Receptor-targeted viral vectors for basic and medical research

Vom Fachbereich Biologie der Technischen Universität Darmstadt

zur Erlangung des akademischen Grades

eines Doctor rerum naturalium

genehmigte Dissertation von

Diplom Biochemikerin Anke Muth geb. Rasbach

aus Friedberg (Hessen)

1. Referentin: Prof. Dr. Beatrix Süß

2. Referent: Prof. Dr. Harald Kolmar

3. Referent: Prof. Dr. Christian Buchholz

Tag der Einreichung: 18.12.2014

Tag der mündlichen Prüfung: 06.03.2015

Darmstadt 2015

D 17

Die vorliegende Arbeit wurde unter der Leitung von Prof. Dr. Christian Buchholz in der Arbeitsgruppe „Molekulare Biotechnologie und Gentherapie“ am Paul-Ehrlich-Institut in Langen angefertigt.

Die Betreuung seitens der Technischen Universität Darmstadt erfolgte durch Prof. Dr. Beatrix Süß vom Fachbereich Biologie.

Parts of this thesis have been published

Rasbach A, Abel T, Münch RC, Boller K, Schneider-Schaulies J & Buchholz CJ (2013). The Receptor Attachment Function of Measles Virus Hemagglutinin Can Be Replaced with an Autonomous Protein That Binds Her2/neu While Maintaining Its Fusion-Helper Function. Journal of Virology (IF[1] 4.648) 87: 6246-6256

Münch RC[2], **Muth A[2]**, Muik AG, Friedel T, Schmatz J, Dreier B, Trkola A, Plückthun A, Büning H & Buchholz CJ (2015). Off-target-free gene delivery by affinity-purified receptor-targeted viral vectors. Nature Communications (IF 10.742), 6: 6246

Münch RC, Janicki H, Völker I, **Rasbach A**, Hallek M, Büning H & Buchholz CJ (2013). Displaying high-affinity ligands on adeno-associated viral vectors enables tumor cell-specific and safe gene transfer. Molecular Therapy (IF 6.425) 21: 109–118

Kneissl S, Abel T, **Rasbach A**, Brynza J, Schneider-Schaulies J & Buchholz CJ (2012). Measles virus glycoprotein-based lentiviral targeting vectors that avoid neutralizing antibodies. PLoS ONE (IF 3.534) 7: e46667

Friedel T, Hanisch LJ, **Muth A**, Honegger A, Abken H, Plückthun A, Buchholz CJ & Schneider IC (2015). Receptor-targeted lentiviral vectors are exceptionally sensitive towards the biophysical properties of the displayed single-chain Fv. Protein Engineering, Design and Selection (IF 2.319), Epub ahead of print

Zhou Q[2], Uhlig KM, **Muth A**, Kimpel J, Lévy C, Münch RC, Seifried J, Trkola A, Coulibaly C, von Laer D, Wels WS, Hartwig UF, Verhoeyen E & Buchholz CJ. Exclusive transduction of human $CD4^+$ T cells upon systemic delivery of CD4-targeted lentiviral vectors. Manuscript in revision.

[1] Impact Factor 2013 Journal Citation Report (Thomson Reuters, 2014)
[2] shared first authors

Oral presentations at international conferences

Rasbach A & Buchholz CJ. Cell surface receptor targeting expanded: from oncolytic measles viruses to lentiviral and AAV vectors.
European Congress of Virology 2013, Lyon, France

Rasbach A, Kirsch N, Abel T, Münch RC, Boller K, Schneider-Schaulies J, Reuter A & Buchholz CJ. Measles virus-pseudotyped lentiviral vectors as tool to understand the fusion complex.
Measles Minisymposium 2013, Annecy, France

Rasbach A, Abel T, Münch RC, Boller K, Schneider-Schaulies J & Buchholz CJ. Receptor attachment is not essential for the measles virus hemagglutinin membrane fusion-helper function.
Annual Meeting of the Society of Virology 2013, Kiel, Germany

Poster presentations at international conferences

Muth A, Münch RC, Muik AG, Plückthun A, Büning H & Buchholz CJ. Adeno-associated viral vectors for targeting circulating tumor cells.
UCT Science Day 2014, Frankfurt, Germany

Rasbach A, Münch RC, Kalicki J, Büning H & Buchholz CJ. Second Generation Entry Targeted AAV Vectors: Reduced Off-Targeting, Flexibility in Receptor Choice and Enhanced Gene Delivery.
American Society of Gene & Cell Therapy Meeting, 2014, Washington DC, USA

Rasbach A, Münch RC, Muik AG, Plückthun A, Büning H & Buchholz CJ. Adeno-associated viral vectors for targeting disseminated and circulating tumor cells.
German Cancer Consortium DKTK Retreat 2014, Heidelberg, Germany

Rasbach A, Abel T, Münch RC, Boller K, Schneider-Schaulies J & Buchholz CJ. The receptor attachment function of measles virus hemagglutinin can be replaced with an autonomous protein that binds Her2 while maintaining its fusion-helper function.
European Congress of Virology 2013, Lyon, France

Rasbach A & Buchholz CJ. Cell surface receptor targeting expanded: from oncolytic measles viruses to lentiviral vectors.
Measles Minisymposium 2013, Annecy, France

Rasbach A, Abel T, Münch RC, Schneider-Schaulies J & Buchholz CJ. A second generation lentiviral vector targeting system displays targeting ligands on a type I transmembrane protein.
German Society of Gene Therapy Meeting 2012, Frankfurt, Germany

Summary

Viral vectors are powerful tools for a steadily increasing number of applications in gene therapy and basic research. In recent years, many proof-of-concept studies and clinical trials resulted in important progress and benefit for patients. Strategies to customize viral vectors will be key to their future success. This thesis deals with viral vectors that were engineered to use a cell surface receptor of choice for cell entry. Such vectors can mediate a restricted gene delivery to a cell type defined by the targeted receptor. The first part of this thesis investigates lentiviral vectors (LVs) carrying engineered glycoproteins of measles virus (MV) to better understand the molecular events during particle cell entry that proceeds via membrane fusion. The second part focuses on adeno-associated viral vectors (AAV) which are non-enveloped particles. AAVs were engineered to assess their potential in detecting rare epithelial cell adhesion molecule (EpCAM)-positive tumor cells.

The first step of MV infection is attachment mediated by the hemagglutinin (H) to one of its receptors which is thought to produce conformational changes in the membrane fusion protein (F) that trigger insertion of its fusion peptide into the target cell membrane. This fusion triggering model was challenged in this thesis by uncoupling the receptor attachment and the fusion-helper function of H by introducing mutations that made it blind to its normal receptors. An artificial receptor attachment protein specific for Her2/neu was incorporated into the membranes of pseudotyped lentiviral particles as a separate transmembrane protein along with H and F. Surprisingly, these particles entered efficiently into Her2/neu-positive SK-OV-3 as well as CHO-Her2 cells. Cell entry was pH-independent, required high-affinity receptor binding and was strictly dependent on the presence of H and F. H-specific monoclonal antibodies as well as mutations in H interfering with H/F interactions blocked cell entry. The vector particles mediated stable and specific transfer of reporter genes into Her2/neu-positive human tumor cells also *in vivo*, while exhibiting improved infectivity and higher titers as compared to conventional Her2/neu-targeted vectors displaying the targeting ligand on H. Additionally, several other targeting ligands were tested in this setting. Extending the current model of MV cell entry, the data suggest that receptor binding of H is not required for its fusion-helper function but particle-cell contact in general may be sufficient to induce the conformational changes in the H/F complex and to activate membrane fusion.

Towards applying AAV targeting technology for the detection, modification or elimination of rare cells expressing EpCAM, which is a marker of circulating tumor cells (CTC), AAVs displaying designed ankyrin repeat proteins (DARPins) specific for EpCAM were generated.

The DARPin Ec1 was displayed on the particle surface and mediated EpCAM-specific gene transfer into receptor-positive cell lines which was further confirmed by competition experiments with the extracellular domain of EpCAM. Transduction was clearly receptor density-dependent and non-malignant EpCAM-positive primary cells were only poorly transducable *ex vivo* and *in vivo*. Performance of vector particles was further enhanced by ion metal affinity chromatography purification. To assess the potency of EpCAM-AAV in detecting rare EpCAM-positive tumor cells, low amounts of MDA-MB-453 tumor cells were mixed with isolated human PBMC. EpCAM-AAV tracked basically all of the tumor cells, even when these made up only 0.3% of the cell mixture. In a next step, the conditions of circulating tumor cells in whole blood were mimicked. As few as 150 tumor cells present in 7.5 milliliters of human blood were readily detected by EpCAM-AAV suggesting that targeted AAVs form a new tool for the detection of rare tumor cells.

The work of this thesis clearly demonstrates that receptor targeting of enveloped and non-enveloped viral vectors is a flexible and versatile technique. Highlighting that both LVs and AAVs can be used not only as gene therapy vectors but also in virological research and diagnostics, these targeting systems open up new possibilities for a broad spectrum of applications.

Zusammenfassung

Virale Vektoren haben sich als nützliche Hilfsmittel für eine immer größer werdende Zahl von Anwendungen in der Gentherapie aber auch in der Grundlagenforschung etabliert. In den letzten Jahren wurde die Weiterentwicklung dieser Vektoren von vielen Machbarkeits- und klinischen Studien vorangetrieben. Strategien um virale Vektoren so anzupassen, dass sie spezifische und individuelle Kriterien erfüllen, werden der Schlüssel zu ihrem weiteren Erfolg sein. Dies könnte zum Beispiel durch Ansteuern eines definierten Rezeptors und somit einen auf bestimmte Zelltypen begrenzten Gentransfer gewährleistet werden. Im ersten Teil dieser Dissertation wurden lentivirale Vektoren untersucht, die veränderte Glykoproteine des Masernvirus tragen, um die molekularen Ereignisse der Membranfusion während des Partikelzelleintritts besser zu verstehen. Im zweiten Teil stehen nicht-behüllte adeno-assoziierte virale Vektoren (AAV) im Fokus. Diese wurden so modifiziert, dass sie seltene Tumorzellen, die das epitheliale Zelladhäsionsmolekül (EpCAM) exprimieren, detektieren können.

Der erste Schritt einer Masernvirusinfektion besteht in der durch das Hämagglutinin (H) vermittelten Anbindung an einen der natürlichen Rezeptoren. Es wird angenommen, dass dies Konformationsänderungen im Fusionsprotein (F) hervorruft, die dann das Einlagern des Fusionspeptids in die Zielzellmembran einleiten. Dieses Fusionsmodell wurde in der vorliegenden Arbeit hinterfragt, indem die Rezeptoranbindung und die Fusionshelferfunktion des H voneinander entkoppelt wurden. Hierfür wurden Mutationen im H eingeführt, die zu einer Verblindung für die natürlichen Rezeptoren führte. Stattdessen wurde ein artifizielles Rezeptoranbindungsprotein, welches spezifisch für Her2/neu ist, zusammen mit H und F in die Membran von pseudotypisierten lentiviralen Vektoren eingebaut. Überraschenderweise waren diese Partikel in der Lage sowohl in Her2/neu-positive SK-OV-3 als auch in CHO-Her2 Zellen einzudringen. Es konnte gezeigt werden, dass der Zelleintritt eine hoch-affine Rezeptoranbindung benötigte, pH unabhängig und grundsätzlich von der Anwesenheit von H und F abhängig war. H-spezifische monoklonale Antikörper so wie eine Mutation in H, welche die H/F Interaktion stört, blockierten den Zelleintritt. Die Vektorpartikel vermittelten stabilen und spezifischen Reportergentransfer in Her2/neu-positive humane Tumorzellen *in vitro* und *in vivo* und wiesen darüber hinaus eine erhöhte Infektiösität und höhere Titer als die konventionellen Her2/neu-Targetingvektoren auf. Zusätzlich wurden verschiedene andere Targetingliganden in diesem System getestet. Als Erweiterung des gegenwärtigen Masernviruszelleintrittmodells legen diese Daten nahe, dass Rezeptoranbindung des H für

dessen Fusionshelferfunktion nicht benötigt wird. Der Kontakt zwischen Partikel und Zelle könnte ausreichend sein, um die Konformationsänderungen im H/F-Komplex hervorzurufen und die Membranfusion auszulösen.

Ein erster Schritt zur Anwendung von AAV-Vektoren für die Detektion, Modifikation oder Eliminierung von seltenen Zellen, die EpCAM, einen Marker für zirkulierende Tumorzellen (CTC), exprimieren, war die Generierung von AAVs, die EpCAM-spezifische „designed ankyrin repeat proteins“ (DARPin) einbauen. Das DARPin Ec1 wurde auf der Kapsidoberfläche des AAV präsentiert und vermittelte spezifischen Gentransfer in EpCAM-positive Zelllinien, was durch Kompetitionsexperimente mit der extrazellulären Domäne von EpCAM bestätigt wurde. Die von EpCAM-AAV vermittelte Transduktion war eindeutig von der Rezeptordichte abhängig und außerdem in nicht-malignen, primären, EpCAM-positiven Zellen, sowohl *ex vivo* als auch *in vivo*, stark eingeschränkt. Des Weiteren konnte die Transduktionseffizienz von EpCAM-AAV durch die chromatographische Abtrennung von DARPin-defizienten AAV Partikeln, die bei der Vektorherstellung als Nebenprodukt entstehen, deutlich erhöht werden. Um das Potential von EpCAM-AAV zur Detektion von seltenen EpCAM-positiven Tumorzellen zu untersuchen, wurde eine geringe Anzahl von MDA-MB-453 Tumorzellen mit isolierten humanen „peripheral blood mononuclear cells“ (PBMCs) gemischt. Fast alle Tumorzellen wurden durch EpCAM-AAV transduziert, auch wenn sie nur 0.3% der Mischung ausmachten. Im nächsten Schritt wurde die Situation von CTCs im Vollblut nachgestellt. Auch wenn nur 150 Tumorzellen in 7.5 ml Blut vorhanden waren, konnten diese mit Hilfe von EpCAM-AAV nachgewiesen werden, was darauf schließen lässt, dass EpCAM-AAV zur Detektion von seltenen Tumorzellen verwendet werden kann.

Die Ergebnisse dieser Arbeit demonstrieren die Flexibilität und Vielseitigkeit des Rezeptortargetings von behüllten und nicht-behüllten viralen Vektoren. Die Tatsache, dass sowohl LVs als auch AAVs nicht nur als Gentherapievektor sondern auch für virologische Fragestellungen und Diagnoseverfahren verwendet werden können, unterstreicht, dass die Targetingsysteme für ein breites Spektrum von Anwendungen neue Möglichkeiten eröffnen.

1 Introduction

Over the past decades gene therapy has become a promising technique and a potential future treatment option for many diseases. Various approaches to replace a mutated gene with a healthy copy or to introduce a therapeutic gene are being developed and by June 2014 more than 2000 clinical gene therapy trials were approved worldwide (http://www.wiley.co.uk/genmed/clinical). The respective genetic information is delivered to a human cell using non-viral or viral vectors. Whereas non-viral vectors are considered as safe albeit rather inefficient alternatives (Schaffer et al, 2008), viruses have evolved to infect host cells and deliver their genomic payload. Engineering viral vectors with new properties to customize them for the respective indication is an emerging field of research. However, a deep understanding of virus biology and structure as well as rational design is required.
This thesis describes the generation and characterization of cell surface receptor-targeted adeno-associated and measles virus-pseudotyped lentiviral vectors for applications in virology and medical research.

1.1 Measles virus

Measles virus (MV) is the causative agent of measles which is a highly contagious disease accompanied by high fever, cough and rash. It is one of the leading causes of death among young children and although a safe and cost-effective vaccine is available, 122.000 deaths were reported globally in 2012 (WHO Fact Sheet N°286). While collaborative efforts of the Measles & Rubella initiative (WHO, UNICEF, the American Red Cross, the United States Centers for Disease Control and Prevention and the United Nations Foundation) aim at controlling and eventually eradicating measles, the virus itself has attracted considerable interest in biomedical research due to its oncolytic properties in recent years. Reports of spontaneous regression of malignancies in children following measles infection have been around since as early as 1971 (Bluming & Ziegler, 1971; Zygiert, 1971; Gross, 1971). Infected tumor cells express the MV glycoproteins which mediate intercellular fusion leading to formation of multinucleated giant cells (syncytia) and apoptotic cell death. But it is only with the use of attenuated vaccine strains which are nonpathogenic to normal tissues, non-persistent and genetically stable that the field of MV virotherapy has moved forward (Russell & Peng, 2009). The MV vaccine strains such as the Edmonston strain acquired CD46 tropism during tissue culture adaption and are known to enter cells predominantly via this receptor

(Dörig et al, 1993; Galanis et al, 2010). CD46, a complement regulatory protein, is expressed by all human nucleated cells but most importantly it is frequently overexpressed in tumor cells (Riley-Vargas et al, 2004; Russell & Peng, 2009). Key to the measles virus attractiveness as oncolytic agent is that cytopathic effects are only observed when CD46 expression level reaches a certain threshold leaving non-malignant tissues unaffected by the virus and leading to preferential killing of tumor cells (Anderson et al, 2004). Nowadays, these favorable characteristics are combined with engineering strategies to monitor virus replication, enhance systemic delivery and tumor specificity and improve efficacy (Miest & Cattaneo, 2014). Promising preclinical results have already led to the initiation of several clinical phase trials. In July 2014, Russel et al. reported complete remission of one patient with advanced incurable myeloma after systemic administration of a high dose recombinant MV engineered to express the human thyroidal sodiumiodide symporter (NIS) allowing noninvasive tumor imaging (Russell et al, 2014; Bell, 2014). Remarkably, this was the first case of intravenous virotherapy to completely eliminate disseminated malignancies.

However, many aspects of MV biology have not yet been fully understood. For the future development and application of MV as biomedical agent as well as treatment and eradication of the measles disease, a detailed understanding and unraveling of viral mechanisms will be necessary.

1.1.1 Virus structure

As a member of the Morbillivirus genus in the family of *Paramyxoviridae*, measles virus is an enveloped, non-segmented negative-strand RNA virus (Moss & Griffin, 2006) (Figure 1A). Its single strand genomic RNA is approximately 16 kb in length and serves as template for synthesis of the positive RNA strand and of the mRNAs that are translated into eight viral proteins (Knipe & Fields, 2007) (Figure 1B). One of the encoded proteins, the large protein (L), is a viral RNA polymerase that is packaged in the virus and is responsible for synthesis of mRNAs once the virus has been uncoated in the cytoplasm of the infected cell. Instead of producing a long positive-strand copy, the polymerase stops at specific sites to release one of six mRNAs and then restarts again. In order to generate a full-length negative-strand RNA genome for new viruses, the same viral RNA polymerase complements the maternal strand but due to accumulation of viral proteins the signals that usually cause the polymerase to stutter are masked (Sompayrac, 2002). Together with the polymerase cofactor phosphoprotein (P) and the nucleoprotein (N), the L protein encloses the viral genome forming the

ribonucleocapsid. The matrix protein (M) is also packaged within the virions and is known to be a mediator between the nucleocapsid and the viral envelope. Interactions between M and the cellular membrane (Hirano et al, 1992; Riedl et al, 2002; Runkler et al, 2007), the N protein (Hirano et al, 1993; Iwasaki et al, 2009; Suryanarayana et al, 1994) and the viral envelope proteins (Cathomen et al, 1998a; Cathomen et al, 1998b; Tahara et al, 2007) are described. It is commonly assumed that M forms a thin layer covering the inner membrane, but recent electron cryotomography data argue that it forms helices coating the ribonucleocapsid to tightly package the genome and recruit it to the budding site (Liljeroos et al, 2011) (Figure 1A).

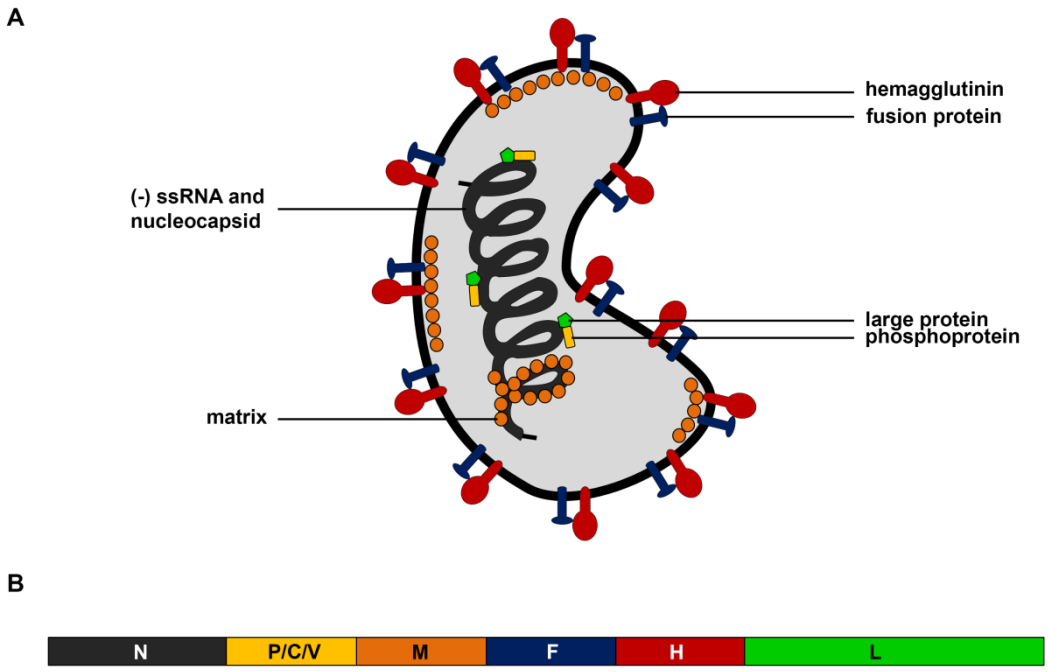

Figure 1: Measles virus structure and genome organization. (A) Schematic representation of the measles virus particle. The pleomorphic enveloped virus contains RNA tightly encapsidated by the nucleoprotein (gray), large protein (green) and phosphoprotein (yellow). The matrix protein (orange) is shown in part as inner layer at the membrane and as layer coating the genome. The envelope glycoproteins hemagglutinin and fusion protein are shown in red and blue, respectively. (B) The non-segmented genome encodes eight proteins, two of which (C and V) are non-structural proteins. Color code corresponds to A.

In addition, two membrane spanning glycoproteins, the hemagglutinin (H) and the fusion protein (F), are transcribed from the viral RNA. They are organized on the viral surface in a hetero-oligomeric complex of F trimers and H tetramers which already forms in the endoplasmic reticulum (Plemper et al, 2001; Paal et al, 2009; Ader et al, 2012). Together, both proteins are the key players for membrane fusion and cell entry of the virus. While H mediates receptor binding and thereby determines the MV cellular tropism, F contains a hydrophobic stretch called fusion peptide that is inserted into the cellular membrane to initiate

virus-cell fusion (Navaratnarajah et al, 2009). Unlike other paramyxovirus attachment proteins, MV H has no neuraminidase activity since it does not bind sialic acid. It is a 617 amino acid type II transmembrane protein which comprises a N-terminal cytoplasmic tail, an integral membrane part, an extracellular stalk region and a globular head domain (Navaratnarajah et al, 2009). The F protein is a highly conserved type I transmembrane protein which is synthesized as 553 amino acid F_0 precursor protein. After cleavage by furin in the trans-Golgi network, the activated protein consists of disulfide-linked F_1 and F_2 subunits (Knipe & Fields, 2007). Besides the six structural proteins N, P, M, F, H and L, two non-structural proteins called C and V are encoded by the viral genome. The basic protein C is alternatively translated in a different reading frame from the P gene using an initiator methionine codon downstream from that of P while V is a product of RNA editing of P mRNA (Knipe & Fields, 2007). Both proteins are described to interfere with the innate immune response by inhibiting interferon signaling and are suggested to modulate viral replication (Ito et al, 2013).

1.1.2 Measles virus propagation and cell entry mechanism

Like most paramyxoviruses, MV enters cells in a pH-independent manner and fuses directly with the plasma membrane (Iorio et al, 2009). However, in contrast to other family members, MV binds to the cell not via sialic acid residues but through direct protein-protein interaction. The wild-type MV clinical isolates enter cells via the signaling lymphocyte activation molecule (SLAM, also known as CD150) (Tatsuo et al, 2000; Erlenhoefer et al, 2001; Hsu et al, 2001) and the adherens junction protein nectin-4 (Mühlebach et al, 2011; Noyce et al, 2011), whereas the vaccine strains additionally use CD46 as cellular receptor (Dörig et al, 1993; Naniche et al, 1993) (Figure 2).

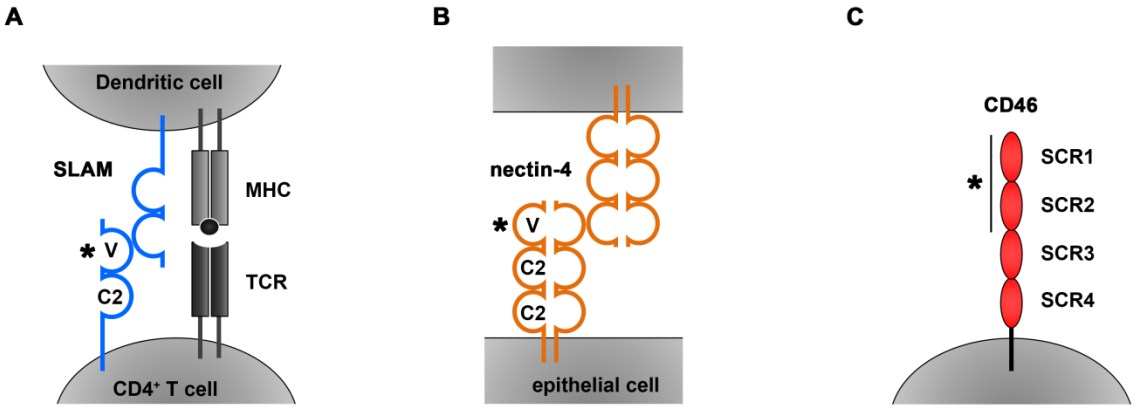

Figure 2: Measles virus receptors. (A) Structure of SLAM. The extracellular part is composed of a variable (V) and a constant (C2) Ig-like repeat. The major histocompatibility complex (MHC) presenting an antigen on dendritic cells as well as the T cell receptor (TCR) on a $CD4^+$ T cell is shown. (B) Structure of nectin-4. Two nectin molecules form a dimer at the cell surface and are able to bind to another dimer on opposing cells. The extracellular domain consists of one V and two C2 Ig-like repeats. (C) Structure of CD46. The third receptor that is exclusively used by laboratory-adapted MV strains has four short consensus repeats (SCR). Interaction of MV with the respective receptor domains are indicated by asterisks. Modified from (Sato et al, 2012).

The use of different receptors with restricted expression in either lymphoid cells such as thymocytes, activated lymphocytes, mature dendritic cells, macrophages and platelets (SLAM) or in epithelial cells (nectin-4) explains the mode of transmission for MV in the human body. Current models postulate that macrophages and dendritic cells in the airway are the first target for the virus entering the respiratory tract (Figure 3). Then, these cells ferry the virus to the lymph nodes from where it spreads throughout the lymphatic organs. Eventually, the infected immune cells transmit the virus to epithelial cells expressing nectin-4 on their basolateral side. After infectious spread of the virus via tight junctions in the airway epithelium, progeny virus is released and expulsed by coughing and sneezing (Mühlebach et al, 2011; Sato et al, 2012). This way, the contagious viral particles can be transmitted to other hosts.

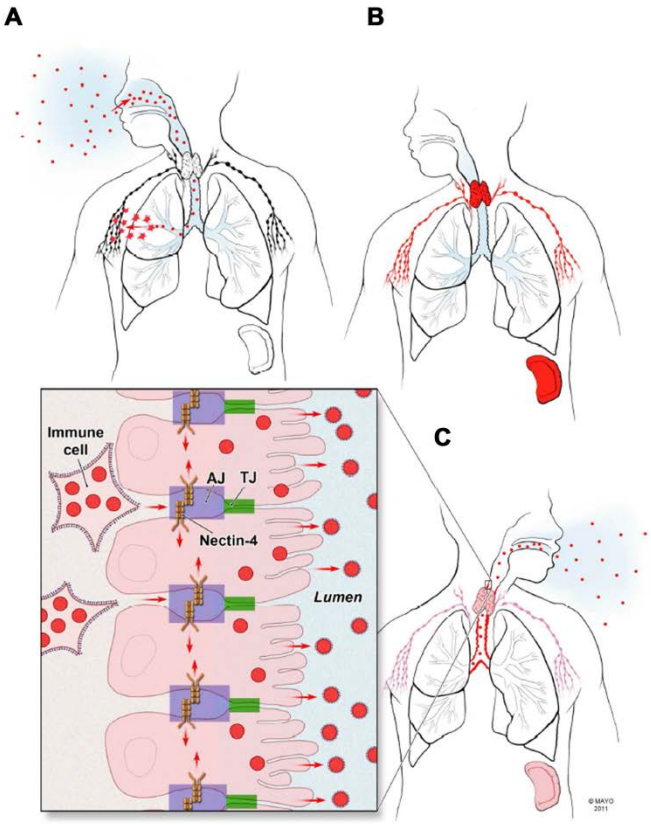

Figure 3: Transmission mode of MV. Infectious viral particles are shown as red spheres; viral glycoproteins are drawn as small spikes on the spheres in the inset close-up. Infected cells and organs are shown in red or pink at or after the peak of infection, respectively. (A) MV enters the human body through the respiratory tract and infects SLAM-positive macrophages and dendritic cells. These cells ferry the virus to the lymph nodes and (B) infection reaches thymus and spleen. (C) Infected immune cells expressing the viral glycoproteins transfer the virus to airway epithelial cells. Viral spread in epithelial cells is adherens junction (AJ, purple rectangles) protein nectin-4-dependent. Once epithelial cells are infected, the virus spreads via tight junctions (TJ, green rectangles). Finally, viral particles are released in the trachea and expulsed via coughing and sneezing. Modified from (Mühlebach et al, 2011).

The first steps of the infectious life cycle depend on virus cell entry mediated by the concerted action of H and F. The structure of an H dimer is best described as a propeller with two cuboidal heads (Figure 4A), each composed of six β-blades (Figure 4B). Binding to the natural MV receptors SLAM and nectin-4 which both belong to the immunoglobulin superfamily is provided by attachment of the globular head to the respective V domains (Figure 2A+B). Residues involved in binding are well characterized and are mainly located in the β5-6 blades (SLAM) or in a hydrophobic groove between β4-5 (nectin-4) (Mateo et al, 2014; Hashiguchi et al, 2011a). The H heads are situated on disulfide-linked long stalk regions, which interact with the globular head of F (Figure 4A) (Paal et al, 2009; Apte-Sengupta et al, 2013). Receptor binding is believed to trigger rearrangements of H which are then transferred to F (fusion-helper function of H) to trigger conformational changes that ultimately expose its fusion peptide to become inserted into the cellular membrane (Plemper

et al, 2011). This H/F interplay is thought to depend on lowering the prefusion F activation energy barrier and thereby initiating the fusion process (Ader et al, 2012).

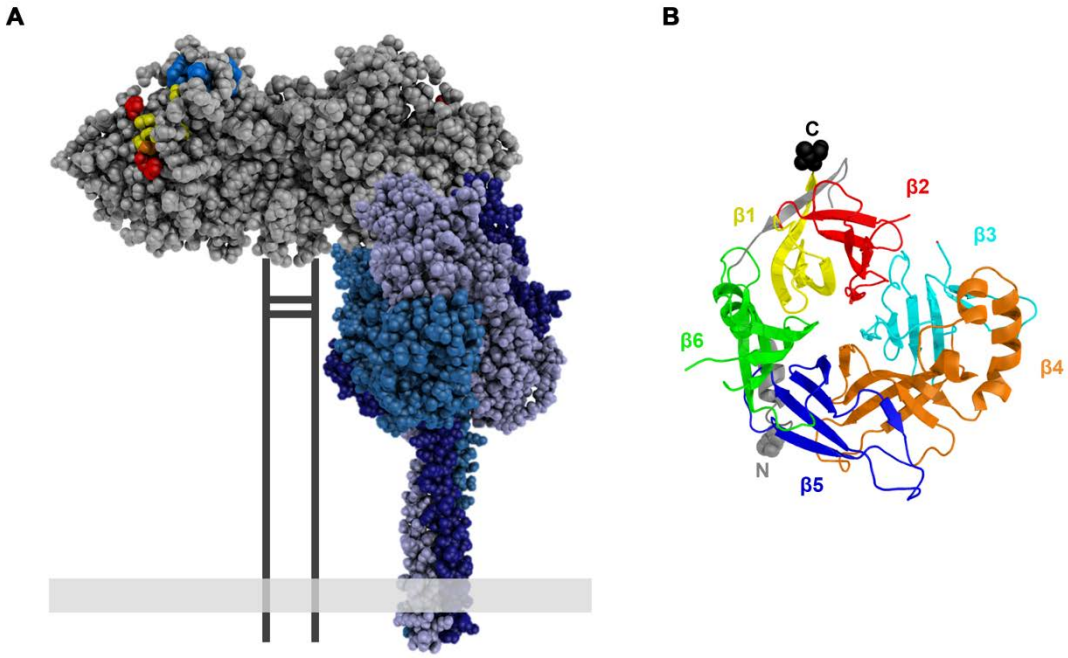

Figure 4: Structure of the MV H and F proteins. (A) Sphere representation of the MV H dimer crystal structure shown in gray (Hashiguchi et al, 2007) and the F trimer of the paramyxovirus parainfluenza virus 5 shown in blue (Yin et al, 2006). The stalk, transmembrane, and cytoplasmic regions of H are depicted as vertical lines, with two horizontal lines indicating disulfide bonds. The residues most important for binding to SLAM (P191-R195, D530, R533), nectin-4 (L482) and CD46 (Y481, L500) are shown in blue, orange and red, respectively. Residues involved in CD46 and nectin-4 binding (L464, F483, Y541, Y543) are colored yellow (Mateo et al, 2014). The virus membrane is illustrated as light gray box. (B) Top view of the six-bladed β-propeller sheet H protein head as cartoon representation. Each blade is represented in a different color. The C terminus is shown in black, the N terminus is shown in gray. The structures (Protein Data Bank [PDB] ID 2ZB5 and 2B9B) were modified using Pymol.

How receptor binding alters the conformation of H and thus initiates the cascade of conformational changes is less well understood, especially when taking the unusual flexibility in using alternative receptors for cell entry into account. Besides the three identified MV receptors, the repertoire of entry receptors has been further extended by H protein engineering. Introducing mutations Y481A, R533A, S548L, and F549S makes the virus deficient for cell entry via its natural receptors (Nakamura et al, 2005; Vongpunsawad et al, 2004). Specificity for a designated receptor was then achieved by fusing a targeting ligand such as a single chain antibody (scAb) or a designed ankyrin repeat protein (DARPin) to the C terminus of H. In this way, a variety of tumor antigens have been shown to be functional as MV receptors (Msaouel et al, 2012).

Contrary to current MV fusion mechanism models, data collected during my diploma thesis indicated that receptor attachment and fusion-helper function can possibly be separated without destroying the fusion competence of the glycoprotein complex (Rasbach, 2010). This

may be achieved by using lentiviral vectors pseudotyped with the MV F and blinded H and a third protein mediating receptor attachment.

1.2 Lentiviral vectors

Many diseases including immunodeficiency disorders, haemophilia or cystic fibrosis are caused by abnormalities in the genome. Patients suffering from one of these genetic conditions would greatly benefit from correction or transfer of the respective genes. Since the relationship between gene defects and diseases has been identified several decades ago, the idea of gene therapy is not very new. Already in 1972, Friedman & Roblin proposed the potential therapeutic use as well as scientific and ethical problems arising from gene therapy (Friedmann & Roblin, 1972). Nowadays, a lot of improvement in gene transfer techniques has been made and many promising gene therapy trials are ongoing. Among the gene delivery vehicles used, vectors derived from retroviruses are probably the most suitable tool for efficient gene transfer and stable integration of the transgene. Especially the development of lentiviral vectors (LV) has gained a lot of attention in the expanding and competitive field of vectorology (Naldini et al, 1996; Schambach et al, 2013). Compared to other retrovirus-derived vectors, as for example γ-retroviral vectors, LVs stand out due to their capacity to transduce non-dividing cells and decreased genotoxicity. The potential of lentiviral vectors is also reflected by the fact that they are used in 4.2% of all vector gene therapy clinical trials (http://www.wiley.co.uk/genmed/clinical). Recently, two studies reported promising results from *ex vivo* clinical trials treating patients with rare hematopoietic diseases using improved lentiviral vectors. Remarkably, patients suffering from metachromatic leukodystrophy or Wiskott-Aldrich syndrome benefitted from treatment with gene-corrected hematopoietic stem cells without any signs of oncogene activation which was a major drawback of previous gene therapy trials using γ-retroviral vectors (Biffi et al, 2013; Aiuti et al, 2013).

1.2.1 HIV-1 derived vectors

Most LVs currently used in clinical trials are derived from the human immunodeficiency virus type I (HIV-1). This complex enveloped virus with a diameter of 100-120 nm and a cone-shaped, cylindrical core is a major human pathogen causing the acquired immunodeficiency syndrome (AIDS) (Knipe & Fields, 2007) (Figure 5). As a member of the family *Retroviridae*, HIV-1 replicates through a unique life cycle. The genome of the virus is composed of two single-stranded RNA copies which are reverse transcribed to DNA upon cell

entry. The discovery of the viral enzyme which mediates this process called reverse transcriptase destroyed the dogma of molecular biology stating that genetic information can only be processed in one way from DNA to RNA to protein and earned David Baltimore, Howard Temin and Renato Dulbecco the Nobel Prize in 1975 (http://www.nobelprize.org). In a next step, the viral DNA is integrated into the host chromosomal DNA and this so-called provirus serves as template for viral genome replication and protein synthesis. The two key enzymes reverse transcriptase and integrase confer on the virus the outstanding ability to maintain a persistent infection and transfer its genetic information vertically.

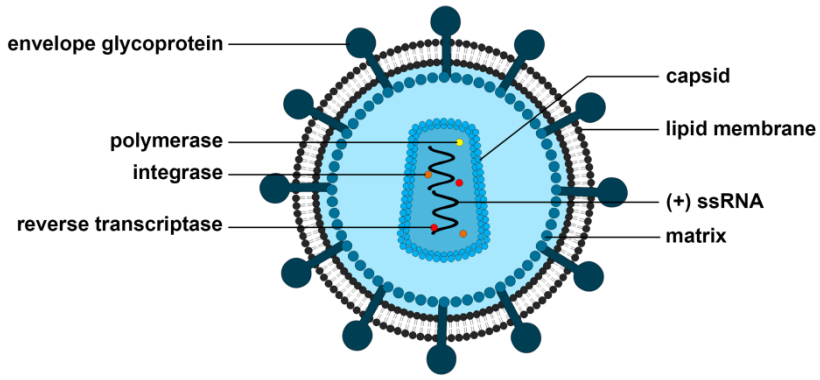

Figure 5: Structure of HIV-1. The enveloped virus has a cylindrical core (capsid) containing two single-stranded RNA genomes which are associated with the nucleocapsid proteins and viral enzymes (polymerase, integrase, reverse transcriptase). The matrix protein forms a thin layer covering the inner membrane. The viral glycoprotein consisting of gp120 and gp41 are shown.

The HIV-1 RNA genome codes for nine viral proteins (Figure 6A). The three main open-reading frames *gag*, *pol* and *env* encode structural proteins and enzymes. While translation products of the *gag* gene are the viral core proteins matrix (MA), capsid (CA), nucleocapsid (NC) and p6 protein, the *pol* sequence provides the information for enzymes required for viral replication such as protease (PR), reverse transcriptase (RT) and integrase (IN). The viral surface glycoprotein gp160 which is eventually cleaved into the gp120 surface (SU) and gp41 transmembrane (TM) protein is encoded by the *env* gene (Knipe & Fields, 2007). In addition, two regulatory proteins transactivating the transcription (Tat) from the viral long terminal repeats (LTR) flanking the genome and controlling splicing and nuclear export of the viral RNA (Rev) are synthesized (Sakuma et al, 2012). The remaining four genes code for the accessory proteins Vif, Vpr, Vpu and Nef that ensure viral survival by evasion of cell-mediated antiviral responses (Malim & Emerman, 2008).

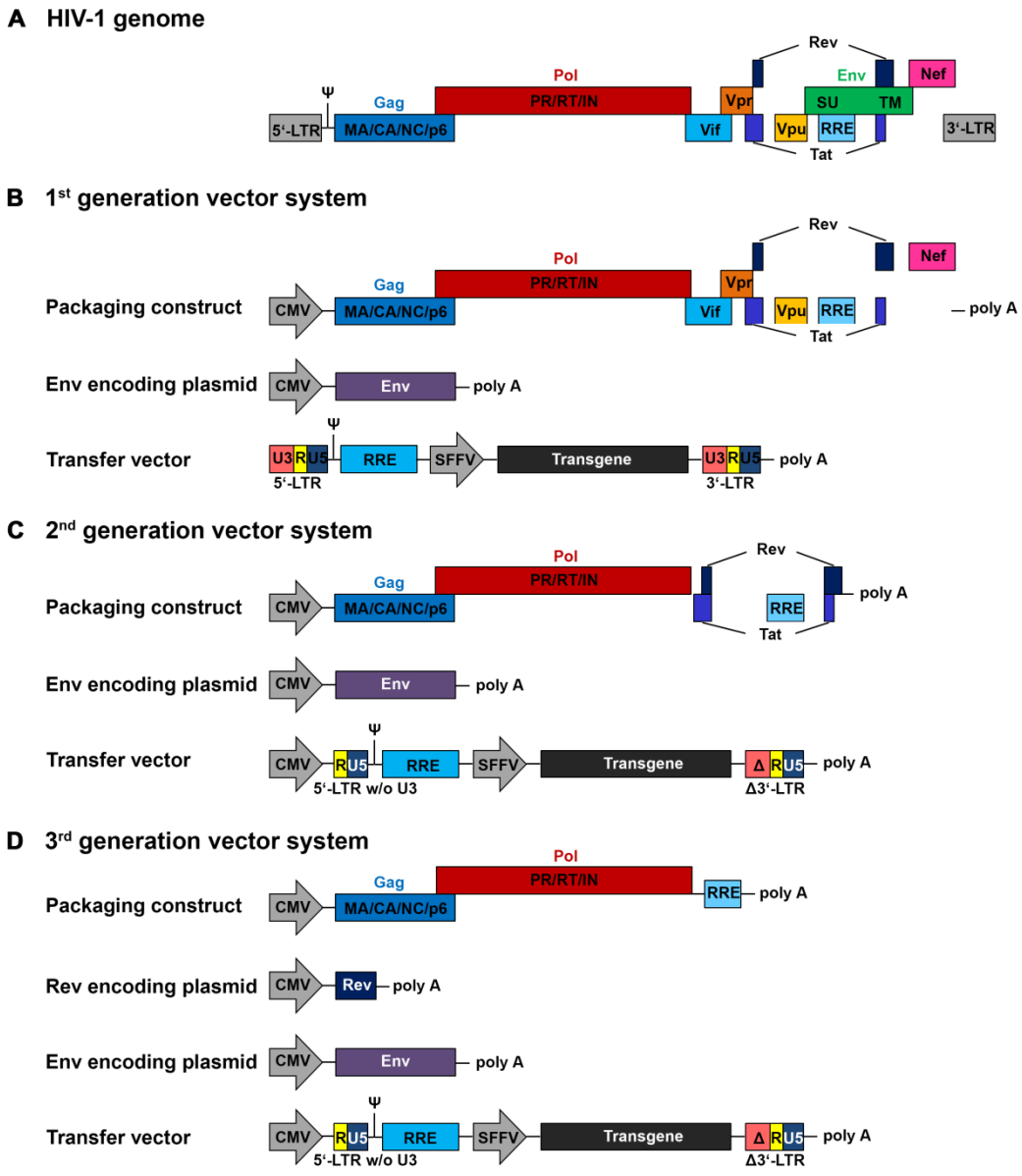

Figure 6: Schematic representation of the HIV-1 genome and HIV-1 vectors. (A) The viral genome encodes three structural (Gag, Pol, Env), two regulatory (Tat, Rev) and four accessory (Vif, Vpr, Vpu and Nef) proteins and is flanked by two long terminal repeats (LTRs). The ψ-signal which is required for packaging of the viral RNA into the virions is located close to the 5'-LTR. The Rev-responsive element (RRE) is also indicated. The Gag precursor protein consists of matrix (MA), nucleocapsid (NC) and p6 protein. The pol sequence provides the information for the enzymes protease (PR), reverse transcriptase (RT) and integrase (IN). The envelope protein is further processed into a surface (SU) and transmembrane (TM) protein. (B) First generation lentiviral vectors are produced by splitting the vector components into three separate plasmids. Only the transfer vector encoding the transgene under control of a strong viral promoter such as the spleen focus-forming virus (SFFV) promoter contains the ψ-signal. (C) In the second generation lentiviral vector system the accessory proteins are excluded to further enhance the safety profile of the vector. (D) The likelihood of recombination is decreased by deleting Tat and Rev from the packaging construct. While Rev is trans complemented with a fourth plasmid, Tat is not required due to replacement of the U3 promotor region in the transfer vector. Modified from (Sakuma et al, 2012) and (Abel, 2013).

In order to develop a replication incompetent viral vector which enables safe and efficient transfer of a specific transgene, sophisticated constructs have been generated. The first generation of HIV-1-derived lentiviral vectors was produced by splitting the vector components into three separate plasmids: the packaging construct encoding Gag/Pol and the

accessory proteins, the Env plasmid, and the transfer vector coding for the transgene (Figure 6B). Prerequisite for the delivery of the transgene without expression of viral proteins in the target cells was that only the transfer vector contained the ψ-signal which is responsible for packaging of the respective RNA into viral particles (Richardson et al, 1993). To further enhance safety, the sequences for the accessory proteins Vif, Vpu, Vpr and Nef counteracting the immune system and promoting HIV-1 propagation and virulence were deleted in the second lentiviral vector generation (Figure 6C) (Sakuma et al, 2012). Although the second generation vectors are often used in research, the third generation vector system is preferred for clinical applications. Here, the likelihood of recombination and thus production of replication competent particles is even more reduced by deleting *tat* and *rev* from the packaging construct. While *rev* is delivered on a separate plasmid, *tat* is not required anymore due to replacement of the U3 promoter region in the transfer vector (Figure 6D) (Sakuma et al, 2012).

1.2.2 Retargeting lentiviral vectors using the measles virus envelope

The cell tropism of a viral vector is determined by its envelope glycoproteins. The HIV-1 gp120 protein uses CD4, a cell surface marker expressed in T-helper cells, monocytes, macrophages and dendritic cells, as its primary receptor (Knipe & Fields, 2007). In order to alter, restrict or expand the host range, envelope proteins derived from other viruses can be incorporated. This process known as pseudotyping enables the combination of unique lentiviral features with the tropism of an expanding list of viral glycoproteins (Cronin et al, 2005). Probably the most popular protein for pseudotyping HIV-1-based vectors is the vesicular stomatitis virus glycoprotein (VSVG). First reported in 1996 by three independent groups (Akkina et al, 1996; Naldini et al, 1996; Reiser et al, 1996), VSVG pseudotypes are still widely used given that the glycoprotein is very stable, allows concentration to high titers and exhibits a broad tropism due to binding to the ubiquitously expressed LDL receptor family (Finkelshtein et al, 2013).

But for some therapeutic applications a restricted gene transfer rather than a wide host range is required. Especially for *in vivo* applications where only one cell type needs to be modified, safety and efficacy can be improved by restricting cell entry of the viral vector (Buchholz et al, 2009). The glycoproteins of other RNA viruses such as Mokola virus or lymphocytic choriomeningitis virus have been exploited to achieve restriction to certain cell types as for example astrocytes or glioma cells (Sakuma et al, 2012). A major limitation is that viral

envelope proteins rarely mediate entry into only one single cell type. The HIV-1 gp120 is one of the few proteins that enable the virus to enter only CD4-positive lymphocytes, but most other viruses either bind to several different receptors or their binding partners are expressed in various cell types. Strikingly, the limited availability of natural envelope proteins can be overcome by engineering glycoproteins to retarget the vector to a cell surface molecule of choice. The measles virus F and H proteins already had been shown to be a powerful tool to redirect oncolytic viruses (chapter 1.1.2) and cytoplasmic tail truncated variants could be efficiently incorporated into lentiviral vectors (Funke et al, 2008; Frecha et al, 2008). An advantage of the measles virus pseudotype is that receptor attachment and fusion are mediated by two different proteins. Therefore, manipulation of the H protein does not interfere with the fusion capacity of F. The MV pseudotyped lentiviral targeting system relies on the same principles as targeted oncolytic viruses. The same four point mutations, namely Y481A, R533A, S548L and F549S, were introduced to ablate the natural tropism of H. Genetic fusion of a targeting ligand to the C terminus of H redirects the vector in cell entry to the receptor of choice. Funke et al. demonstrated the first set of MV pseudotyped lentiviral vectors that specifically targeted CD20 or the epidermal growth factor receptor (Funke et al, 2008), but since then the list of cell surface markers used has been further extended to proteins relevant in immunology, hematology, neurobiology and cancer research (Anliker et al, 2010; Ageichik et al, 2011; Zhou et al, 2012; Münch et al, 2011).

1.3 Adeno-associated viral vectors

Another promising viral vector system is based on the adeno-associated virus (AAV). Depending on the application, vectors constructed from AAVs are favorable due to features inherent to their viral biology. They are non-pathogenic, have low immunogenic potential, are capable of transducing dividing and non-dividing cells and although they usually do not insert genetic material into the host chromosomes, long-term gene expression can be sustained in non-dividing cells (Clark et al, 1997; Büning et al, 2008; Mingozzi & High, 2007). Many clinical trials using AAV gene therapy have achieved promising results in diseases such as congenital blindness and haemophilia (Mingozzi et al, 2013) and have led to the pioneering first market authorization of a gene therapy product in Europe. The product with the trade name Glybera is an AAV1 vector delivering an intact copy of the human lipoprotein lipase (LPL) gene to restore the enzyme’s activity in LPL deficiency patients suffering from severe or multiple pancreatitis attacks (Ylä-Herttuala, 2012; Flemming, 2012).

In combination with techniques to tackle the drawbacks of AAV vectors such as the presence of neutralizing antibodies in human serum or their limited cell specificity, AAV gene therapy is expected to progress even further and will have an impact on modern medicine.

1.3.1 AAV biology

AAV is a small, non-enveloped virus with an icosahedral shape of approximately 20-26 nm. The first human AAV was discovered in 1965 as contaminant in adenovirus preparations. Since it usually requires co-infection with a helper virus such as adenovirus or herpesvirus for productive infection, AAV is considered replication-deficient and is classified as member of the *Dependovirus* genus in the *Parvoviridae* family (Knipe & Fields, 2007). In the absence of a helper virus, AAV will integrate preferentially into the AAVS1 locus on chromosome 19 (Kotin et al, 1990; Samulski et al, 1991) (Figure 7). This biphasic life cycle in combination with the ability for site-specific integration makes AAV unique among eukaryotic DNA viruses (Young et al, 2000).

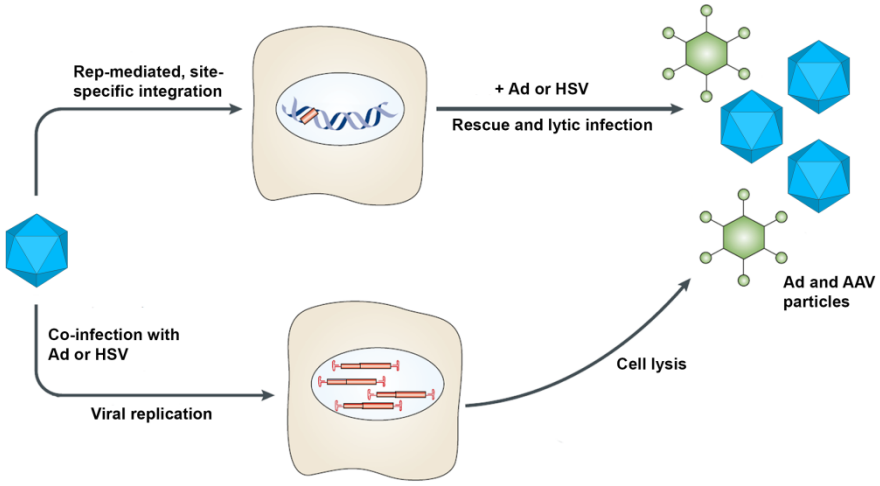

Figure 7: Biphasic life cycle of adeno-associated virus. In absence of helper virus, AAV integrates site-specifically into the human chromosome 19 (red) and persists in a latent form. If the cell is co-infected with adenovirus (Ad) or herpes simplex virus (HSV) the necessary factors for active AAV replication are provided. Modified from (Vasileva & Jessberger, 2005).

The 4.7 kb single-stranded DNA genome can be of positive or negative polarity contains three open reading frames (ORF) flanked by two inverted terminal repeats (ITRs) (Berns, 1974) (Figure 8). The ITRs forming T-shaped hairpin structures are important for genome packaging and integration (Cao et al, 2002). Additionally, they contain Rep-binding elements and a terminal resolution site necessary for genome replication. Current models also propose that

the ITR is the origin of replication and serves as primer for second strand synthesis. The four non-structural AAV proteins Rep40, Rep52, Rep68 and Rep78 are encoded by the *rep* ORF and their expression is regulated by the viral promoters p5 and p19. The two overlapping mRNAs of Rep52 and Rep78 can be subject to splicing and give rise to Rep 40 and Rep68, respectively (Knipe & Fields, 2007). A common feature of all four proteins is their ATPase and helicase activity. The larger Rep proteins Rep68 and Rep78 are known to regulate viral replication and gene expression. In the presence of helper virus they transactivate transcription and contribute to the replication of the AAV genome whereas in the absence of helper virus they repress the promoters p5 and p19 and mediate site-specific integration (Pereira et al, 1997; Young et al, 2000). The small Rep proteins Rep40 and Rep52 are involved in viral assembly and packaging (King et al, 2001).

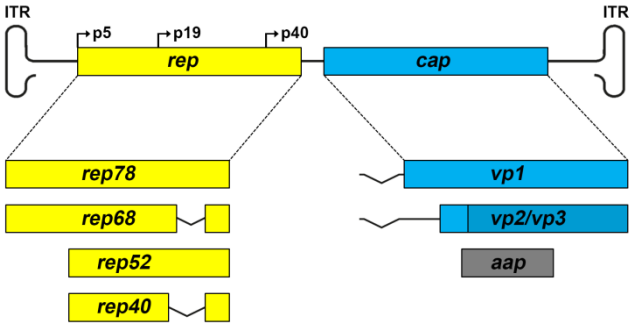

Figure 8: Genome organization of AAV. The 4.7 kb single-stranded DNA genome is flanked by two T-hairpin shaped inverted terminal repeats (ITRs) and contains three open reading frames (ORFs). The *rep* ORF encodes the non-structural proteins Rep78, Rep68, Rep52 and Rep40. The *cap* ORF encodes the three structural proteins VP1, VP2 and VP3 that form the viral capsid with the aid of the assembly-activating protein (AAP) which is encoded by an alternative ORF within *cap*. The promoters p5, p19 and p40 drive expression of the viral proteins. The respective transcripts are shown below. Modified from (Kotterman & Schaffer, 2014).

The *cap* gene encodes the three structural proteins VP1, VP2 and VP3 that form the viral capsid (Figure 8). They are produced from the p40 mRNA which is further processed using two different splice acceptors located in the intron between the *rep* and *cap* ORF. The longer splice variant contains the natural start codon and leads to the expression of VP1. In the second variant, this codon has been spliced out. An unusual ACG codon is used for the expression of VP2 and a conventional AUG further downstream is the initiator codon for VP3 (Knipe & Fields, 2007). This regulation of gene expression leads to a common C-terminal end for all three structural proteins. The use of unusual start codons and splice variants results in a transcriptional gradient of 1:1:10 for VP1, VP2 and VP3. Assembly of the capsid is assisted by the assembly-activating protein (AAP) which is the gene product of a recently identified ORF within the *cap* gene (Sonntag et al, 2010).

The capsid comprises 60 VP monomers arranged with *T*=1 icosahedral symmetry. Several three-dimensional structures of different AAV serotypes have been determined by X-ray crystallography or cryo-electron microscopy reconstruction (Kronenberg et al, 2001; Xie et al, 2002; Walters et al, 2004; Govindasamy et al, 2006; Nam et al, 2007; Lerch et al, 2010; Ng et al, 2010; Govindasamy et al, 2013). Common features to the capsid proteins of all serotypes are a small α-helix (αA) and an eight-stranded anti-parallel β-barrel (βB-βI) (Figure 9A). The large loops connecting the β-strands are divided in distinctive HI and DE loops as well as nine variable regions (VR-I to VR-IX) (Tseng & Agbandje-McKenna, 2014; Govindasamy et al, 2006). These VRs form the exterior surface of the capsid and contribute to structural and functional differences between AAV serotypes, including receptor attachment, transduction efficiency and antigenic specificity (Drouin & Agbandje-McKenna, 2013).

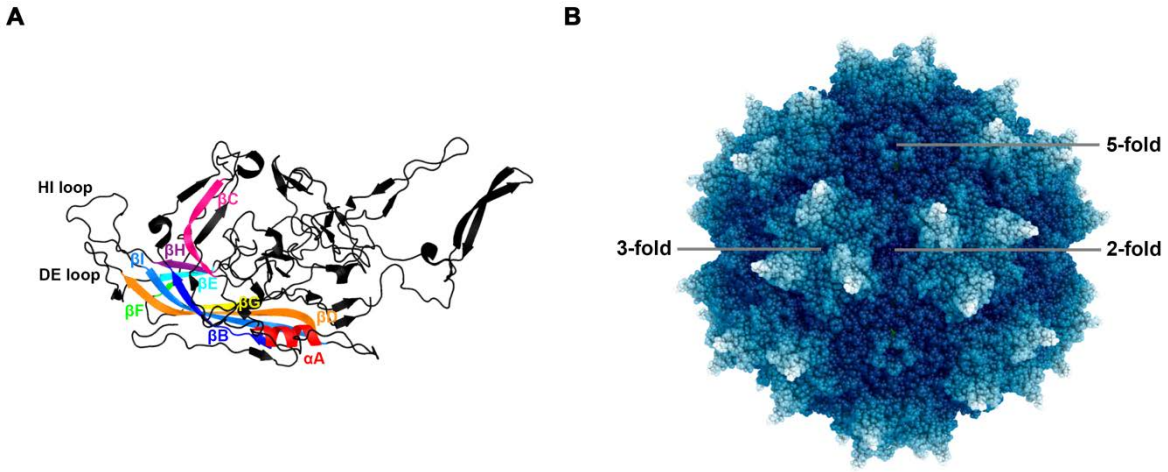

Figure 9: Capsid structure of adeno-associated virus. (A) Structure of the VP3 monomer of AAV2 as cartoon representation. The conserved αA helix (red), the β-barrel core motif (βB-βI, each strand in a different color according to (Govindasamy et al, 2006)), the DE and HI loops are indicated. (B) Sphere representation of the surface of the assembled AAV2 capsid radially colored (from capsid center to surface). The approximate two-, three- and five-fold symmetry axes are indicated. The structures (Protein Data Bank [PDB] ID 1LP3) (Xie et al, 2002) were modified using Pymol.

Assembly of the capsid proteins is structured by two-, three- and five-fold symmetry-related interactions (Figure 9B). The two-fold axis formed by two monomers is marked by a depression while characteristic spiky protrusions arise at the three-fold axis. The latter is described to be important for receptor binding and to contain prominent antigenic epitopes (Gurda et al, 2013; Wu et al, 2000; Opie et al, 2003). The DE loops of five assembled monomers form the central pore complex at the five-fold axis which is surrounded by a canyon region. These cylindrical channels link the outside of the virus with the interior of the capsid. Mutational analyses revealed that this region is important for genome packaging and serves as portal for the VP1 and VP2 N-termini externalization (Bleker et al, 2005; Bleker et

al, 2006). The N-termini harbor a conserved catalytic phospholipase A2 domain and three clusters of basic amino acids which seem to be necessary for endosomal escape, nuclear import and virus infectivity (Girod et al, 2002; Grieger et al, 2006; Kronenberg et al, 2005; Popa-Wagner et al, 2012).

To date, various AAV serotypes and variants have been isolated from humans and nonhuman primates but also horse, cow, chicken, snake and other tissues (Wu et al, 2006b; Asokan et al, 2012). The most prevalent and best characterized strain found in the human population is the AAV2 serotype. Many AAV gene therapy approaches are based on AAV2 vectors which are described to transduce muscle, liver, brain, retina and lungs (Daya & Berns, 2008). They bind to heparan sulfate proteoglycan (HSPG) as primary receptor but internalization is enhanced by interaction with various co-receptors such as fibroblast/hepatocyte growth factor receptor, laminin receptor and integrin αVβ5/α5β1 (Summerford & Samulski, 1998; Qing et al, 1999; Akache et al, 2006; Kashiwakura et al, 2005; Summerford et al, 1999; Asokan et al, 2006). Other serotypes exhibit differences in tissue tropism, transduction efficiencies and prevalence of preexisting humoral immunity which enabled the rapid transition to potential candidates as gene therapy vectors depending on the medical indication.

1.3.2 AAV vector engineering

For gene transfer applications, AAV vectors are generated by modifying the viral genome and producing recombinant, replication-deficient AAV vector particles employing double or triple transfection of HEK293 cells (Figure 10). The gene of interest replaces both, *rep* and *cap*, and is inserted between the viral ITRs which are the only *cis*-acting elements necessary for packaging into the AAV capsid. The *rep* and *cap* genes are provided in trans on a second plasmid along with the adenoviral helper genes required for replication. Alternatively, the adenoviral helper proteins E2A, E4 and VA RNA are provided by transfection of a third plasmid. The resulting AAV vectors can then be purified by CsCl or iodixanol density gradient centrifugation and/or chromatography-based methods (Burova & Ioffe, 2005).

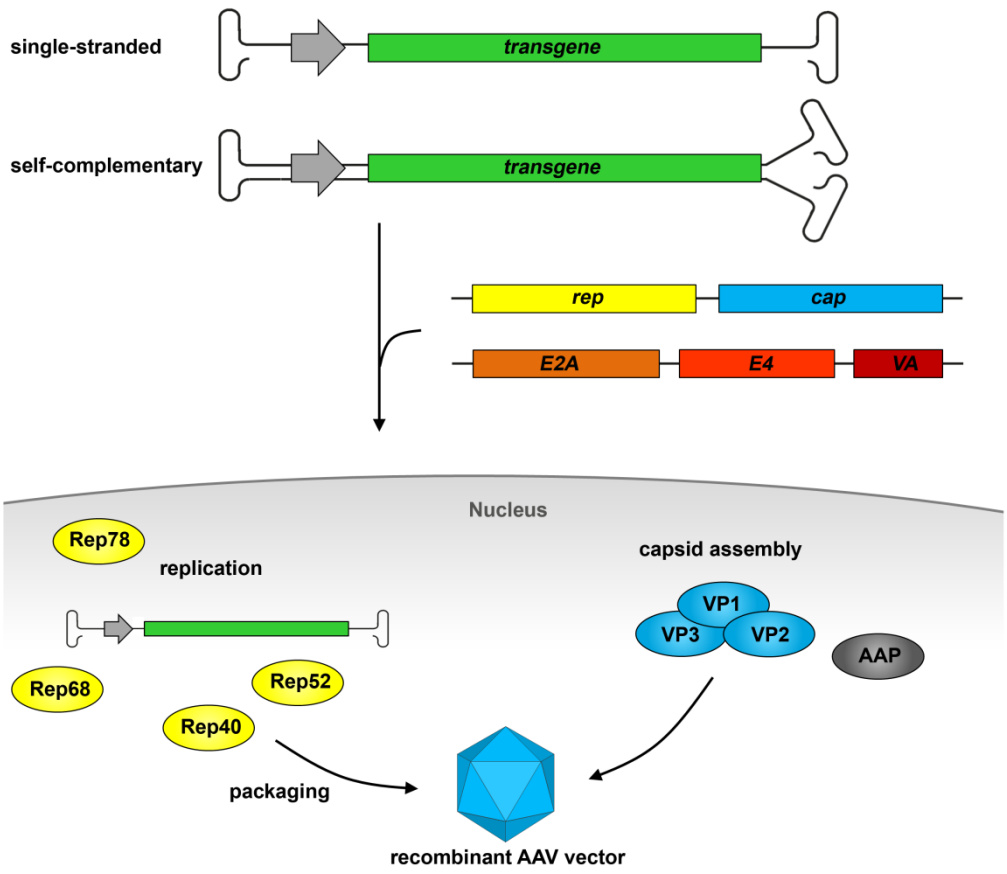

Figure 10: Generation of recombinant AAV vectors. To generate AAV vectors, a transgene of choice is inserted between the viral ITRs in the single-stranded or self-complementary conformation. The *rep*, *cap* and adenoviral helper genes *E2A*, *E4* and *VA* are provided in trans on separate plasmids. After triple transfection of HEK293 cells, the transfer vector is replicated and packaged into assembled capsids in the nucleus. Rep78, Rep68, Rep52 and Rep40 are non-structural proteins assisting replication and packaging. The capsid proteins VP1, VP2 and VP3 form the capsid with the help of the assembly-activating protein (AAP). Modified from (Kotterman & Schaffer, 2014).

Because recombinant AAV vectors do not encode Rep proteins and lack a *cis*-acting element called integration efficiency element (IEE), the transgene persists primarily episomally (Philpott et al, 2002). One of the rate-limiting steps of transduction, besides trafficking and capsid uncoating, is the second strand DNA synthesis prior to gene expression which depends on the host cell replication machinery (Ferrari et al, 1996; Fisher et al, 1996). The development of self-complementary AAV (scAAV) genomes bypasses this natural barrier, shortens the lag time before transgene expression and improves efficiency *in vitro* and *in vivo* (McCarty et al, 2001; Wang et al, 2003; McCarty et al, 2003). This genome organization takes advantage of the preference for the formation of self-complementary DNA which was increased by deleting the terminal resolution site sequence from one ITR and thus preventing the Rep proteins from nicking at this position. The resulting dimeric genome in the inverted repeat configuration contains two wildtype ITRs at both ends and one mutated ITR in the middle (Figure 10) (McCarty, 2008). As consequence, the maximal transgene capacity is

reduced. Nevertheless, a scAAV2 construct of 3,300 bp exceeded what was assumed originally for the maximal encapsidation of large genomes (Wu et al, 2007).

1.3.2.1 Receptor-targeted AAV vectors

The development of adeno-associated viral vectors targeting certain tissues or subtypes of cells has been driven by several different strategies. Among the most prominent ones is the so-called capsid shuffling followed by directed evolution. Here, capsid genes from different natural AAV isolates are fragmented, randomly reassembled for diversification and selected for desired properties (Kay, 2011). Another method relies on the use of chimeric capsids with inserted peptide sequences for retargeting (Choi et al, 2005). However, these methods are often labor-intensive and rarely result in vectors specific for only one cell type.

Recently, clear-cut receptor specificity of an AAV vector targeting Her2/neu has been achieved by rational design. Natural receptor binding of the AAV2 vector to HSPG was ablated by introduction of the two point mutations R585A and R588A in the capsid proteins (Kern et al, 2003; Opie et al, 2003; Boucas et al, 2009). Then, a DARPin specific for Her2/neu was fused to the N-terminus of the VP2 capsid protein conferring a redirected viral tropism (Münch et al, 2013). The specificity for tumor cells overexpressing the Her2/neu receptor was shown *in vitro* as well as *in vivo* and benefit of suicide gene transfer in a therapeutic xenograft setting was substantial. In order to prevent off-targeting *in vivo* which is caused by vector particles composed of only VP1 and VP3 and to enhance gene delivery efficiency, an additional purification step can be performed (Münch, 2013). Fusion of a His-tag at the N-terminus of the DARPin-VP2 protein allows immobilized metal ion affinity chromatography and increases targeting vector quality.

1.4 Objectives

This thesis describes two different projects using receptor-targeted viral vectors. The aim of the first project was a better understanding of the molecular events during MV cell entry and to challenge the hypothesis that MV receptor contact triggers the conformational changes required for cell entry. The second project aimed at developing and characterizing an AAV vector targeting the human epithelial cell adhesion molecule (EpCAM) which is overexpressed in most epithelial malignancies and circulating tumor cells.

To reach the first goal, lentiviral vectors pseudotyped with the measles virus glycoproteins could be used. In order to assess whether receptor attachment of H is required for fusion

triggering, a third protein mediating binding to the cellular receptor had to be incorporated into vector particles. Primary aim was to gain significance for results obtained previously (Rasbach, 2010) and to further analyze vector particles for protein composition, surface presentation of envelope proteins and titers as well as cell entry characteristics. Several different targeting ligands should be assessed for their potential as attachment domains. Additionally, gene transfer efficiency of this new vector type should be evaluated *in vitro* and *in vivo* in a xenograft tumor model.

For the generation of human EpCAM-specific AAV vectors, a recently established targeting system using high affinity binders should be employed (Münch et al, 2013). Therefore, highly specific DARPins had to be fused to the N-terminus of the VP2 protein for incorporation into the viral capsid. Generated vector particles had to be analyzed for their morphology, protein content, surface exposure of the DARPin, genomic titers and packaging efficiency. Furthermore, targeting specificity should be confirmed on different receptor-positive and receptor-negative cell lines as well as on primary cells and in a transgenic mouse model. Purity and efficiency of the vector particles should be further improved using affinity-chromatography. Ultimately, the potential of EpCAM-AAV to detect and modify rare tumor cells in blood samples should be assessed.

2 Material and Methods

2.1 Material

2.1.1 Equipment

Name	Model	Manufacturer
Bacteria incubator shaker	Innova™ 4200	New Brunswick Scientific
Cell incubator	BBD6220	Heraeus, Thermo Scientific
Cell sorter	MoFlo	Beckman Coulter
Centrifuge	Multifuge X3, Multifuge 3	Heraeus, Thermo Scientific
Chemiluminescence detection	Fusion FX7	Vilber Lourmat
Electron microscope	EM 109	Zeiss
Flowcytometer	MACSQuant Analyzer	Miltenyi Biotec
Flowcytometer	LSRII	Becton Dickinson
Fluorescence microscope	Axiovert 200	Zeiss
Gel documentation station	Gel Imager	Intas
Gel electrophoresis system	n/a	Bio-Rad
HPLC system	Smartline	Knauer
In vivo imaging system	IVIS Spectrum	PerkinElmer
Laminar Flow Cabinet Class II	SterilGARD® III	The Baker Company
Laser scanning microscope	LSM 510	Zeiss
Light microscope	Axiovert 25	Zeiss
LightCycler	LightCycler®	Roche
Micropipettes	Research plus®	Eppendorf
Microplate reader	THERMOmax	Molecular Devices
Multichannel pipettes	Finnpipette F2	Thermo Scientific
Pipetboy	Accu-jet®	Brand
Spectrophotometer	NanoDrop 2000c	Thermo Scientific
Table-top processor	Curix 60™	Agfa
Thermo cycler	PTC 200	MJ Research
Ultracentrifuge	Optima™ L-70k	Beckman Coulter

2.1.2 Kits

Name	Supplier
GeneJET Plasmid Miniprep Kit	Thermo Scientific
EndoFree® Plasmid Maxi Kit	QIAGEN
JETStar NoEndo Jetfilter Giga Kit	Genomed
GeneJET Gel Extraction Kit	Thermo Scientific
Rapid DNA Ligation Kit	Fermentas
DNeasy® Blood & Tissue Kit	QIAGEN
FastStart DNA Master^{PLUS} SYBR Green I	Roche
RETROtek HIV-1 p24 Antigen ELISA	ZeptoMetrix

2.1.3 Enzymes

Name	Supplier
Restriction endonucleases	New England Biolabs
Trypsin 2.5% (Melnick)	Paul-Ehrlich-Institut
Phusion Hot Start II High Fidelity DNA Polymerase	Thermo Scientific
DreamTaq DNA Polymerase	Thermo Scientific
Benzonase® Nuclease	Sigma-Aldrich

2.1.4 Antibiotics

Name	Supplier
Penicillin/Streptomycin	Paul-Ehrlich-Institut
Geniticin	Gibco
Puromycin	Sigma-Aldrich

2.1.5 Buffers and chemicals

Name	Composition/Supplier
AAV lysis buffer	50 mM Tris-HCl, 150 mM NaCl in PBS
D-Luciferin	Perkin Elmer
DNA loading buffer 6x	Thermo Scientific

Name	Composition/Supplier
ECL Plus Western Blotting detection reagent	Amersham
ELISA blocking buffer	PBS, 0.05% Tween-20, 3% BSA, 5% sucrose
ELISA washing buffer	PBS, 0.05% Tween-20
FACS washing buffer	2% FCS in PBS
FACS fix	1% formaldehyde in PBS
FACS sorting buffer	10 mM HEPES, 2% FCS, 0.5 mM EDTA in PBS
Freezing medium	90% FCS, 10% DMSO
Histopaque®-1077	Sigma-Aldrich
IMAC binding buffer	20 mM imidazole, 20 mM sodium phosphate, 0.5 M NaCl
IMAC elution buffer	300 mM imidazole, 20 mM sodium phosphate, 0.5 M NaCl
OptiPrep™	Sigma-Aldrich
PBS	Lonza
PBS M/K	2.5 mM KCl, 1 mM MgCl2 in PBS
PEI	18 mM polyethylenimine in H2O
S.O.C medium	Sigma-Aldrich
SDS running buffer	25 mM Tris, 192 mM Glycine, 1% SDS
TAE	40 mM Tris, 20 mM Acetic acid, 1 mM EDTA
TBS-T	10 mM Tris pH 8.0, 150 mM NaCl, 0.1% Tween-20
TMB liquid substrate	Sigma-Aldrich
TNE	25 mM Tris pH 7.4, 150 mM NaCl, 5 mM EDTA
Transfer buffer	48 mM Tris, 39 mM Glycine, 20% Methanol
Triton X-100	Sigma-Aldrich
Trypsin solution	PBS, 2 mM EDTA, 0.25% Trypsin-Melnick
Tween-20	Sigma-Aldrich

2.1.6 Antibodies

Name	Application	Dilution	Supplier
α-MV F, rabbit serum (F431)	WB	1:4,000	R. Cattaneo
α-MV H, rabbit serum (H606)	WB	1:1,000	R. Cattaneo
α-HIV-1 p24, mouse	WB	1:1,000	Gentaur

Name	Application	Dilution	Supplier
α-HA tag, mouse (12CA5)	WB	1:1,000	Roche
α-AAV VP1/VP2/VP3, mouse (B1)	WB	1:20	Progen
α-rabbit-HRP, goat	WB	1:2,000	DAKO
α-mouse-HRP, rabbit	WB	1:2,000	DAKO
α-AAV intact particle, mouse (A20)	ELISA	1:4	Progen
α-myc tag, mouse	ELISA	1:1,000	Abcam
α-mouse-biotin, donkey	ELISA	1:25,000	Jackson ImmunoResearch
Streptavidin-HRP	ELISA	1:500	Jackson ImmunoResearch
α-HA tag, mouse (16B12)	IF, EM	1:800	Covance
α-mouse-10 nm gold, goat	EM	1:50	British BioCell
α-MV F, mouse (Y503)	FC, IF	1:250	R. Cattaneo
α-MV H, mouse (K83)	FC, IF	1:10-20	J. Schneider-Schaulies
α-mouse IgG2a AlexaFluor546, goat	IF	1:250	Invitrogen
α-mouse IgG1 AlexaFluor633, goat	IF	1:250	Invitrogen
α-mouse-PE, goat	FC	1:20	Sigma-Aldrich
α-MV H, mouse (L77)	NA, FC	variable	J. Schneider-Schaulies
α-MV H, mouse (Nc32)	NA, FC	variable	J. Schneider-Schaulies
α-MV H, mouse (K71)	NA, FC	variable	J. Schneider-Schaulies
α-MV H, mouse (K29)	NA, FC	variable	J. Schneider-Schaulies
α-Her2/neu-PE, mouse	FC	1:20	BD Pharmingen
α-EpCAM-PE, mouse	FC	1:20	Miltenyi Biotec
α-HA tag-PE	FC	1:20	Miltenyi Biotec
FcR blocking reagent, human	FC	1:10	Miltenyi Biotec

WB: western blot, ELISA: enzyme-linked immunosorbent assay, IF: immunofluorescence, EM: immunoelectron microscopy, FC: flow cytometry, NA: neutralization assay

2.1.7 Oligonucleotides

Oligonucleotides were synthesized by Eurofins MWG Operon or Sigma-Aldrich.

Name	Sequence (5’ – 3’)
GFP-for	GCTACCCCGACCACATGAAG
GFP-rev	GTCCATGCCGAGAGTGATCC

luc-for	TTCGGCTGGCAGAAGCTATG
luc-rev	GCTCGCGCTCGTTGTAGATG
DARPin-for	GGAAGGACCGGTATGGACCTGGGTAAGAAACTG
$DARPin_{corr}$-rev	GTCCGAGCACTTGTACAGATTAAGCTTCGCCGCTTT
His-for	GGAAGGACCGGTATGCATCACCATCACCATCACATCGAGGG AAGGGACCTGGGTAAGAAACTGCTG
Myc-for	GGAAGGACCGGTATGGAACAAAAACTTATTTCTGAAGAAGA TCTGATCGAGGGAAGGGACCTGGGTAAGAAACTGCTG
EpCAM-for	TTAATAGGCGCGCCAGTCCTCCGACAGACTGAGTCGCCCGGG GGGGATCCACCGGTCGCCACCATGGCGCCCCCGCAGGTCCTCG
EpCAM-rev	GATGCACCGACTGACTAGTTAGTTATGCATTGAGTTCCCTATGC
oIMR8744	CAAATGTTGCTTGTCTGGTG
oIMR8745	GTCAGTCGAGTGCACAGTTT
oIMR8558	TCAGATAAAGGAGATGGGTGAGA
oIMR8559	GGCAGCTTTCAATCACAAATCAG

2.1.8 Plasmids

Name	**Description**	**Source**
pCMVΔR8.91	HIV-1 packaging plasmid	U. Blömer (Zufferey et al, 1998)
pSEW	HIV-1 transfer vector encoding GFP under control of the SFFV promoter	M. Grez (Demaison et al, 2002)
pS-luc2-W	HIV-1 transfer vector encoding luciferase under control of the SFFV promoter	(Abel et al, 2013)
pS-EGFP-I-puro-W	Bicistronic HIV-1 transfer vector encoding GFP and puromycin	Irene C. Schneider
pS-hEpCAM-I-puro-W	Bicistronic HIV-1 transfer vector encoding human EpCAM and puromycin	This thesis
pCMV6-AC-EpCAMcDNA	Human full-length TruClone™ with human EpCAM cDNA	Origene
pMD2.G	Encodes the VSV glycoprotein	D. Trono

pCG-FΔ30	Encodes MV F with a truncated cytoplasmic tail of 30 aa under control of the CMV promoter	(Funke et al, 2008)
pCG-HΔ18	Encodes MV H with a truncated cytoplasmic tail of 18 aa under control of the CMV promoter	(Funke et al, 2008)
pCG-H_{mut}Δ18	Encodes MV H with a truncated cytoplasmic tail of 18 aa and the four point mutations Y481A, R533A, S548L, F549S under control of the CM promoter	(Funke et al, 2008)
pCG-H^{*}_{mut}Δ18	Encodes MV H with a truncated cytoplasmic tail of 18 aa and the five point mutations F111N, Y481A, R533A, S548L, F549S under control of the CM promoter	(Rasbach et al, 2013)
pCG-H_{mut}Δ18-DARPin-9.29	Encodes MV H_{mut}18 fused to the Her2/neu-specific DARPin 9.29	(Münch et al, 2011)
pCR2.1-Helical Linker	Contains the sequence for the helical linker HL7 flanked by *NotI* and *SalI* restriction sites	Eurofins MWG Operon
pDisplay-$D^{9.29}$	Encodes the Her2/neu-specific DARPin 9.29 fused to the PDGFR TMD under control of the CMV promoter	(Rasbach et al, 2013)
pDisplay-D^{G3}	Encodes the Her2/neu-specific DARPin G3 fused to the PDGFR TMD under control of the CMV promoter	(Rasbach et al, 2013)
pDisplay-$D^{9.26}$	Encodes the Her2/neu-specific DARPin 9.26 fused to the PDGFR TMD under control of the CMV promoter	This thesis
pDisplay-$D^{9.16}$	Encodes the Her2/neu-specific DARPin 9.16 fused to the PDGFR TMD under control of the CMV promoter	This thesis
pDisplay-$D^{9.01}$	Encodes the Her2/neu-specific DARPin 9.01 fused to the PDGFR TMD under control of the CMV promoter	This thesis

pDisplay-D^{H14R}	Encodes the Her2/neu-specific DARPin H14R fused to the PDGFR TMD under control of the CMV promoter	This thesis
pDisplay-HL7-$D^{9.29}$	Encodes the Her2/neu-specific DARPin 9.29 fused to a helical linker and the PDGFR TMD under control of the CMV promoter	This thesis
pDisplay-HL7-D^{G3}	Encodes the Her2/neu-specific DARPin G3 fused to a helical linker and the PDGFR TMD under control of the CMV promoter	This thesis
pDisplay-HL7-$D^{9.26}$	Encodes the Her2/neu-specific DARPin 9.26 fused to a helical linker and the PDGFR TMD under control of the CMV promoter	This thesis
pDisplay-HL7-$D^{9.16}$	Encodes the Her2/neu-specific DARPin 9.16 fused to a helical linker and the PDGFR TMD under control of the CMV promoter	This thesis
pDisplay-HL7-$D^{9.01}$	Encodes the Her2/neu-specific DARPin 9.01 fused to a helical linker and the PDGFR TMD under control of the CMV promoter	This thesis
pDisplay-HL7-D^{H14R}	Encodes the Her2/neu-specific DARPin H14R fused to a helical linker and the PDGFR TMD under control of the CMV promoter	This thesis
pDisplay-$D^{57.2}$	Encodes the CD4-specific DARPin 57.2 fused to the PDGFR TMD under control of the CMV promoter	This thesis
pDisplay-$D^{29.2}$	Encodes the CD4-specific DARPin 29.2 fused to the PDGFR TMD under control of the CMV promoter	This thesis

pDisplay-$D^{27.2}$	Encodes the CD4-specific DARPin 27.2 fused to the PDGFR TMD under control of the CMV promoter	This thesis
pDisplay-$D^{55.2}$	Encodes the CD4-specific DARPin 55.2 fused to the PDGFR TMD under control of the CMV promoter	This thesis
pDisplay-HL7-$D^{57.2}$	Encodes the CD4-specific DARPin 57.2 fused to a helical linker and the PDGFR TMD under control of the CMV promoter	This thesis
pDisplay-HL7-$D^{29.2}$	Encodes the CD4-specific DARPin 29.2 fused to a helical linker and the PDGFR TMD under control of the CMV promoter	This thesis
pDisplay-HL7-$D^{27.2}$	Encodes the CD4-specific DARPin 27.2 fused to a helical linker and the PDGFR TMD under control of the CMV promoter	This thesis
pDisplay-HL7-$D^{55.2}$	Encodes the CD4-specific DARPin 55.2 fused to a helical linker and the PDGFR TMD under control of the CMV promoter	This thesis
pDisplay-D^{Ac1}	Encodes the EpCAM-specific DARPin Ac1 fused to the PDGFR TMD under control of the CMV promoter	This thesis
pDisplay-D^{Ec1}	Encodes the EpCAM-specific DARPin Ec1 fused to the PDGFR TMD under control of the CMV promoter	This thesis
pDisplay-HL7-D^{Ac1}	Encodes the EpCAM-specific DARPin Ac1 fused to a helical linker and the PDGFR TMD under control of the CMV promoter	This thesis
pDisplay-HL7-D^{Ec1}	Encodes the EpCAM-specific DARPin Ec1 fused to a helical linker and the PDGFR TMD under control of the CMV promoter	This thesis
pDisplay-$scFv^{A5}$	Encodes the CD105-specific scFv A5 fused to the PDGFR TMD under control of the CMV promoter	(Rasbach, 2010)

pDisplay-HL7-scFv^{A5}	Encodes the CD105-specific scFv A5 fused to a helical linker and the PDGFR TMD under control of the CMV promoter	This thesis
pDisplay-scFv^{CD20}	Encodes the CD20-specific scFv fused to the PDGFR TMD under control of the CMV promoter	(Rasbach, 2010)
pDisplay-HL7-scFv^{CD20}	Encodes the CD20-specific scFv fused to a helical linker and the PDGFR TMD under control of the CMV promoter	This thesis
pDisplay-scFv$^{141.7}$	Encodes the CD133-specific scFv 141.7 fused to the PDGFR TMD under control of the CMV promoter	This thesis
pDisplay-scFv^{AC133}	Encodes the CD133-specific scFv AC133 fused to the PDGFR TMD under control of the CMV promoter	This thesis
pDisplay-HL7-scFv$^{141.7}$	Encodes the CD133-specific scFv 141.7 fused to a helical linker and the PDGFR TMD under control of the CMV promoter	This thesis
pDisplay-HL7-scFv^{AC133}	Encodes the CD133-specific scFv AC133 fused to a helical linker and the PDGFR TMD under control of the CMV promoter	This thesis
pDisplay-scFv^{CD30}	Encodes the CD30-specific scFv fused to the PDGFR TMD under control of the CMV promoter	This thesis
pDisplay-HL7-scFv^{CD30}	Encodes the CD30-specific scFv fused to a helical linker and the PDGFR TMD under control of the CMV promoter	This thesis
pDisplay-scFv^{CD8}	Encodes the CD8-specific scFv fused to the PDGFR TMD under control of the CMV promoter	This thesis
pDisplay-HL7-scFv^{CD8}	Encodes the CD8-specific scFv fused to a helical linker and the PDGFR TMD under control of the CMV promoter	This thesis

pDisplay-nb^{s-14}	Encodes the Art2.2-specific nanobody s-14 fused to the PDGFR TMD under control of the CMV promoter	This thesis
pDisplay-nb^{l-17}	Encodes the Art2.2-specific nanobody l-17 fused to the PDGFR TMD under control of the CMV promoter	This thesis
pDisplay-HL7-nb^{s-14}	Encodes the Art2.2-specific nanobody s-14 fused to a helical linker and the PDGFR TMD under control of the CMV promoter	This thesis
pDisplay-HL7-nb^{l-17}	Encodes the Art2.2-specific nanobody l-17 fused to a helical linker and the PDGFR TMD under control of the CMV promoter	This thesis
pXX6-80	Adenoviral helper plasmid encoding E2A, E4 and VA	H. Büning
pscGFP-SFFV	Self-complementary AAV transfer vector encoding GFP under control of the SFFV promoter	(Münch et al, 2013)
pscluc2-SFFV	Self-complementary AAV transfer vector encoding luciferase under control of the SFFV promoter	(Münch et al, 2013)
pRC	Encodes the AAV2 rep and cap proteins	H. Büning
pRC-VP2$_{KO}$-HSGP$_{mut}$	Encodes the AAV2 rep and cap proteins with mutated VP2 start codon and the point mutations R585A and R588A	H. Büning
pDARPin-9.29-VP2	Encodes the Her2/neu-specific DARPin 9.29 fused to the N-terminus of the AAV2 VP2 protein containing the point mutations R585A and R588A	(Münch et al, 2013)
pDARPin-9.29^{Myc}-VP2	Encodes the Myc-tagged Her2/neu-specific DARPin 9.29 fused to the N-terminus of the AAV2 VP2 protein containing the point mutations R585A and R588A	(Münch et al, 2013)

pDARPin-Ec1-VP2	Encodes the EpCAM-specific DARPin Ec1 fused to the N-terminus of the AAV2 VP2 protein containing the point mutations R585A and R588A	This thesis
pDARPin-Ec1^{Myc}-VP2	Encodes the Myc-tagged EpCAM-specific DARPin Ec1 fused to the N-terminus of the AAV2 VP2 protein containing the point mutations R585A and R588A	This thesis
pDARPin-Ec1^{His}-VP2	Encodes the His-tagged EpCAM-specific DARPin Ec1 fused to the N-terminus of the AAV2 VP2 protein containing the point mutations R585A and R588A	This thesis
pDARPin-Ac1-VP2	Encodes the EpCAM-specific DARPin Ac1 fused to the N-terminus of the AAV2 VP2 protein containing the point mutations R585A and R588A	This thesis

2.1.9 Bacterial strains and mammalian cells

Name	**Description**	**Source**
E. coli Top10	Chemically competent bacterial strain	Life Technologies
E. coli SURE	Chemically competent bacterial strain (Stop Unwanted Rearrangement Events)	Stratagene
HEK-293T	Human embryonic kidney cell line, genetically engineered to express the SV40 T antigen	ATCC CRL-11268
SK-OV-3	Human ovarian carcinoma cell line	ATCC HTB-77
CHO-K1	Chinese hamster ovary cell line	ATCC CCL-61
CHO-Her2	Chinese hamster ovary cell line genetically engineered to express Her2/neu	(Münch et al, 2011)
MDA-MB-453	Human breast cancer cell line	ATCC HTB-131

Name	Description	Source
MCF-7	Human breast cancer cell line	ATCC HTB-22
LNT-229	Human glioblastoma cell line	ATCC CRL-2611
CHO-EpCAM	Chinese hamster ovary cell line genetically engineered to express EpCAM	This thesis
CHO-EpCAM L1	Chinese hamster ovary cell line genetically engineered to express EpCAM	This thesis
CHO-EpCAM M6	Chinese hamster ovary cell line genetically engineered to express EpCAM	This thesis
CHO-EpCAM H1	Chinese hamster ovary cell line genetically engineered to express EpCAM	This thesis
HMECs	Human mammary epithelial cells	Lonza

2.1.10 Culture media

Name	Description	Source
Luria-Bertani (LB) broth	1% tryptone, 0.5% yeast extract, 1% NaCl in H_2O pH 7.2	Paul-Ehrlich-Institut
S.O.C. medium	2% Tryptone, 0.5% yeast extract, 10 mM NaCl, 2.5 mM KCl, 10 mM $MgCl_2$, 10 mM $MgSO_4$, 20 mM glucose in H_2O	Invitrogen
Dulbecco's modified Eagle medium (DMEM)	Supplemented with 10% FCS and 2 mM L-glutamine as culture medium for HEK-293T, CHO-K1, MDA-MB-453, MCF-7, LNT-229 and all CHO-EpCAM cells	Lonza
McCoy's medium	Supplemented with 10% FCS and 2 mM L-glutamine as culture medium for SK-OV-3 cells	Sigma-Aldrich
Mammary Epithelial Cell Growth Medium BulletKit™	Culture medium for HMECs	Lonza

2.2 Methods of molecular biology

2.2.1 Transformation of chemically competent bacteria

For transformation, chemically competent *E. coli* Top10 or SURE bacteria were thawed on ice and 50 ng DNA or 5 µl ligation reaction mix were added. After 30 min incubation, bacteria were heat-shocked at 42°C for 45 seconds in a thermomixer and immediately cooled on ice. For initial recovery, cells were diluted with 500 µl S.O.C. medium and incubated for 30 min at 37°C and 600 rpm. Transformed bacteria were then plated on LB agar plates containing the corresponding antibiotics and incubated over night at 37°C or for 3 days at 25°C.

2.2.2 Plasmid preparation

Plasmid DNA from transformed bacteria was purified using the GeneJET Plasmid Miniprep Kit, EndoFree® Plasmid Maxi Kit or JETStar NoEndo Jetfilter Giga Kit according to the manufacturer's instructions. These kits are based on the use of silica membranes binding DNA in the presence of high concentrations of chaotropic salts or anion-exchange columns. Thus, cellular components can be washed away prior to DNA elution with low-salt buffers. For purification of low, medium and high amounts of DNA, 5 ml, 200 ml or 2400 ml LB medium supplemented with the corresponding antibiotic were inoculated with a single bacteria clone and cultivated overnight at 37°C. The grown bacteria were pelleted by centrifugation at 2,000 × g (low amounts, Multifuge 3) or 6,000 rpm (medium and high amounts, Sorvall Rc26 plus) for 15 min at 4°C. The concentration of purified DNA was determined photometrically (NanoDrop 2000c).

2.2.3 Restriction of DNA

Analytical or preparative restrictions of DNA were performed using restriction endonucleases from New England Biolabs according to the manufacturer's instructions. Standard restriction reaction mix was prepared as follows:

	Analytical	Preparative
DNA	1 µg	5 µg
10x restriction buffer	3 µl	5 µl
Enzyme(s)	5 U	20 U
H_2O	ad 30 µl	ad 500 µl
Incubation time	1-2 hours	5-16 hours

For digestions with two or more enzymes the optimal buffer conditions for all endonucleases were chosen. If different incubation temperatures were required, digestions were performed sequentially.

2.2.4 DNA Ligation

Ligation of double-stranded DNA fragments with either cohesive or blunt termini was carried out using the Rapid Ligation Kit (Fermentas) according to the manufacturer's instructions. In total 50 ng – 200 ng DNA was used for each reaction in a molar ratio of 3:1 for insert/linearized vector DNA. The ligation mix, which contained Rapid Ligation buffer and the T4-DNA ligase to catalyze the formation of phosphodiester bonds, was incubated for 5-15 min at room temperature. The ligated DNA was directly used for transformation of chemically competent bacteria or frozen at -20°C.

2.2.5 Agarose gel electrophoresis

Agarose gel electrophoresis was used to analyze and separate DNA fragments of different sizes. This technique is based on the molecular sieve properties of polymerized agarose gels and the distinct migration behavior of negatively-charged DNA according to its size in the electrical field. Agarose gels with different concentrations were produced by adding the corresponding amount of agarose to 100 ml TAE buffer and heating until the agarose powder dissolved. After addition of 50 µg/ml ethidium bromide which intercalates into DNA strands and can be visualized under UV light, the solution was casted into a tray to allow polymerization. For separation of fragments > 1 kb, 0.7-1% agarose gels were prepared, whereas 1.5-2% agarose gels were used for smaller fragments.

DNA samples were supplemented with 5x loading buffer and loaded into the gel pockets in a Bio-Rad WIDE MINI-SUB chamber. Electrophoresis was performed at 100-120 V until

fragments were sufficiently separated. Results were analyzed under UV light and compared to a 2-Log DNA ladder (New England Biolabs).

2.2.6 Isolation of DNA from agarose gels

DNA fragments of interest were cut out of the agarose gel and transferred into an Eppendorf tube. Purification of DNA was performed using the GeneJET Gel Extraction Kit according to the manufacturer's instructions.

2.2.7 Isolation of DNA from tissue and vector particles

For the purification of total DNA from tissues or vector particles, the DNeasy Blood & Tissue Kit was used according to the manufacturer's instructions. Subsequently, DNA obtained from 0.5 cm mouse tail was used for genotyping transgenic mice by polymerase chain reaction. Genomic DNA obtained from 10 µl AAV preparations was used for determination of genomic titers by quantitative polymerase chain reaction.

2.2.8 Polymerase chain reaction

Polymerase chain reaction (PCR) allows amplification of specific DNA sequences using two or more primers. Additionally, primer-dependent extensions and mutations can be introduced into the amplified DNA sequences, emphasizing the importance of this powerful technique in molecular biology. A typical PCR reaction consists of several thermal cycles with multiple steps: (i) initial denaturation, (ii) annealing of the primers to the complementary DNA sequence and (iii) elongation of DNA by a DNA polymerase. The annealing and elongation temperatures have to be adjusted according to the primers, the amplicon length and the applied polymerase.

For cloning purposes, the Phusion Hot Start II High Fidelity DNA polymerase was used, offering high proofreading capacity and fast elongation rates. Due to a reversible bound affibody inhibiting the DNA polymerase activity at room temperature, amplification of nonspecific products is prevented. The reaction mix was prepared as follows:

Component	
Template DNA	5-50 ng
5x Phusion HF buffer	10 µl
10 mM dNTPs	1 µl
Primer for	0.5 µM
Primer rev	0.5 µM
Phusion Hot Start II HF DNA Polymerase (2 U/µl)	0.5 µl
H_2O	ad 50 µl

The PCR was performed using the manufacturer's cycling instructions, repeating steps 2-4 25-times:

1.	Initial denaturation	98°C	30 s
2.	Denaturation	98°C	5-10 s
3.	Annealing	52-72°C*	10-30 s
4.	Extension	72°C	15-30 s/kb
5.	Final Extension	72°C	5 min

*depending on the primers

For genotyping of human EpCAM transgenic mice, a *Taq* DNA polymerase PCR protocol was used:

Component	
Template DNA (isolated from mouse tail)	7.5 µl
10x DreamTaq Buffer	3 µl
10 mM dNTPs	0.67 µl
Primer oIMR8744 (100 µM)	0.75 µl
Primer oIMR8745 (100 µM)	0.75 µl
Primer oIMR8558 (100 µM)	1.5 µl
Primer oIMR8559 (100 µM)	1.5 µl
DreamTaq (5 U/µl)	0.25 µl
H_2O	ad 30 µl

The PCR was performed using the manufacturer's cycling instructions, repeating steps 2-4 34-times:

1.	Initial Denaturation	95°C	3 min
2.	Denaturation	95°C	30 s
3.	Annealing	55°C	60 s
4.	Extension	72°C	60 s
5.	Final Extension	72°C	2 min

Using two different primer pairs, a transgene-specific sequence of 383 bp and an internal positive control sequence of 200 bp can be amplified and detected simultaneously.

2.2.9 Quantitative polymerase chain reaction

Quantitative PCR (qPCR) was performed to determine the genomic titer of AAV vectors. Key feature of this method is a dye e.g. SYBR Green I which intercalates specifically into the double strand of the amplified PCR product. By measuring the increase of fluorescence after each cycle monitoring of the amplification is enabled. For the determination of genomic titers, the FastStart DNA Master^{PLUS} SYBR Green I kit was used according to the manufacturer's instructions. DNA isolated from AAV vectors (2.2.7) served as template. Plasmid DNA containing the respective sequence was used as standard.

Component	
H_2O	14 µl
Primer for (20 pmol/µl)	0.5 µl
Primer rev (20 pmol/µl)	0.5 µl
FastStart DNA Master^{PLUS} SYBR Green I (1a+1b)	4 µl
Template DNA (isolated from AAV vectors)	1 µl

Depending on the packaged transgene, the primer pairs GFP-for/GFP-rev or luc-for/luc-rev were used and the qPCR program was adapted accordingly:

1.	Initial denaturation	95°C	10 min	slope: 20°C/s
2.	Quantification (40 cycles)			
	a.	95°C	10 s	slope: 20°C/s
	b.	64°C	4 s*, 5 s#	slope: 20°C/s
	c.	72°C	7 s*, 10 s#	slope: 20°C/s
3.	Melting curve			
	a.	95°C	0 s	slope: 20°C/s
	b.	67°C	10 s	slope: 20°C/s
	c.	95°C	0 s	slope: 0.1°C/s

*for GFP transferring AAV vectors, #for luciferase transferring AAV vectors

2.3 Protein biochemical methods

2.3.1 SDS-polyacrylamide gel electrophoresis

Sodium dodecyl sulfate polyacrylamide gel electrophoresis (SDS-PAGE) is a commonly used technique for separating proteins based on their molecular mass. The anionic detergent SDS denatures proteins thus removing secondary and tertiary protein structures. Additionally, SDS coats the proteins mostly proportional to their molecular weight conferring a negative charge to the linearized protein. When applied to an electrical field, the negatively charged proteins migrate to the anode and can be separated by the gel matrix of a polyacrylamide gel according to their molecular mass, analogous to agarose gel electrophoresis.

Vector particles or flotation assay fractions were mixed with 2x urea sample buffer and incubated at 95°C for 10 min. Then, samples were loaded to 10% SDS polyacrylamide gels and separated using the Bio-Rad Mini Protein II chamber system. The Precision Plus Protein™ Standard Kaleidoscope™ marker, commercially available from Bio-Rad, was used as protein standard. SDS-PAGE was performed at 70 V until samples entered the resolving gel and then at 120 V until the desired marker protein reached the end of the gel.

	Resolving gel (10%)	Stacking gel (5%)
30% acrylamide	3.33 ml	0.83 ml
1 M Tris, pH 8.8	3.9 ml	-
1 M Tris, pH 6.8	-	0.63 ml
50% glycerine	0.82 ml	-
10% SDS	55 µl	25 µl
Aqua bidest	1.9 ml	3.5 ml
TEMED	13 µl	10 µl
20% APS	26 µl	20 µl
Food coloring	-	20 µl

2.3.2 Western blot analysis

Following SDS-PAGE (2.3.1), the separated proteins can be transferred onto a protein-binding surface e.g. a nitrocellulose membrane for subsequent visualization by immunostaining. This so-called western blot analysis was performed using the Bio-Rad Trans-Blot SD Semi-Dry transfer cell. Whatman filter papers, nitrocellulose membrane and the SDS polyacrylamide gel were shortly incubated in transfer buffer before they were carefully layered into the transfer cell. After blotting at 180 mA for 90 min, unspecific membrane binding sites were blocked with blocking buffer (TBS-T with 5% horse serum or 5% milk powder) for one hour at room temperature. For specific detection of proteins, membranes were incubated with primary antibody diluted in blocking buffer over night at 4°C. The next day, membranes were washed five times with TBS-T and then incubated with the respective secondary antibody conjugated to horseradish peroxidase (HRP). After a second washing step, detection was performed using the ECL Plus Western Blotting detection reagent. The reagent contains luminol which can be oxidized, a process catalyzed by HRP, resulting in an excited product emitting light with a wavelength of 425 nm. Signals were visualized using chemiluminescence films or the Fusion FX7 imager.

2.3.3 Dot blot analysis

Fractions collected during affinity chromatography of AAV vectors were analyzed by dot blot. This method is a simple way to detect the presence or absence of a protein in a sample without electrophoretic protein separation prior to analysis. For the detection of AAV2 capsid proteins, 25 µl of collected fractions were mixed with 1% SDS and incubated for 10 min at

95°C. Whatman filter papers and nitrocellulose membrane pre-incubated first in water and then PBS were layered into the dot blot apparatus and samples were transferred onto the membrane according to the manufacturer's instructions. Subsequent, immunostaining and detection of chemiluminescence was performed as described for western blot analysis (2.3.2).

2.3.4 Flotation assay

Detergent-resistant membranes (DRMs) were isolated by flotation assay. This method is based on the specific properties of the sphingolipid- and cholesterol-rich detergent-resistant membranes. They are not solubilized by detergents under certain conditions and can therefore be separated from the rest of the cellular material using density centrifugation. For DRM isolation, vector particle-producing cells were scraped and lysed in ice-cold TNE buffer containing 0.5% Triton X-100. Lysates were homogenized through a 23-gauge needle and incubated with constant agitation for 30 min at 4°C. Then, they were mixed with 1 ml OptiPrep™, transferred to ultracentrifuge tubes and overlaid with an OptiPrep™ gradient (2 ml of 30% followed by 1 ml of 25, 20, 17.5, 15, 12.5 and 5% OptiPrep™ in TNE buffer). Centrifugation was performed for 16 h at 39,000 rpm and 4°C in a Beckman SW41 rotor. Gradient fractions were analyzed by SDS-PAGE and western blotting.

2.3.5 Enzyme-linked immunosorbent assay

The enzyme-linked immunosorbent assay (ELISA) is used to detect and quantify a substance in solution. Antigens or antibodies are adsorbed to a well-plate followed by blocking, washing and detection using enzyme-conjugated antibodies.

Quantification of p24 gag in lentiviral vector particle preparations was performed using the RETROtek HIV p24 antigen ELISA kit according to the manufacturer's instructions.

For capsid titer determination, immunoplates (Nunc) were coated with serial dilutions of vector particles over night at 4°C. The next day, plates were washed three times with ELISA washing buffer and blocked with ELISA blocking buffer for 2 hours at room temperature. Primary antibody incubation with the α-AAV2 intact capsid antibody diluted in ELISA blocking buffer was performed for one hour at room temperature, followed by another washing step and incubation with the anti-mouse Biotin-conjugated secondary antibody for one hour at room temperature. Again, the plate was washed and then incubated with streptavidin-HRP diluted in ELISA blocking buffer. After final washing steps with ELISA washing buffer and water, coated capsids were detected using the TMB liquid substrate

system and a microplate reader according to the manufacturer's instructions. Previously analyzed vector preparations were used as standard.
For the detection of surface-exposed DARPins on AAV particles, immunoplates were coated with α-myc tag antibody diluted in PBS over night at 4°C. After washing and blocking, serial dilutions of AAV vector preparations were added for 2 hours at room temperature. Detection of captured AAV particles was performed as described for the capsid ELISA.

2.3.6 Immobilized-metal affinity chromatography

Immobilized-metal affinity chromatography (IMAC) is a method to separate proteins and molecules based on the interaction with metal ions. Proteins containing a polyhistidine tag can be retained in a HisTrap HP column (GE Healthcare) due to formation of chelat complexes between the tag and the nickel ions of the stationary phase. Then, bound proteins can be eluted by addition of the aromatic heterocycle imidazole.
For IMAC purification of DARPin-displaying AAV vector particles a Knauer HPLC system was used according to the manufacturer's instructions. Prior to sample loading, columns were washed with 15 column volumes water and equilibrated with 15 column volumes IMAC binding buffer. Vector particles were diluted in IMAC binding buffer and were loaded onto the column at a flow rate of 0.1 ml/min followed by washing with 10 column volumes. For elution of bound vector particles, columns were washed with another 3 column volumes IMAC binding buffer and then eluted with 5 column volumes IMAC elution buffer at a flow rate of 0.2 ml/min. A final elution step to clean the columns was performed with buffer containing 500 mM imidazole. During loading, washing and elution, flow through was collected by an autosampler.

2.3.7 Dialysis

Iodixanol density gradient- or IMAC-purified AAV vectors were dialyzed using Slide-A-Lyzer® dialysis cassettes (7,000 Da molecular weight cut-off, Thermo Scientific) according to the manufacturer's instructions. AAV preparations were injected into the cassettes with a 21-gauge needle and dialyzed against 2 liters of PBS for 12 hours at 4°C.

2.3.8 Immunofluorescence microscopy

For immunofluorescence microscopy, HEK-293T cells were seeded into a covered chamber of an 8-well LabTek plate and transfected with 0.25 µg pDisplay-$D^{9.29}$, pCG-$H_{mut}\Delta 18$ and pCG-FΔ30. After 24 hours, cells were washed with PBS and fixed with 4% formaldehyde for 20 min at room temperature. Cells were permeabilized with 0.5% Triton X-100 in PBS for 8 min before they were washed again and incubated with blocking solution (PBS, 5% chicken serum) for 45 min at room temperature. Subsequently, cells were incubated with α-MV H and α-HA tag antibody for one hour at 37°C. Secondary antibodies conjugated to Alexa Fluor dyes 546 and 633, respectively, were added and left for one hour at 37°C. Finally, cells were washed twice with PBS and were analyzed using a laser scanning microscope (LSM 510). Micrographs shown as false-color images were assembled using the LSM Image Browser (Zeiss, Jena, Germany).

2.3.9 Electron microscopy

For immunoelectron microscopy, lentiviral vector-producing HEK-293T cells were fixed with 2% formaldehyde, washed three times with PBS and incubated with blocking solution (PBS, 5% chicken serum). Primary antibody directed against HA tag was added to the cells and left for one hour at 37°C. After two additional washing steps, cells were incubated with secondary anti-mouse-10 nm gold antibody for one hour at 37°C following glutaraldehyde fixation, epoxy embedding and preparation of ultrathin sections. For this, detached cells were embedded in agarose, fixated with 1% osmium tetroxide and contrasted with 2% uranyl acetate. Stepwise dehydration of the samples was performed using 30%, 50%, 70%, 80%, 90%, 96% and 100% ethanol. Finally, samples were embedded into epoxy, cut into ultrathin sections and mounted on Formvar-coated 200-mesh copper grids.

For electron microscopy of AAV vector preparations, Formvar-coated 200-mesh nickel were placed on a suspension drop containing AAV2, Her2-AAV or EpCAM-AAV particles for 10 min at room temperature. Then, the grids were washed three times with H_2O and stained for 15 seconds in 2% uranyl acetate.

All samples were analyzed using an EM109 transmission electron microscope.

2.4 Cell culture and virological methods

2.4.1 Cultivation of cell lines

Cells were cultivated in the appropriate medium (2.1.10) in a humidified incubator at 37°C, 5% CO_2 and 90% humidity. They were passaged twice a week. For this purpose, medium was aspirated and adherent cells were washed with PBS and then detached using trypsin for 5 min at 37°C. An appropriate fraction of the resulting suspension was seeded into a new culture flask with fresh medium.
All cell lines were regularly checked for contaminations with mycoplasma by PCR.

2.4.2 Freezing and thawing of cell lines

Adherent cells were detached as described (2.4.1), resuspended in cell culture medium and centrifuged for 4 min at 800 rpm and 4°C. The cell pellet was resuspended in cold freezing medium (2.1.5), aliquoted into cryotubes and frozen at -80°C using a 5100 Cryo Freezing Container (Nalgene). 24 hours later, cells were transferred to the gas phase of liquid nitrogen for long-term storage at -155°C.
Frozen cells were thawed in a 37°C water bath and immediately transferred to a cell culture flask containing pre-warmed medium. The next day, cell culture medium was exchanged.

2.4.3 Transfection of cell lines

Mammalian cells were transfected using the cationic polymer polyethylenimine (PEI). Positively-charged PEI/DNA complexes bind to the cell surface, are endocytosed and eventually released into the cytoplasm of a cell.
For transfection of HEK-293T cells, 1.4 x 10^5 cells per cm^2 cell culture vessel were seeded. The next day, cell culture medium was replaced with DMEM supplemented with 15% FCS and 3.2 mM glutamine. Then, 0.2 µg DNA/cm^2 and 0.8 µl PEI/cm^2 (2.1.5) were each diluted with DMEM and vortexed. Both solutions were combined and again vortexed thoroughly. After incubation for 20 min at room temperature, the transfection mix was added to the cells. Another medium exchange was performed 24 hours later to remove residual PEI/DNA complexes.

2.4.4 Cultivation of primary cells

Primary cells are freshly derived from a living organism and resemble more closely the physiological state of cells in the body. They undergo only a predetermined number of cell divisions and are usually less robust than immortal cell lines. HMECs were cultivated in Mammary Epithelial Cell Growth Medium (2.1.10) according to the distributor's instructions using supplied subculture reagents.

2.4.5 Isolation of human peripheral blood mononuclear cells

Human peripheral blood mononuclear cells (PBMCs) were isolated from freshly collected healthy donor blood or buffy coats (Blutspendedienst Hessen) by density centrifugation. For this purpose, either Vacutainer CPT Cell Preparation tubes (Becton Dickinson) were used according to the manufacturer's instructions or Histopaque®-1077 gradients were prepared. After density centrifugation, erythrocytes and granulocytes were pelleted and the mononuclear cell layer (lymphocytes, monocytes and macrophages) was aspirated from the interphase. PBMCs were washed twice with PBS and remaining erythrocytes were subsequently lysed for 20 min at 37°C using 0.86% ammonium chloride. After two additional washing steps, PBMCs were counted and resuspended in cell culture medium.

2.4.6 Vector production and concentration

Lentiviral and AAV vector particles were generated by transient transfection of HEK-293T cells using the PEI transfection protocol (2.4.3). Production scales ranged from one 6-well up to 40 cell culture dishes à 147.8 cm^2 growth surface.

For production of lentiviral vector particles, co-transfection of pCG-FΔ30, pCG-H_{mut}Δ18, pDisplay-$D^{9.29}$, pCMVΔR8.91 and transfer vector in a ratio of 5:3:6:20:21 was performed. Two days after transfection, cell culture supernatant containing vector particles was filtered with a 0.45 µm PTFE syringe filter and concentrated over a 20% sucrose cushion by ultracentrifugation in a SW28 rotor (Beckman Coulter) for 3 hours at 28,000 rpm and 4°C or for 24 hours at 4,500 × g and 4°C. The pellet was resuspended in PBS and aliquots were stored at -80°C.

AAV vector particles were produced using the adenovirus helper-free AAV packaging strategy (Xiao et al, 1998). The plasmids pRC-$VP2_{KO}$-$HSPG_{mut}$, pDARPin-VP2, pXX6-80 and the transfer vector were co-transfected into HEK-293T cells in a ratio of 1:1:1:3. Two

days after transfection, cells were scraped off the cell culture dish and centrifuged for 7 min at 1000 rpm. Cell pellets were resuspended in AAV lysis buffer (2.1.5) and subjected to three freeze/thaw cycles in liquid nitrogen and a 37°C water bath. After benzonase treatment (50 U/ml) for 30 min at 37°C, cell debris was removed by centrifugation for 20 min at 3700 × g and 4°C. Vector particle containing supernatant was diluted with PBS M/K (2.1.5) and transferred to a Quick-Seal® ultracentrifugation tube (Beckman Coulter). Subsequently, a gradient of 9 ml 15%, 6 ml 25%, 5 ml 40% and 6 ml 60% OptiPrep™ was underlayered. Density gradient centrifugation was performed in a 70Ti rotor (Beckman Coulter) for two hours at 63,000 at 4°C. AAV vector particles were recovered from the 40% OptiPrep™ fractions, aliquoted and stored at -80°C.

2.4.7 Transduction and titration

For titration, serially diluted viral particle solutions were added to cells. At 72 h after transduction, the percentage of GFP-positive cells was determined by flow cytometry analysis. Dilutions with 2 to 20% of GFP-positive cells were used to calculate the titer in transducing units/ml.

For transduction, 8 x 10^3 to 1.2 x 10^4 cells were seeded into a single well of a 96-well plate. The next day, vector particle dilutions were added to the cells, from which in advance medium was aspirated.

For spinfection experiments, cells and vector dilutions were centrifuged at 700 × g and 4°C for 1 h. After 72 h, titers were calculated based on the percentage of green fluorescent cells determined by flow cytometry.

2.4.8 Flow cytometry und fluorescence-activated cell sorting

Flow cytometry is a laser-based technique to measure and analyze characteristics of cells. Single cells flow in a sheath fluid through a beam of light and properties such as relative size, granularity, or fluorescence intensity can be determined based on scattered and emitted light.

For flow cytometry analysis of cells, medium was aspirated and cells were washed with FACS washing buffer and then detached using trypsin. After centrifugation at 800 rpm for 4 min, cells were either stained with antibodies or directly fixed with FACS fix.

For fluorescence-activated cell sorting (FACS) of CHO-EpCAM cells, cells were detached as described above. After centrifugation at 800 rpm for 4 min, cells were stained with anti-EpCAM-PE antibody and washed again. Cells were resuspended in FACS sorting buffer and

filtered through a 50 µm cell strainer. EpCAM-positive single cells were sorted into 96-wells and cultivated in conditioned medium.

2.4.9 Neutralization assay

Lentiviral vector particles were incubated with or without H-specific MAbs (0.001 µg, 0.01 µg, 0.1 µg or 1 µg in 100 µl) for 1 h at room temperature and then added to SK-OV-3 cells at an MOI of 0.3. The percentage of GFP-positive cells was determined after 72 h by flow cytometry.

2.4.10 Binding assay

Vector particles (0.14 µg p24) were incubated with 1 µg MAbs for 1 h at room temperature. Subsequently, 1.5×10^5 SK-OV-3 cells were added following 1 h of incubation at 4°C. Cell-particle complexes were then stained with anti-HA tag PE-coupled antibody, fixed and analyzed by flow cytometry.

2.4.11 Competition assay

For the competition of EpCAM-AAV with soluble recombinant protein, vector particles were incubated with increasing amounts (0, 0.001, 0.01, 0.1, 1 or 10 µg/ml) of the extracellular domain of human or murine EpCAM for 1 h at 4°C. Then, samples were used to transduce EpCAM-positive cells. Analysis of GFP expression was performed 72 h post transduction.

2.4.12 Detection of tumor cells in whole blood samples

Mimicking the conditions of circulating tumor cells in blood samples derived from patients, MDA-MB453 tumor cells were mixed with 7.5 ml blood of healthy donors. PBMCs were purified as described in chapter 2.4.5, plated in a 10 cm^2 cell culture dish and 3×10^{10} vector genomes EpCAM-AAV were added. After 48 h, cells were completely removed from the cell culture dish using trypsin, washed, incubated with human FcR blocking reagent for 15 min on ice (20 µl per 10^7 cells) and stained with anti-CD326-PE (diluted 1:10) and anti-CD45-APC (diluted 1:5) for another 15 min. Samples were washed again, fixed with 1% formaldehyde in PBS and analyzed by flow cytometry. A gating strategy to exclude debris, doublets and high

$CD45^+$ cells was performed. Remaining $GFP^+/EpCAM^+$ cells were analyzed using version 4.07 of the FCS Express software (De Novo).

2.5 Experimental mouse work

2.5.1 Injection of tumor cells

SK-OV-3 cells were cultured and detached as described (2.4.1), centrifuged for 4 min at 800 rpm and washed with PBS. After an additional centrifugation step, cells were resuspended in PBS and counted. Then, CB17 SCID female mice (6 to 8 weeks old; Harlan Laboratories, Eystrup, Germany) were anaesthetized with 2.5% isoflurane. The cell suspension was briefly vortexed and 5 x 10^6 cells in 100 µl were injected subcutaneously using a 23 gauge needle into the right flank of the mice.

2.5.2 Injection of vector particles

For intravenous injection (i.v.) of vector particles, mice were transferred to a restrainer and 200 µl vector particles diluted in PBS were injected into a lateral tail vein using a 30 gauge needle.
For intraperitoneal injection (i.p.), mice were restrained and tilted so that the head was facing downwards and 200 µl vector particles diluted in PBS were injected into the abdomen using a 30 gauge needle.

2.5.3 *In vivo* imaging

The *in vivo* imaging technology allows non-invasive visualization of bioluminescence signals in small animals. In order to detect luciferase expression, mice were injected i.p. with 150 mg D-Luciferin/kg body weight (2.1.5). After 5 min, mice were anaesthetized with 2.5% isoflurane in a XGI-8 induction chamber for 2 min and placed into the IVIS Spectrum imaging chamber. Imaging data were obtained 10 - 20 min after substrate injection. Data were analyzed using the software Living Image 4.2 (Caliper Life Sciences).

3 Results

This thesis describes the generation and characterization of two types of receptor-targeted viral vectors for the application in basic research as well as potentially in cancer treatment and diagnosis. A lentiviral vector pseudotyped with the measles virus (MV) glycoproteins was used to separate the receptor attachment and fusion-helper function provided by the MV H protein. It was shown that H is still able to perform its fusion-helper function without attaching to the receptor. The resulting vector particles achieved specific and efficient gene transfer *in vitro* and *in vivo*. Furthermore, AAV vectors targeted to the human epithelial cell adhesion molecule (EpCAM) were developed. Fusion of a designed ankyrin repeat protein (DARPin) to the N-terminus of the VP2 capsid protein did not affect vector particle integrity and resulted in high specificity for EpCAM-positive cells. Since EpCAM-positive cells play a major role in metastases initiation and can be an indicator of the efficacy of cancer therapy, the vector's ability to detect rare tumor cells in blood was assessed.

3.1 Using MV-pseudotyped lentiviral vectors to separate the fusion-helper function from receptor attachment

3.1.1 Setting up the system

To separate the receptor attachment function from H, three transmembrane proteins had to be incorporated into the envelope membrane of LV particles: i) the cytoplasmic tail-truncated F protein variant FΔ30, ii) the cytoplasmic tail-truncated H variant H_{mut}Δ18 which is in addition mutated in its natural receptor binding sites, and iii) an artificial transmembrane protein composed of the transmembrane domain (TMD) of the platelet-derived growth factor receptor (PDGFR) and a targeting ligand mediating attachment to the receptor of choice (pDisplay-TL) (Figure 11). Different types of targeting ligands were applied including DARPins and scFvs. Figure 11 provides an overview on the design and elements present in the different plasmids, also including a number of control constructs and variants. Among these are the plasmids encoding the unmutated HΔ18 variant, the H^{*}_{mut}Δ18 additionally harboring the F111N mutation, a conventional H_{mut}Δ18 fused with a targeting ligand and the glycoprotein of the vesicular stomatitis virus (VSV).

Initially, the coding sequence of DARPin 9.29, which is specific for Her2/neu, a receptor

tyrosine kinase overexpressed on cancer cells, was fused to the PDGFR TMD resulting in pDisplay-D$^{9.29}$ (Figure 11) (Rasbach, 2010).

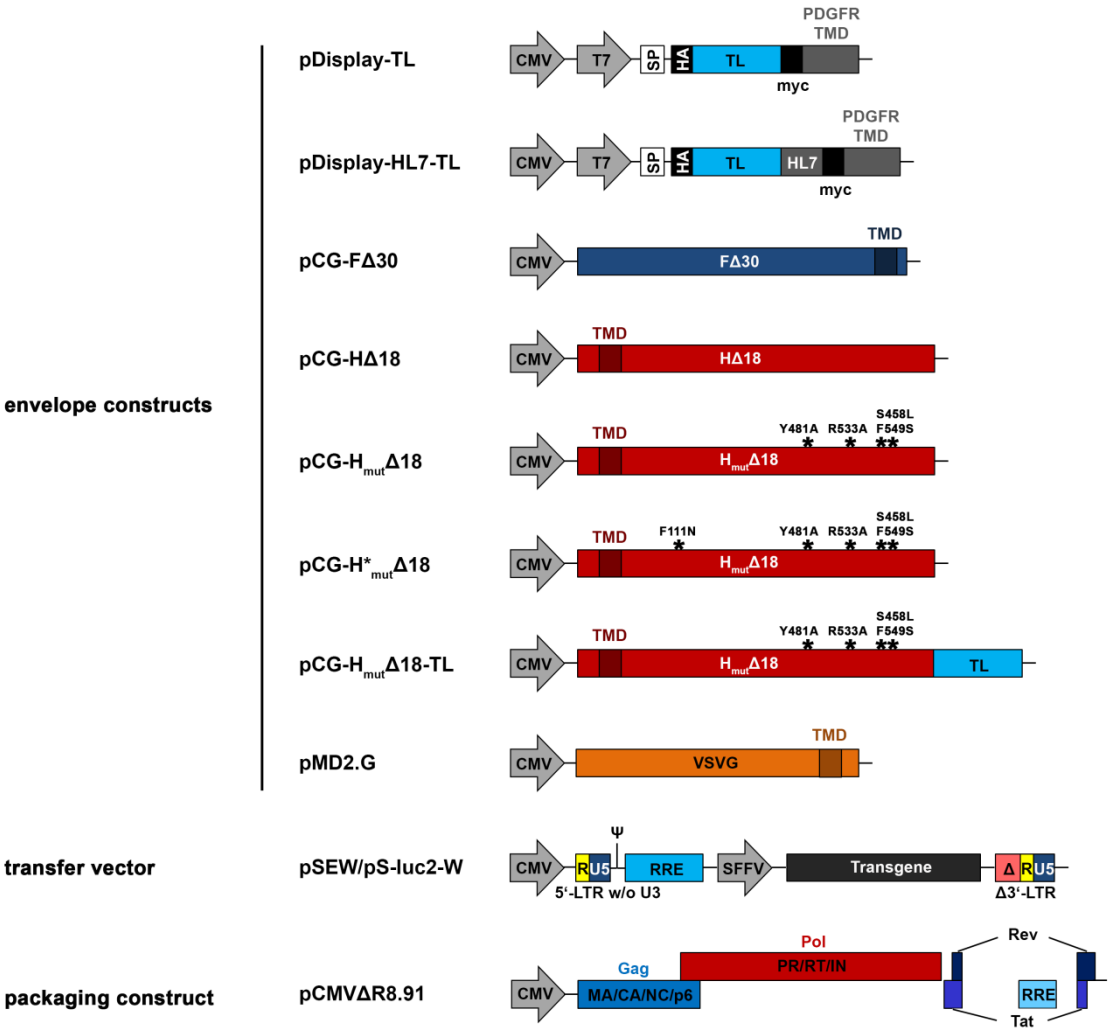

Figure 11: Schematic drawing of constructs used for the generation of lentiviral vectors. A targeting ligand (TD) is fused between the HA and myc-tag of the pDisplay (Invitrogen). Resulting proteins are presented on the platelet-derived growth factor receptor (PDGFR) transmembrane domain (TMD). The signal peptide (SP) sequence at the N-terminus targets the protein to the secretory pathway. The construct pDisplay-HL7-TD contains an additional sequence coding for a helical linker (HL7) between the TL and myc-tag. Asterisks mark mutations introduced to ablate natural receptor recognition of H (H_{mut}) or the F111N glycosylation site (H^*mut). For retargeting the H protein to a cell surface marker of choice, a TL was fused in frame in construct pCG-H_{mut}Δ18-TL. In order to generate control vectors pseudotyped with VSVG, the plasmid pMD2.G was used. The transfer vector pSEW or pS-luc2-W encoding the GFP or luciferase reporter genes and the packaging construct pCMVΔR8.91 are shown.

In order to generate D$^{9.29}$-LV particles having incorporated D$^{9.29}$, H_{mut}Δ18 and FΔ30, cotransfection of five plasmids into HEK-293T cells was performed. The plasmids pDisplay-D$^{9.29}$, pCG- H_{mut}Δ18, pCG- FΔ30 as well as the GFP encoding transfer vector plasmid pSEW (Münch et al, 2011; Demaison et al, 2002) and the packaging construct pCMVΔR8.91 (Zufferey et al, 1997) are required for production and release of the respective vector particles

into the supernatant (Figure 11, Figure 12). Supernatants of transfected cells were collected after 48 hours and subsequently purified and concentrated by centrifugation over a sucrose cushion.

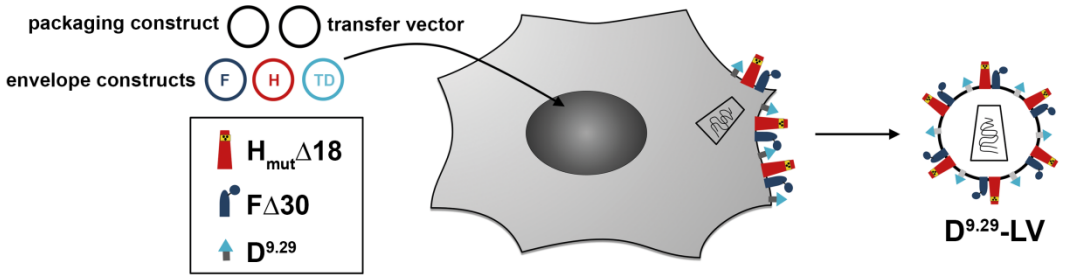

Figure 12: Principle of virus particle generation by transfection of HEK-293T cells. Transfection with the five plasmids shown gives rise to D$^{9.29}$-LV particles pseudotyped with H$_{mut}$Δ18 (red), FΔ30 (dark blue) and D$^{9.29}$ (light gray and blue).

Proteins can only become incorporated into the LV particle envelope if they are efficiently expressed at the cell surface of producer cells. Fluorescence microscopy of cells expressing H$_{mut}$Δ18 and D$^{9.29}$ had revealed that both proteins were well expressed on the surface of HEK-293T cells (Rasbach, 2010), meeting the critical prerequisite for efficient incorporation into LVs. Moreover, H$_{mut}$Δ18 and D$^{9.29}$ colocalized (Figure 13A).

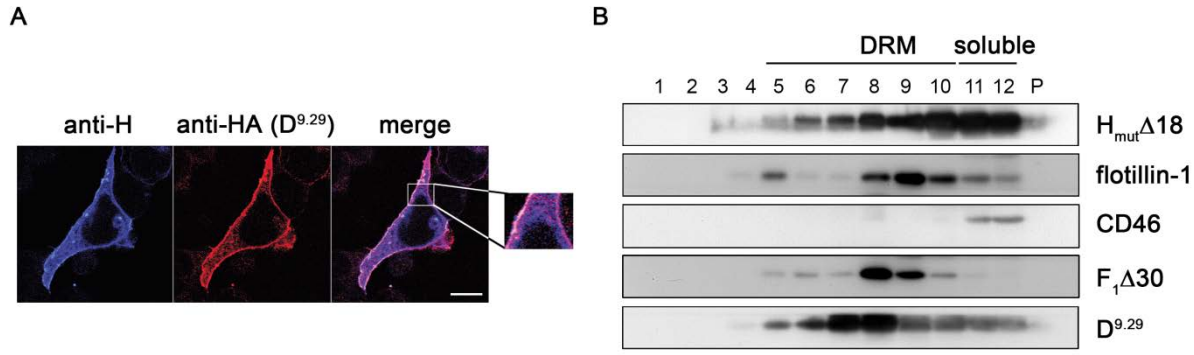

Figure 13: D$^{9.29}$ colocalizes with MV glycoproteins. (A) H$_{mut}$Δ18 and D$^{9.29}$ coimmunostaining one day after HEK-293T cells were transfected with 0.25 µg of pCG-H$_{mut}$Δ18, pCG-FΔ30, and pDisplay-D$^{9.29}$. Fixed and permeabilized cells were stained with anti-H and then with anti-HA antibody. Secondary antibodies conjugated with Alexa Fluor dyes 546 and 633 were used for detection. Scale bar, 10 µm. Modified from (Rasbach, 2010). (B) D$^{9.29}$ resides within the same membrane fractions as the MV glycoprotein complex. Detergent-resistant membranes (DRM) from HEK-293T cells transfected with pCMVR8.9, pSEW, pCG-H$_{mut}$Δ18, pCG-FΔ30, and pDisplay-D$^{9.29}$ were separated by flotation assay. The distribution of proteins within fractions (fraction 1 represents the top of the gradient) and the pellet (P) was assessed by immunoblotting with antibodies specific for H, F, the HA tag of D$^{9.29}$, the DRM marker flotillin 1, and the non-DRM marker CD46. (Rasbach et al, 2013)

It is known that H and F form a tight complex already within the endoplasmic reticulum (Plemper et al, 2001) and are then transported together to the cell surface. Supposedly, they do not distribute randomly within the membrane but are enriched in detergent-resistant membranes (DRM) (Avota et al, 2004; Vincent et al, 2000). Therefore, it was evaluated whether $D^{9.29}$ can also be found in these distinct membrane populations together with $H_{mut}\Delta18$ and $F\Delta30$ by membrane flotation assay and subsequent western blot analysis.

For this assay, vector particle producing HEK-293T cells were lysed in TNE buffer which only disrupts membrane parts that are not cholesterol-rich and therefore not detergent-resistant. In an OptiPrep™ step gradient DRMs were separated from soluble components by ultracentrifugation and resulting fractions were analyzed for their protein content. The DRMs were present in fractions 5-10 as determined by use of the DRM marker flotillin-1 (Langhorst et al, 2005), with the soluble membranes in fractions 11 and 12 as indicated by use of the non-DRM marker CD46 (Hogue et al, 2011). $F\Delta30$ as well as a significant amount of $H_{mut}\Delta18$ were detected in the DRM fractions (Figure 13B). Although the MV H protein alone has not been described to be sorted into DRMs, it is known that it is associated up to 30% with DRMs upon coexpression with MV F (Vincent et al, 2000). The modifications in the F and H cytoplasmic tails thus did not alter their DRM association. Interestingly, the vast majority of $D^{9.29}$ was also found in the DRM fractions, thus suggesting a colocalization with $F\Delta30/H_{mut}\Delta18$ at the cell membrane.

3.1.2 Characterization of vector particles

Besides incorporation into the virus membrane, a proper display of the DARPin 9.29 and the efficient release of functional viral particles are crucial for evaluating whether cell entry was still possible although receptor attachment had been uncoupled from H. To assess the quality of vector preparations, the particles were analyzed for their protein content, accessibility of the $D^{9.29}$, transduction performance as well as infectivity.

3.1.2.1 $D^{9.29}$ is incorporated into the viral membrane and accessible

In addition to $D^{9.29}$-LV, a series of particles was generated as control: by omitting one of each of the three plasmids encoding $H_{mut}\Delta18$, $F\Delta30$, or $D^{9.29}$ and replacing the DNA with an empty plasmid called pCG-1, particles with only two of the three transmembrane proteins were generated (Figure 14). Moreover, a $H_{mut}\Delta18$ variant ($H^{*}_{mut}\Delta18$) was used in which F93 (correlates to position 111 in the untruncated H protein) was replaced by an asparagine to

introduce an additional N-glycosylation site (Figure 11, Figure 14). This mutation has been described to interfere with H/F complex formation (Paal et al, 2009) and was shown to be well expressed in HEK-293T cells (Rasbach, 2010). As positive control conventional 9.29-LV particles were generated where the DARPin 9.29 has been fused to the C terminus of $H_{mut}\Delta18$ (Figure 11) (Münch et al, 2011) thereby integrating the tasks of receptor attachment and fusion helper function to H (Figure 14).

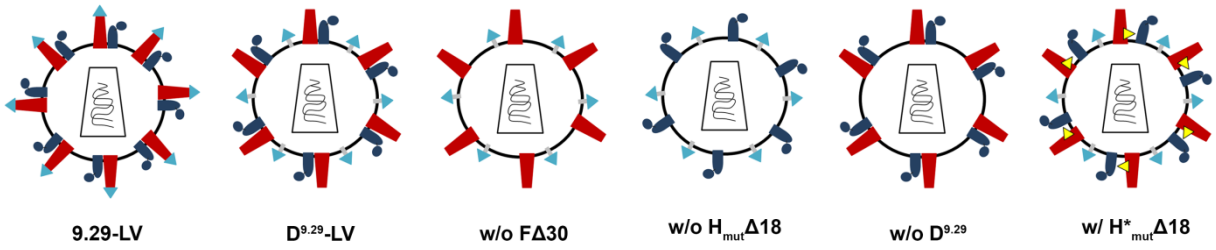

Figure 14: Schematic drawing of $D^{9.29}$-LV and its variants. $D^{9.29}$-LV contains FΔ30 (dark blue) and $H_{mut}\Delta18$ (red) and the DARPin (light blue) presented on the PDGFR TMD (gray) in its envelope. The conventional targeting vector 9.29-LV displays the DARPin as fusion protein with H. Control vectors w/o FΔ30, w/o $H_{mut}\Delta18$, w/o $D^{9.29}$ or with the $H^{*}_{mut}\Delta18$ variant characterized by an additional N-glycosylation site (yellow) are shown.

All particles were analyzed by western blotting for the presence of H, F_1, which is a subunit of F linked to the smaller subunit F_2 by a disulfide bond after cleavage of the F_0 precursor protein, and $D^{9.29}$ (HA tag) as well as the HIV-1 gag protein p24. For $D^{9.29}$-LV, all three types of transmembrane proteins, i.e. $D^{9.29}$, $H_{mut}\Delta18$ and FΔ30, were found to be efficiently incorporated. Notably, $H_{mut}\Delta18$ and FΔ30 were incorporated at similar levels to those in the conventional 9.29-LV vector (Figure 15A, lanes 1 and 2). $H^{*}_{mut}\Delta18$ was also detected in the particles (Figure 15, lane 6) and migrated below the 9.29-$H_{mut}\Delta18$ protein due to the smaller size of the $H_{mut}\Delta18$ variants compared to the DARPin-H fusion protein. Consistent with the omission of one plasmid encoding for each one transmembrane protein during production, no $F_1\Delta30$, $H_{mut}\Delta18$ or $D^{9.29}$ were detected in the respective samples (Figure 15A, lanes 3-5).

To further confirm the presence and accessibility of $D^{9.29}$ on the surface of released particles, immunoelectron microscopy was performed. HEK-293T producer cells were fixed, stained against the HA tag of $D^{9.29}$, embedded in epoxy and ultrathin sectioned. It was expected that mature viral particles were not only released from the cells but that they were displaying the DARPin protein on their surface as indicated by gold labelling (arrow head) (Figure 15B). Thus, viral vectors exhibited the expected protein composition, had HIV-1 like morphology and had incorporated the additional $D^{9.29}$ protein.

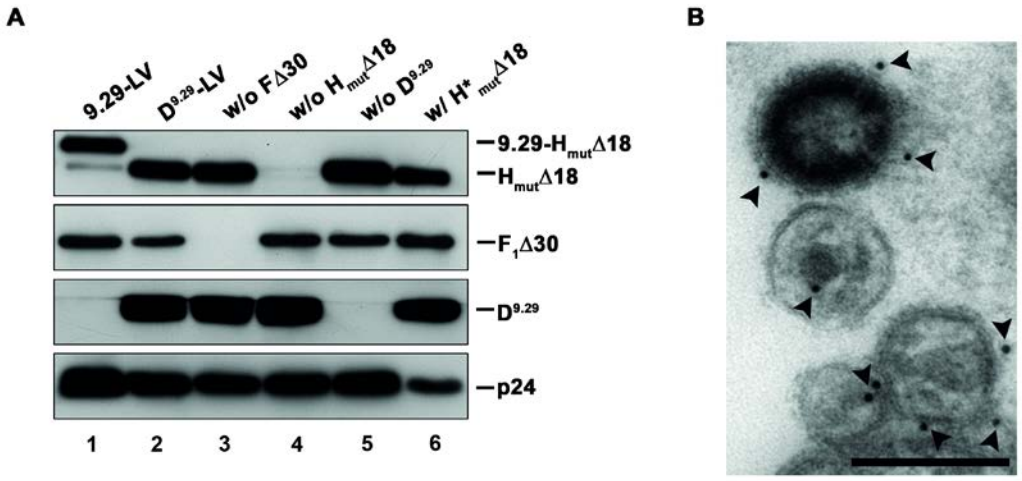

Figure 15: MV-pseudotyped virus incorporates $D^{9.29}$. (A) Western blot analysis for incorporation of FΔ30, $D^{9.29}$, p24, and H_{mut}Δ18 or 9.29-H_{mut}Δ18 in vector particles 9.29-LV, $D^{9.29}$-LV, and variants of $D^{9.29}$-LV in which FΔ30 (w/o FΔ30), H_{mut}Δ18 (w/o H_{mut}Δ18), or $D^{9.29}$ (w/o $D^{9.29}$) was omitted, respectively, or H_{mut}Δ18 was replaced by H^*_{mut}Δ18 (w/ H^*_{mut}Δ18). (B) Immunoelectron microscopy of ultrathin sections of HEK-293T producer cells releasing $D^{9.29}$-LV vector particles. $D^{9.29}$ was detected with a primary antibody directed against the HA tag and secondary anti-mouse antibody conjugated with 10-nm gold particles (arrow heads) following epoxy embedding and ultrathin sectioning. Scale bar, 200 nm. (Rasbach et al, 2013)

3.1.2.2 $D^{9.29}$-LV is able to enter Her2/neu-positive cells

As demonstrated in the previous chapter, $D^{9.29}$-LV particles were successfully produced and revealed the expected physical properties. But the key question was whether these particles will be able to bind to Her2/neu-positive cells via the $D^{9.29}$ protein and, more importantly, then fuse with the cell membrane to enter the cytoplasm.

To address this question, Her2/neu-positive SK-OV-3 cells were incubated with $D^{9.29}$-LV and its control vectors. $D^{9.29}$-LV was able to enter the cells which was indicated by strong GFP fluorescence and transduced even more cells than the conventional vector 9.29-LV where the DARPin was fused to H (Figure 16A). None of the control particles lacking one of the three transmembrane proteins or particles containing H^*_{mut}Δ18 were able to mediate any significant transfer of the *egfp* gene (Figure 16A). Upon performance of transduction experiments in serial dilutions to titrate the vectors it could be shown that an almost 10-fold-higher transduction efficiency was achieved with $D^{9.29}$-LV than with 9.29-LV (8.5×10^6 t.u./ml compared to 8.9×10^5 t.u./ml) (Figure 16B). One possible explanation for the increase in transduction efficiency and titer upon presentation of the DARPin 9.29 on the PDGFR transmembrane domain instead of H was that more particles were released from $D^{9\text{-}29}$-LV producing cells eventually leading to higher concentrated vector stocks.

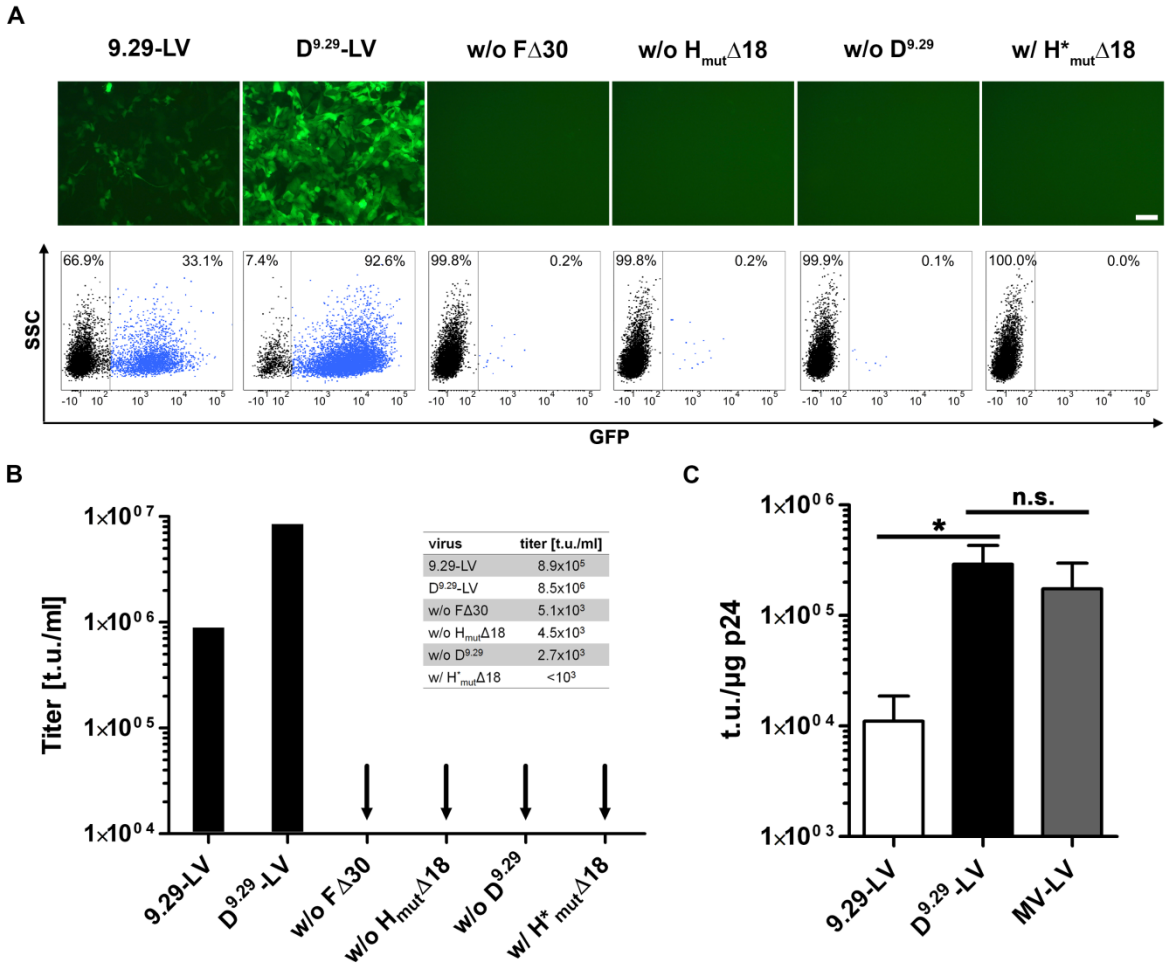

Figure 16: $D^{9.29}$-LV mediates efficient gene delivery. Equal amounts of *egfp* gene-delivering virus particles 9.29-LV, $D^{9.29}$-LV, and variants of $D^{9.29}$-LV in which FΔ30 (w/o FΔ30), H_{mut}Δ18 (w/o H_{mut}Δ18), or $D^{9.29}$ (w/o $D^{9.29}$) was omitted, respectively, or H_{mut}Δ18 was replaced by H^*_{mut}Δ18 (w/ H^*_{mut}Δ18) were added to SK-OV-3 cells. (A) Representative pictures and flow cytometry dot plots of SK-OV-3 cells 3 days after addition of virus. Scale bar, 100 µm. (B) Titers on SK-OV-3 cells as determined by flow cytometry analysis. Arrows indicate titers of < 1×10^4 transducing units (t.u.)/ml. (C) Infectivity determined as ratio of transducing units (t.u.) per µg p24 for 9.29-LV, $D^{9.29}$-LV, and MV-LV (n = 4; mean±standard deviations [SD] are shown; *, $P < 0.01$; n.s., not significant by unpaired t test). (Rasbach et al, 2013)

To determine the amount of particles, the HIV-1 capsid protein p24 was used as an indicator. Calculations of titers and quantification of p24 by ELISA for four different virus stocks revealed a 26-fold-higher infectivity-to-particle-number ratio (n = 4, $P < 0.01$) for D^{9-29}-LV than for 9.29-LV and a ratio similar to that for the nontargeted MV-LV (Figure 16C). These findings ruled out that better transduction performance was due to higher concentrated $D^{9.29}$-LV stocks but rather suggested that less particles were produced compared to 9.29-LV. It is well known that not all LVs released from producer cells are infectious and functional but it seemed that $D^{9.29}$-LV particles were significantly more infectious than the conventional targeting vector and comparable to MV-LV.

3.1.2.3 Different targeting ligands can be used as receptor binding domain

To validate that these findings were not just DARPin 9.29 specific, the whole panel of Her2/neu-specific DARPins, that were already described to work for redirecting lentiviral vector particles, were applied (Münch et al, 2011). In total five other DARPins, namely G3, H14R, 9.26, 9.16 and 9.01, were used (Table 1). Except for DARPin G3 which was selected and affinity-maturated using ribosome display (Zahnd et al, 2006; Zahnd et al, 2007), all other Her2-specific DARPins were selected from a large phage library by using signal recognition particle (SRP) phage display (Steiner et al, 2008). In contrast to conventional phage display, a signal sequence directs the proteins to the SRP translocation pathway. This route enables translocation of proteins cotranslationally and thus results in much higher display levels of stable and fast-folding proteins (Steiner et al, 2008; Steiner et al, 2006).

Table 1: Applied Her2/neu-specific DARPins

	9.29[c,e]	**G3[d,e]**	**H14R[c]**	**9.26[c,e]**	**9.16[c]**	**9.01[c]**
K_D (nmol/l)[a]	3.83	0.09	0.20	1.36	6.90	N/A
DARPin type[b]	N3C	N2C	N3C	N3C	N3C	N3C
Her2/neu binding	I	IV	IV	I	I-III	N/A

[a] Dissociation constant, [b] Number of ankyrin repeats; N represents the N-capping repeat, internal binding repeats are indicated by numbers, C represents the C-capping repeat, [c] (Steiner et al, 2008), [d] (Zahnd et al, 2007), [e] (Jost et al, 2013)

In a first experiment, particles displaying the DARPin G3 on the PDGFR transmembrane domain were generated (D^{G3}-LV). This DARPin binds the membrane-proximal Her2/neu domain IV, whereas DARPin 9.29 is directed against the membrane-distal domain I (Jost et al, 2013). Compared to particles presenting the DARPin G3 directly fused to H (G3-LV), D^{G3}-LV revealed lower transduction efficiency. Only 16% SK-OV-3 cells were GFP-positive, whereas G3-LV transduced up to 30% of the cells (Figure 17A, left and middle).

Since one of the main differences between G3 and 9.29 is their Her2/neu binding domain, this could be the reason for the efficiency drop. Therefore, the distance between DARPin and Her2/neu domain IV was compensated by inserting a helical linker (HL) between the PDGFR transmembrane domain and the DARPin G3.

The coding sequence for the helical linker RGSGA-$(EAAAK)_7$-ALGS was synthesized (pRC2.1-Helical Linker) and inserted into the *NotI/SalI* digested pDisplay-D^{G3}. The resulting pDisplay-HL7-D^{G3} (Figure 11) was used for production of $D^{HL7\text{-}G3}$-LV particles. Remarkably,

titers increased dramatically and resulted in more than 80% positive SK-OV-3 cells (Figure 17A, right).

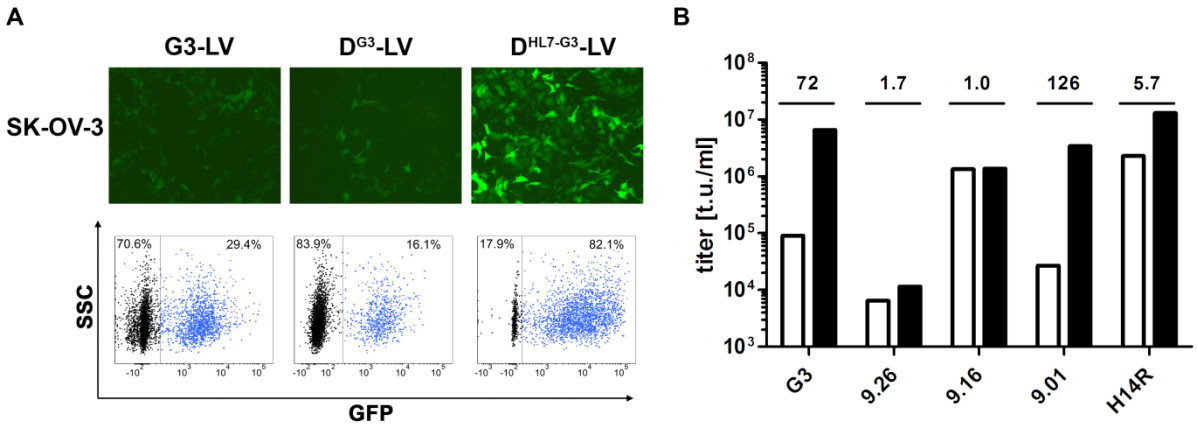

Figure 17: Panel of Her2/neu-specific DARPins as alternative targeting ligands. (A) SK-OV-3 cells were transduced with particles presenting the Her2/neu-specific DARPin G3 fused to H (G3-LV), to the PDGFR transmembrane domain (D^{G3}-LV), or to the PDGFR transmembrane domain connected by a helical linker ($D^{HL7\text{-}G3}$-LV). Representative pictures of GFP-expressing cells were taken 72 h after transduction, and the percentage of GFP-positive cells was determined by flow cytometry. Scale bar, 100 µm. (B) SK-OV-3 cells were transduced with particles presenting the DARPin G3, 9.26, 9.16, 9.01 or H14R either fused to the PDGFR transmembrane domain (white bars) or to the PDGFR transmembrane domain connected by a helical linker (black bars). Titers as determined by flow cytometry are shown and fold changes are indicated. (Rasbach et al, 2013)

After production of all five D^{X}-LV and $D^{HL7\text{-}X}$-LV (X stands for the respective Her2/neu-specific DARPin) variants, titers were determined on SK-OV-3 cells. Consistently, for particles presenting a DARPin directed against domain IV, titers increased 72-fold for $D^{HL7\text{-}G3}$-LV and 5.7-fold for $D^{HL7\text{-}H14R}$-LV compared to D^{G3}-LV and D^{H14R}-LV. In contrast, the helical linker did neither increase nor decrease titers of particles presenting DARPins 9.26 and 9.16. The strongest fold-change was observed for the vector pair $D^{9.01}$-LV/$D^{HL7\text{-}9.01}$-LV. Although the Her2/neu binding domain of this specific DARPin is not known, it can be speculated that it is sterically not favorable when the DARPin is presented directly on the PDGFR transmembrane domain.

Regardless of their size, binding domain or Her2/neu affinity, all five DARPins could be successfully used for generating particles that were able to enter cells although receptor attachment was uncoupled from H. Interestingly, it could be shown that the distance between receptor attachment domain and membrane influences the transduction efficiency.

In a next step, other receptor types than Her2/neu were addressed. CD4- and EpCAM-specific DARPins (Schweizer et al, 2008; Stefan et al, 2011), single-chain variable fragments (scFv) directed against CD105, CD20, CD133, CD30 and CD8 (Abel et al, 2013; Funke et al, 2008; Anliker et al, 2010; Friedel et al; Zhou et al, 2012) and nanobodies binding to rat ADP-

ribosyltransferase (Art2.2) (Koch-Nolte et al, 2007) were tested as targeting ligands without and with helical linker in this system (Table 2).

Table 2: Summary of targeting ligands used for pDisplay constructs and vector particles.

Target	Targeting ligand	w/o linker D^{X}-LV	w/ linker D^{HL7}-X-LV
Human Her2/neu	DARPin 9.29	#	
	DARPin G3	#	
	DARPin 9.26		
	DARPin 9.16		
	DARPin 9.01		
	DARPin H14R		
Human CD4	DARPin 57.2[a]		
	DARPin 29.2[a]		
	DARPin 27.2[a]		
	DARPin 55.2[a]		
Human EpCAM	DARPin Ac1[b]		
	DARPin Ec1[b]		
Human CD105	scFv A5[c]	#	
Human CD20	scFv CD20[d]	#	
Human CD133	scFv 141.7[e]		
	scFv AC133[e]		
Human CD30	scFv CD30[f]		
Human CD8	scFv CD8[g]		
Rat Art2.2	Nanobody s-14[h]		
	Nanobody l-17[h]		

	> 10^{6} t.u./ml
	> 10^{5} t.u./ml
	> 5×10^{3} t.u./ml
	not detectable

Different designed ankyrin repeat proteins (DARPins), single-chain variable fragments (scFv) or nanobodies were cloned into pDisplay (w/o linker) or pDisplay-HL7 (w/linker) using *SfiI/NotI* restrictions enzymes. Vector particles generated using the respective plasmids were titrated on receptor-positive cell lines. [a](Schweizer et al, 2008), [b](Stefan et al, 2011), [c](Völkel et al, 2004; Abel et al, 2013), [d](Funke et al, 2008), [e](Anliker et al, 2010), [f](Friedel et al) , [g](Zhou et al, 2012), [h](Koch-Nolte et al, 2007), #(Rasbach, 2010)

After cloning of all the respective plasmid constructs and production of the vector particles, titers were determined on receptor-positive cell lines. Whereas gene transfer into CD4-positive cells could not be observed at all, moderate transduction was detected on EpCAM-positive cells using DARPin Ac1 as targeting ligand. Interestingly, not only DARPins could be used as targeting proteins but also scFvs. Gene transfer into human CD105-positive endothelial cells as well as into cells expressing the stem cell marker CD133 was successful.

On the other hand, lymphocyte cell marker CD20, CD30 and CD8 failed to work as cell entry receptors for the respective LVs. As third class of targeting domains, nanobodies selected to bind to rat ADP ribosyltransferase 2.2 (Art2.2) expressed exclusively by mature rat T cells was used. All four resulting vector particle variants were able to transfer the *gfp* transgene into target cells with $D^{HL7\text{-}s\text{-}14}$-LV exhibiting the highest titer.

Although some targeted receptors did not mediate entry, it was clearly shown that several different receptors can be used as cell entry portals. Transduction efficiency varied depending on the target and the targeting ligand and with no other targeting ligand were higher or comparable titers achieved than with the Her2/neu-specific DARPins. Consequently, further experiments and characterization was carried out using $D^{9.29}$-LV.

3.1.3 Characterization of $D^{9.29}$-LV cell entry

Having shown that $D^{9.29}$-LV is able to fuse with the cell membrane and to transfer the *gfp* gene very efficiently, a panel of experiments was performed to characterize the molecular prerequisites for its cell entry. First, the dependence on Her2/neu was assessed to clarify that receptor binding was indeed mediated via the $D^{9.29}$ protein. Second, the function of the MV fusion machinery was tested.

3.1.3.1 Her2/neu binding is required for cell entry

To confirm that Her2/neu binding is necessary for efficient transduction, a spinfection experiment was performed. Here, $D^{9.29}$-LV and its control vectors were centrifuged onto SK-OV-3 cells. This way, viruses and cells were artificially brought into close contact, potentially circumventing the need for high-affinity receptor binding.

Without centrifugation the same transduction pattern was observed as in Figure 16A, strengthening the fact that transduction only occurred after addition of 9.29-LV or $D^{9.29}$-LV, but not when the MV glycoprotein complex was not intact or when $D^{9.29}$ was missing (Figure 18A). The spinfection increased transduction by $D^{9.29}$-LV and 9.29-LV, whereas still no remarkable transduction was observed for the control vectors (Figure 18B). Although this experiment shows that one can enhance the transduction using spinfection, it clearly demonstrates that high-affinity receptor binding is needed and close contact of virus and cell is not enough for cell entry of $D^{9.29}$-LV.

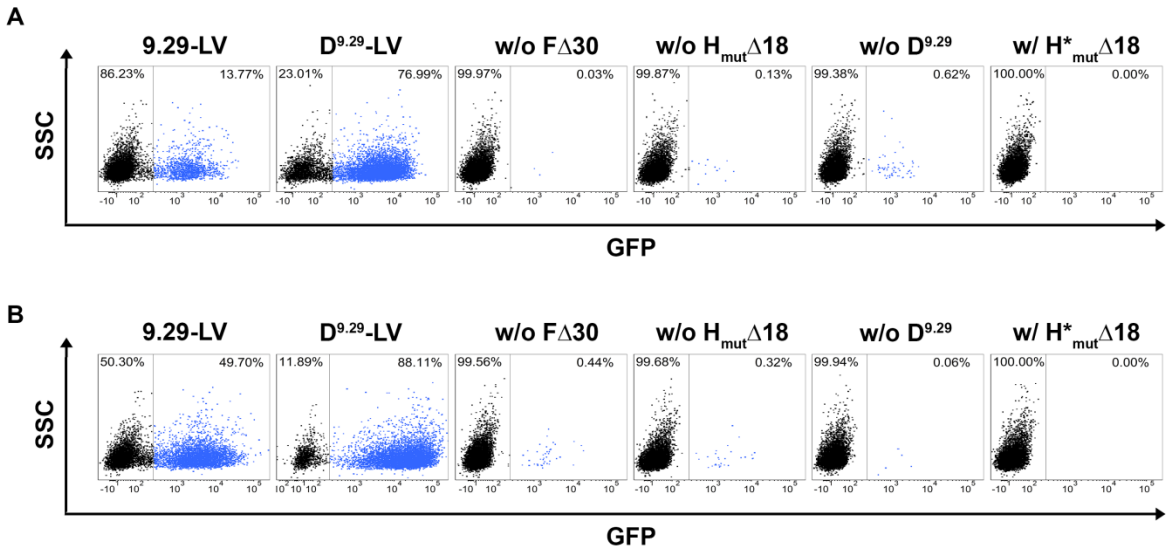

Figure 18: High-affinity receptor binding is needed for virus entry. SK-OV-3 cells were incubated with equal amounts of *egfp* gene-delivering virus particles 9.29-LV, $D^{9.29}$-LV, and variants of $D^{9.29}$-LV in which FΔ30 (w/o FΔ30), H_{mut}Δ18 (w/o H_{mut}Δ18), or $D^{9.29}$ (w/o $D^{9.29}$) was omitted, respectively, or H_{mut}Δ18 was replaced by H^*_{mut}Δ18 (w/ H^*_{mut}Δ18) either without centrifugation (A) or with additional centrifugation at 700 × g for 1 h (B). Flow cytometry analysis was performed 72 h after transduction. (Rasbach et al, 2013)

As described in chapter 3.1.1, the vector particles generated were adapted from the targeting system using MV-pseudotyped lentiviral vector particles first described by Funke et al. (Funke et al, 2008). One key to retarget these particles was to ablate the natural receptor binding by introducing several point mutations in H (Nakamura et al, 2005; Vongpunsawad et al, 2004). This was shown to be sufficient to prevent binding to the MV receptors SLAM, CD46 or Nectin-4. However, upon presentation of the attachment domain on a third protein and thereby potentially taking away a shielding effect from H, residual recognition of a so far unidentified MV receptor might be present. If this was true, receptor attachment and fusion helper function would not have been completely uncoupled.

To assess whether $D^{9.29}$-LV cell entry occurred also in absence of the MV receptors, CHO cells stably expressing Her2/neu (Münch et al, 2011) were transduced. While the parental CHO-K1 cells which expressed neither Her2/neu nor any of the natural MV receptors remained untransduced, CHO-Her2 cells were readily transduced by $D^{9.29}$-LV (Figure 19). Although the percentage of GFP-positive CHO-Her2 cells was lower than that of transduced SK-OV-3 cells, which is likely due to the lower susceptibility of rodent cells to LVs compared to that of human cells, the data demonstrate that cell entry of $D^{9.29}$-LV is Her2/neu dependent. Hence, receptor binding in $D^{9.29}$-LV particles must have been uncoupled from H while still mediating efficient cell entry.

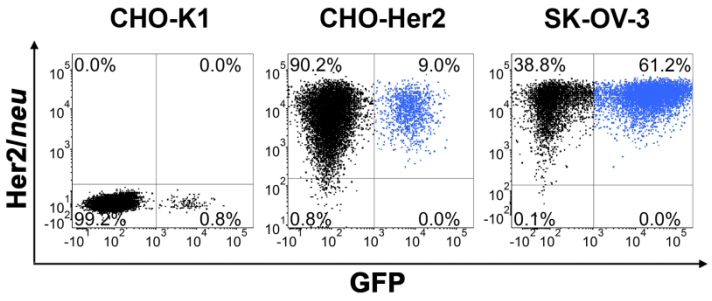

Figure 19: Cell entry is Her2/neu dependent. Parental CHO-K1, CHO-Her2 cells stably expressing Her2/neu or SK-OV-3 cells were transduced with $D^{9.29}$-LV. After 72 h cells were stained with anti-Her2/neu-PE antibody and analyzed by flow cytometry for receptor and GFP expression. (Rasbach et al, 2013)

3.1.3.2 Cell entry relies on the MV membrane fusion mechanism

$D^{9.29}$-LV particles have been proven to enter cells upon high-affinity receptor binding in a Her2/neu-dependent manner. Furthermore, these particles could enter cells in absence of MV receptors confirming that cell entry was not due to recognition of an unidentified natural receptor.

To assess whether $D^{9.29}$-LV cell entry relies on F-mediated membrane fusion, acidification of endosomes was blocked with chloroquine to prove that virus particle entry was pH independent. Besides 9.29-LV, MV-LV virus particles pseudotyped with FΔ30/HΔ18 entering into cells pH independently via CD46 or Nectin-4 (Funke et al, 2008), as well as LV particles pseudotyped with the glycoprotein G of vesicular stomatitis virus (VSV), which enter cells pH dependently (Hernandez et al, 1996), were used as controls (Figure 20A).

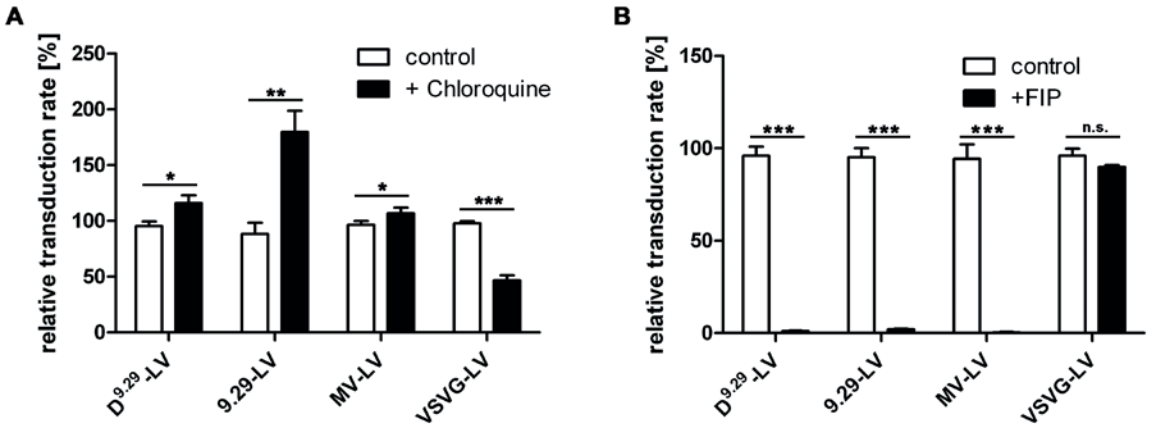

Figure 20: Membrane fusion is MV F dependent. (A) SK-OV-3 cells (1×10^4) were treated with 150 µM chloroquine before the indicated virus particles were added. Relative transduction rates compared to that for cells transduced in the absence of chloroquine were determined by flow cytometry analysis. (B) MV-pseudotyped LV particles (0.07 µg p24) and VSVG-LV (0.008 µg p24) were incubated with (+ FIP) or without (control) 200 µM FIP for 1 h at room temperature and then added to SK-OV-3 cells at an MOI of 0.3. The percentages of GFP-positive cells were determined by flow cytometry after 72 h and transduction rates relative to that obtained with untreated particles were calculated (n = 3; means ± SD are shown; *, $P < 0.05$; **, $P < 0.01$; ***, $P < 0.0001$; n.s., not significant by unpaired t test). (Rasbach et al, 2013)

As expected, chloroquine treatment of SKOV-3 cells reduced the transduction rate mediated by VSVG-LV substantially (Figure 20A). In contrast, the transduction mediated by $D^{9.29}$-LV and MV-LV was slightly but significantly enhanced in presence of chloroquine. The strongest effect was observed for 9.29-LV, were the relative transduction rate reached 200% after chloroquine treatment (Figure 20A). Possibly, blocking endocytosis allowed more virus particles to enter cells at the plasma membrane.

In order to show that F is actively taking part in the fusion process, the fusion inhibitory peptide (FIP) (Norrby, 1971; Richardson & Choppin, 1983) was applied to specifically block F. While FIP did not influence VSVG-LV-mediated gene transfer, which was expected since FIP cannot bind to any VSVG-LV component, it almost completely inhibited gene transfer of all three MV-pseudotyped particles (Figure 20B). These experiments clearly demonstrated that F is required for cell entry proving that at least one component of the MV glycoprotein complex is actively taking part in the fusion process.

One important question remained: Why is H needed although receptor attachment is mediated by a third protein? It has been shown in chapter 3.1.2.2 that w/o $H_{mut}\Delta 18$-LV was not able to transduce cells implying that presence of H is essential. Possible explanations could be that H is required as passive stabilizer of the MV glycoprotein complex or that it fulfills a mechanistic function during the fusion process. Therefore, the role of H in $D^{9.29}$-LV cell entry was assessed by applying neutralizing H-specific monoclonal antibodies (MAbs). The selected MAbs recognize conformational epitopes on H which have been roughly mapped by competition assays and mutational analysis of MV escape variants (Liebert et al, 1994; Moeller et al, 2001). Putative MAb binding sites as well as the mutations introduced in $H_{mut}\Delta 18$ to ablate the natural receptor usage are localized on the dimeric globular head domain of the H protein. MV-LV particles, which served as a positive control for the neutralizing activities of the MAbs, were completely neutralized in the presence of 0.1 µg of K71 or L77 and 1 µg of Nc32 or K29 (Figure 21A). In contrast, VSVG-LV was not affected by any of the four MAbs, thus excluding any interference with virus particle cell entry in general (Figure 21A). The strongest effect on $D^{9.29}$-LV was exerted by L77, whereas MAbs Nc32 and K29 impaired gene delivery of $D^{9.29}$-LV or 9.29-LV moderately. Remarkably, one of the MAbs, K71, was unable to neutralize both Her2/neu-targeted viruses (Figure 21A) which could be due to the ablation of its epitope in $H_{mut}\Delta 18$.

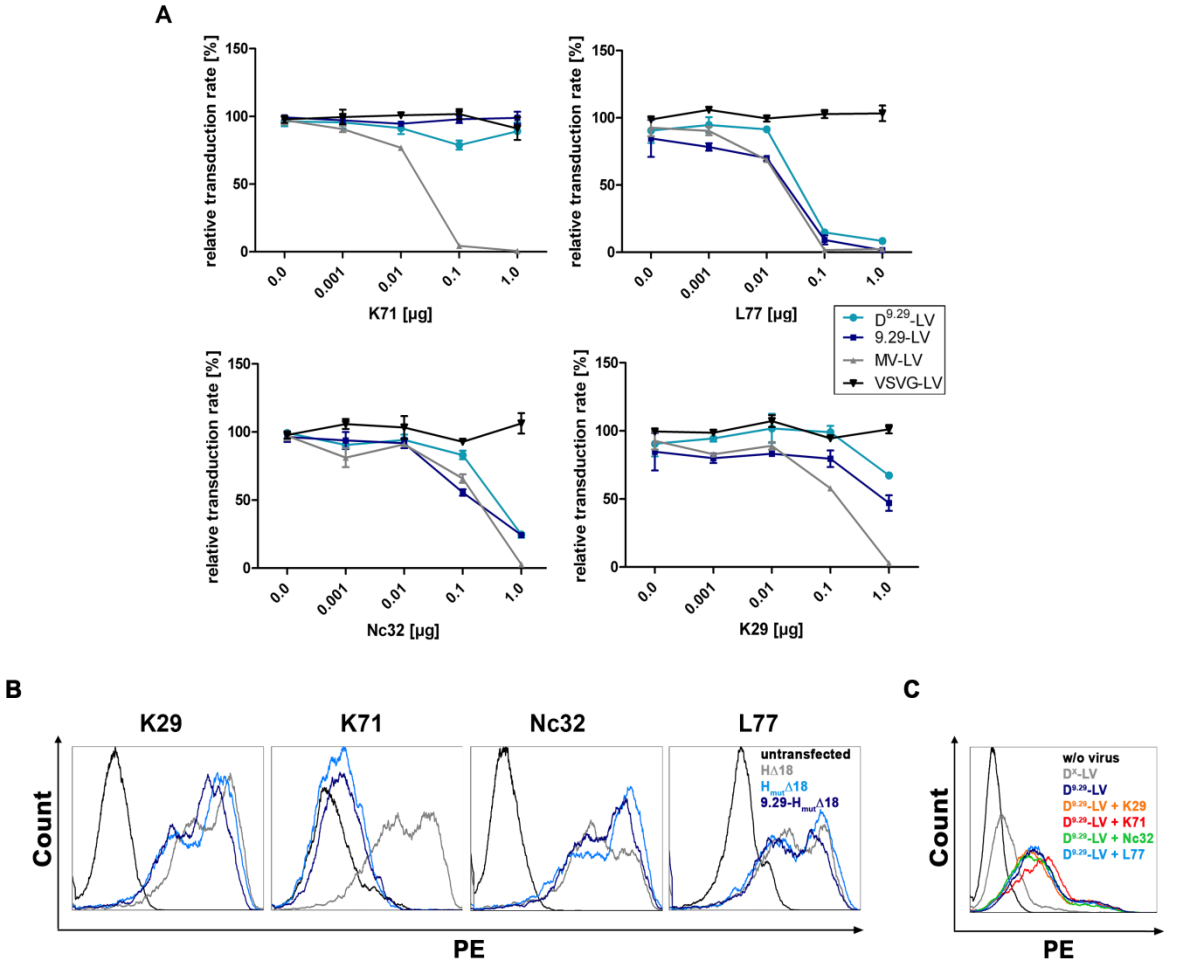

Figure 21: Neutralization of $D^{9.29}$-LV by H-specific monoclonal antibodies. (A) MV-pseudotyped LV (0.1 µg p24) and VSVG-LV (0.004 µg p24) particles were incubated with or without H-specific MAbs K71 (top left), L77 (top right), Nc32 (bottom left), and K29 (bottom right) for 1 h at room temperature and then added to SK-OV-3 cells at an MOI of 0.3. The percentages of GFP-positive cells were determined by flow cytometry after 72 h, and transduction rates relative to that obtained in the absence of MAbs were calculated (n = 3; means ± SD are shown). (B) HEK-293T cells (1×10^6) transiently transfected with pCG-HΔ18, pCG-H_{mut}Δ18, or pCG-H_{mut}Δ18-DARPin-9.29 were stained with K29, K71, Nc32, or L77. Secondary anti-mouse-PE was used for detection in flow cytometry. (C) Binding of virus particles to SK-OV-3 cells. $D^{9.29}$-LV was incubated with 1 µg K29, K71, Nc32, or L77 for 1 h at room temperature, and then SK-OV-3 cells were added and left for another hour. Samples were stained against the HA tag of particles using an anti-HA PE-coupled antibody. Cells incubated only with virus or virus displaying an attachment domain unable to bind to Her2/neu (D^X-LV) were used as positive and negative controls, respectively. Fluorescence of cell-particle complexes was analyzed using flow cytometry. (Rasbach et al, 2013)

To confirm that the inability of K71 to neutralize $D^{9.29}$-LV and 9.29-LV relies on the disruption of the antibody epitope in H_{mut}Δ18, cells expressing HΔ18, H_{mut}Δ18 or 9.29-H_{mut}Δ18 were stained with all four MAbs and flow cytometry was performed to determine potential differences in avidity.

As expected, only cells transfected with HΔ18 were recognized by K71. The mutated H variants showed signals comparable to that of untransfected cells (Figure 21B). K29, Nc32 and L77 bound all three H proteins with similar efficiencies whether it was mutated, fused to the DARPin or in its native form. These data prove that cell entry and transduction of $D^{9.29}$-LV can be inhibited by presence of H-specific neutralizing MAbs. But conceivably, this

neutralization could simply be due to interference with receptor attachment because of steric hindrance upon antibody binding. That in turn would not prove an active role of H in the virus cell fusion. To rule out steric hindrance as neutralization cause, a binding assay of $D^{9.29}$-LV to SK-OV-3 cells in presence of the MAbs was performed. None of the four MAbs impaired binding of $D^{9.29}$-LV particles to Her2/neu-expressing cells (Figure 21C). The fluoresecence signals were comparable to that of $D^{9.29}$-LV binding cells in absence of MAbs and clearly stronger than that of the negative control, cells incubated with virus displaying an attachment domain unable to bind to Her2/neu (D^{X}-LV). Thus, three of four tested MAbs neutralized $D^{9.29}$-LV to at least some extent without interfering with virus receptor attachment. $H_{mut}\Delta 18$ must therefore fulfill an essential role during cell entry of $D^{9.29}$-LV particles.

3.1.4 $D^{9.29}$-LV as a gene transfer vector

For the safe and successful use of viral vectors in gene therapy, the design of the vector has to meet a set of strict requirements. Ideally for *in vivo* applications, the transgene of choice is delivered precisely and efficiently into a target organ or cell population upon systemic administration. That MV-pseudotyped lentiviral vectors are able to target not only specific tissues but cells defined by a single surface marker *in vitro* and *in vivo*, as for example $CD8^+$ T lymphocytes, $CD105^+$ endothelial cells or $Her2/neu^+$ tumor cells, has been reported (Zhou et al, 2012; Abel et al, 2013; Münch et al, 2011).
In chapter 3.1.2.2 it was shown that $D^{9.29}$-LV was even more infectious and transduced Her2/neu cells more efficiently than 9.29-LV. Therefore, the potential of $D^{9.29}$-LV as a novel type of cell entry-targeted vector for gene transfer was assessed. First, vector production was optimized and then the ability to mediate stable gene transfer evaluated *in vitro*. Finally, targeting tumor cells *in vivo* was tested in a xenograft mouse model.

3.1.4.1 Optimizing $D^{9.29}$-LV production

One prerequisite for the application of viral vectors in *in vivo* gene therapy is to have high titers. Funke et al. (Funke et al, 2008) showed that the ratio of H and F-encoding plasmids in packaging cells can be optimized to increase LV titers. It is known that after infection with MV, cells produce less H than F mRNA (Cattaneo et al, 1987), suggesting that once production conditions are adjusted accordingly the release of infectious particles would be optimal. Moreover, LV particles displaying three different transmembrane proteins had not been described before.

Therefore, vector particle production was optimized in two consecutive steps. First, the amounts of F- and H-encoding plasmids were varied, and then, based on one of the optimal F-to-H ratios (5:3) (Figure 22A), the amount of pDisplay-$D^{9.29}$ plasmid was varied. In general, it was beneficial to transfect more pDisplay-$D^{9.29}$ than pCG-$H_{mut}\Delta18$ (Figure 22B), thus a ratio of 5:3:6 for F-, H-, and $D^{9.29}$-encoding plasmids was used for further vector production.

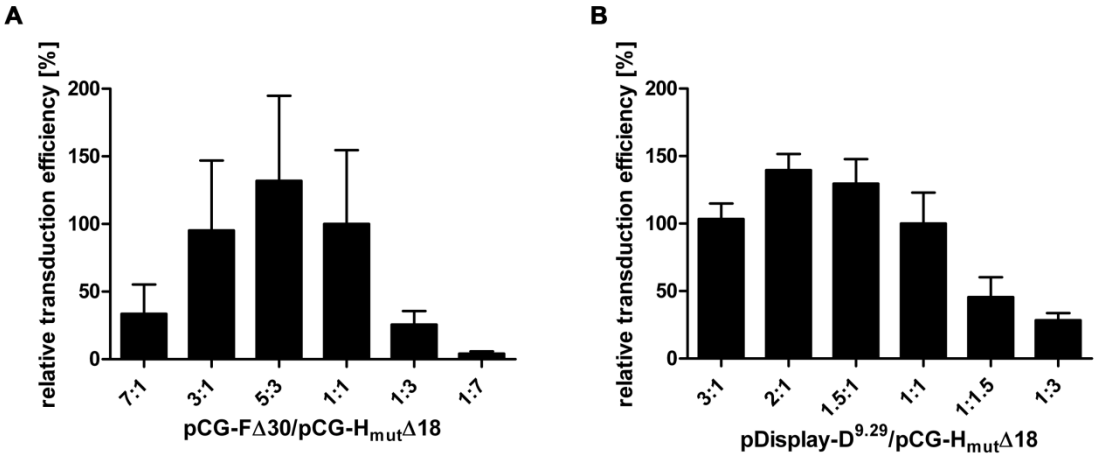

Figure 22: Optimizing $D^{9.29}$-LV production. Titers of $D^{9.29}$-LV stocks were optimized by (A) keeping the amount of pDisplay-$D^{9.29}$ constant and varying that of pCG-FΔ30 to pCG-H_{mut}Δ18 or (B) keeping the amounts of pCG-FΔ30 and pCG-H_{mut}Δ18 constant and varying that of pDisplay-$D^{9.29}$ for transfection of HEK-293T cells along with pCMVΔ8.91 and pSEW. For each ratio, pseudotyped vectors were titrated on SK-OV-3 cells and their relative titer normalized to that obtained after transfection of a 1:1 plasmid ratio (100%) is shown (n = 3; means ± SD are shown). (Rasbach et al, 2013)

3.1.4.2 $D^{9.29}$-LV mediates stable gene transfer

$D^{9.29}$-LV showed high titers on SK-OV-3 as well as CHO-Her2 cells. To confirm that gene transfer was long lasting and to exclude that observed titers were attributable to pseudotransduction, which means GFP protein transfer from the producer to the target cells, the sensitivity of $D^{9.29}$-LV and its control vector VSVG-LV towards a reverse transcriptase inhibitor was tested (Liu et al, 1996). A contribution of protein transfer to titers was well possible since it is known and was also observed for $D^{9.29}$-LV that during production of MV pseudotyped vector particles syncytia are formed. These multinucleated cells result from cell fusion and are prone to enhanced vesicle production and release. Formation of syncytia and, in late stages of vector production, cell death was especially pronounced for $D^{9.29}$-LV compared to 9.29-LV. In contrast to protein transfer which would be unaffected by reverse transcriptase inhibitors, treatment with 3'-azido-3'-deoxythymidine (AZT) inhibits the reverse transcription of the transfer vector in transduced cells and thereby prevents GFP expression.
SK-OV-3 cells were transduced with $D^{9.29}$-LV or as positive control VSVG-LV either in

presence or absence of 10 µM AZT. After three days cells were analyzed by flow cytometry and transduction was compared. In the presence of AZT, gene transfer rates dropped substantially to extents that were similar for both $D^{9.29}$-LV and VSVG-LV (Figure 23A).

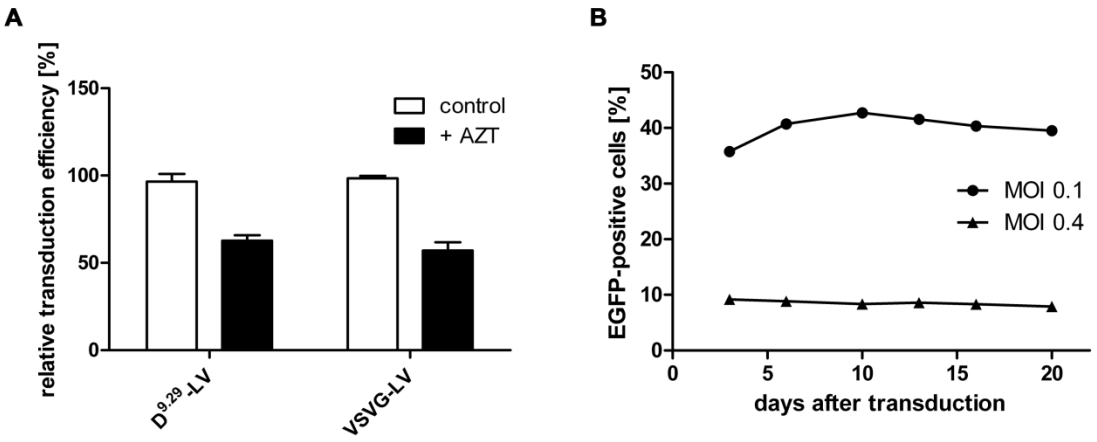

Figure 23: $D^{9.29}$-LV mediates stable gene transfer. (A) SK-OV-3 cells were transduced with $D^{9.29}$-LV or VSVG-LV in the presence or absence of 10 µM reverse transcriptase inhibitor azidothymidine (AZT) to verify that vectors mediated transgene integration. Relative transduction efficiency is shown (n = 3; means ± SD are shown; $P < 0.001$ by unpaired t test). (B) In order to demonstrate stable transduction, SK-OV-3 cells were cultivated for 20 days after transduction with $D^{9.29}$-LV at an MOI of 0.4 or 0.1. The percentage of EGFP-positive cells was determined at the indicated time points by flow cytometry analysis. (Rasbach et al, 2013)

To further verify that gene expression was stable, SK-OV-3 cells were transduced with $D^{9.29}$-LV at MOI 0.1 or 0.4 and the number of GFP-positive cells was determined over a period of 20 days. Constant levels of 10% or 40% GFP-positive cells were detected over the whole observation period.

Because $D^{9.29}$-LV was sensitive towards reverse transcriptase inhibition and able to mediate long lasting GFP expression, the data demonstrate stability of gene integration and that pseudotransduction was not the cause for observed high titers.

3.1.4.3 Tumor targeting of $D^{9.29}$-LV in a xenograft mouse model

After having demonstrated that $D^{9.29}$-LV transfers genes stably into receptor-positive cells, its *in vivo* targeting potential was assessed in a xenograft mouse model carrying a subcutaneously growing SK-OV-3 tumor. To follow tumor targeting by *in vivo* imaging and enabling the analysis of the distribution after systemic administration, vector particles were equipped with a *luciferase* reporter gene. CB17 SCID mice were subcutaneously injected with the Her2/neu-positive human cell line SK-OV-3 that has been proven to be susceptible for $D^{9.29}$-LV (chapter 3.1.2.2). Tumor growth was monitored until tumors had reached a volume of about

50 mm^3. Subsequently, $D^{9.29}$-LV or control particles pseudotyped with FΔ30 and H_{mut}Δ18 but devoid of $D^{9.29}$ (w/o $D^{9.29}$-LV^{luc}) were injected systemically through the lateral tail vein. Several time points after vector administration, mice were analyzed by *in vivo* imaging. $D^{9.29}$-LV^{luc} resulted in luciferase activity already 3 days after vector administration, which steadily increased over time in the SK-OV-3 tumor (Figure 24A). In contrast, even after 2 weeks no luciferase signals could be detected in the tumor tissue of w/o $D^{9.29}$-LV^{luc}-injected mice (Figure 24B).

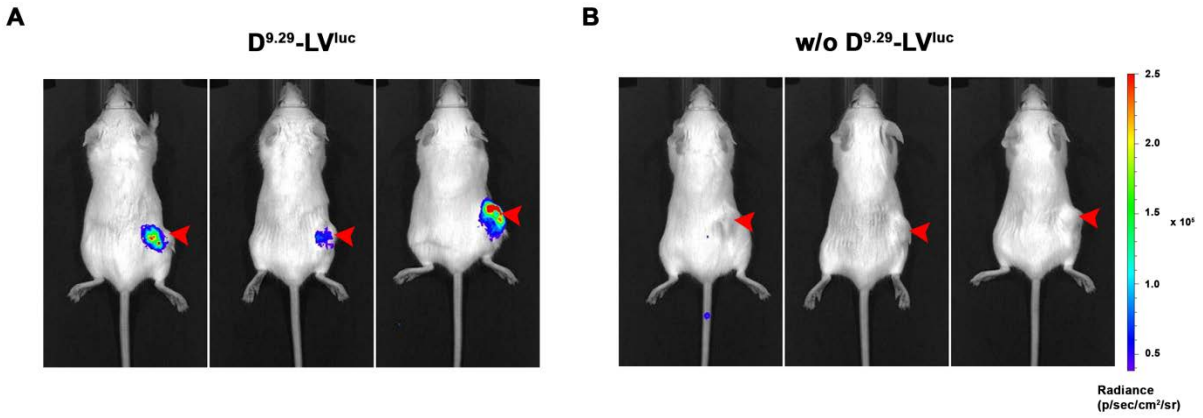

Figure 24: $D^{9.29}$-LV selectively targets Her2/neu-positive tumors *in vivo*. CB17 SCID mice were injected with 5×10^6 SK-OV-3 cells into the right flank (arrowheads). Once tumors had reached a volume of about 50 mm^3, $D^{9.29}$-LV^{luc} (8 µg p24) or w/o $D^{9.29}$-LV^{luc} (15 µg p24) was injected into the tail vein, and luciferase signals were analyzed by *in vivo* imaging 1 week later. Luciferase signal intensity is expressed as photons/second/square centimeter/steradian. (Rasbach et al, 2013)

Thus, it is clear that $D^{9.29}$-LV is directed to the tumor cells by $D^{9.29}$ and that in its absence an MV-pseudotyped lentiviral vector containing a receptor-blinded H is not able to specifically target SK-OV-3 cells *in vivo*.

3.2 Adeno-associated viral vector targeted to EpCAM-positive tumor cells

The human epithelial cell adhesion molecule (EpCAM) is a surface marker of normal epithelia, but it is also highly overexpressed in primary tumors and metastases of many epithelial tumors (Simon et al, 2013). In addition to its role in cell adhesion, EpCAM is a signaling molecule described to be involved in oncogenic pathways activating and engaging c-myc and Wnt signaling (Litvinov et al, 1994; Yamashita et al, 2007; Münz et al, 2004; Maetzel et al, 2009). In recent years, it has attracted a lot of attention in biomedical research due to reports that it is also expressed on cancer stem cells (CSCs) and ciruculating tumor cells (CTCs) (Dalerba et al, 2007; Pantel et al, 2008). These rare cell populations are difficult to track, modify and eventually destroy. Therefore, a viral vector directed against EpCAM

could be useful in basic research as well as therapeutic settings.

To this end, the recently described strategy to generate receptor-targeted AAV2-derived vector particles was employed (Münch et al, 2013). AAVs displaying EpCAM-specific DARPins were generated, characterized and tested for their capacity to detect rare tumor cells.

3.2.1 Generation and characterization of EpCAM-AAV

The successful incorporation of the Her2/neu-specific DARPin 9.29 into the AAV capsid was previously shown by Münch et al (Münch et al, 2013). Here, a fusion of the DARPin to the VP2 capsid protein of AAV2 was chosen. This site was selected because EGFP-VP2 fusion proteins were already described to be tolerated and did not interfere with viral assembly, packaging efficiency of the genome or infectivity (Lux et al, 2005). The same was true for Her2-AAV particles combined with an unprecedented capacity to target Her2/neu-positive tumor cells and to mediate safe gene transfer *in vitro* and *in vivo* (Münch et al, 2013).

Producing receptor-targeted AAV relies on an adenovirus helper free, four-plasmid transfection system. Naturally, a plasmid encoding the DARPin-VP2 fusion protein is essential. The sequence of the EpCAM-specific DARPin Ec1 (Stefan et al, 2011) was amplified by PCR using the primers DARPin-for and $DARPin_{corr}$-rev. Then, the PCR product was inserted into the *AgeI/BsrGI* digested pDARPin-9.29-VP2, thereby replacing the sequence of the Her2/neu-specific DARPin and resulting in pDARPin-Ec1-VP2, coding for Ec1 N-terminally fused to VP2. In this construct, the start codon for the VP2 protein was mutated to prevent expression of the unmodified VP2 protein (Figure 25). For expression of the other two capsid proteins VP1 and VP3 as well as the nonstructural proteins Rep78, Rep68, Rep52, Rep40 and AAP, the plasmid pRC-VP2ko was used. Of course, the same mutation as in pDARPin-VP2 disrupting the VP2 start codon was present in this construct. Additionally, both plasmids harbor mutations resulting in exchange of arginines 585 and 588 for alanines which prevent binding to the natural receptor HSPG (Kern et al, 2003; Opie et al, 2003; Boucas et al, 2009; Münch et al, 2013) (Figure 25).

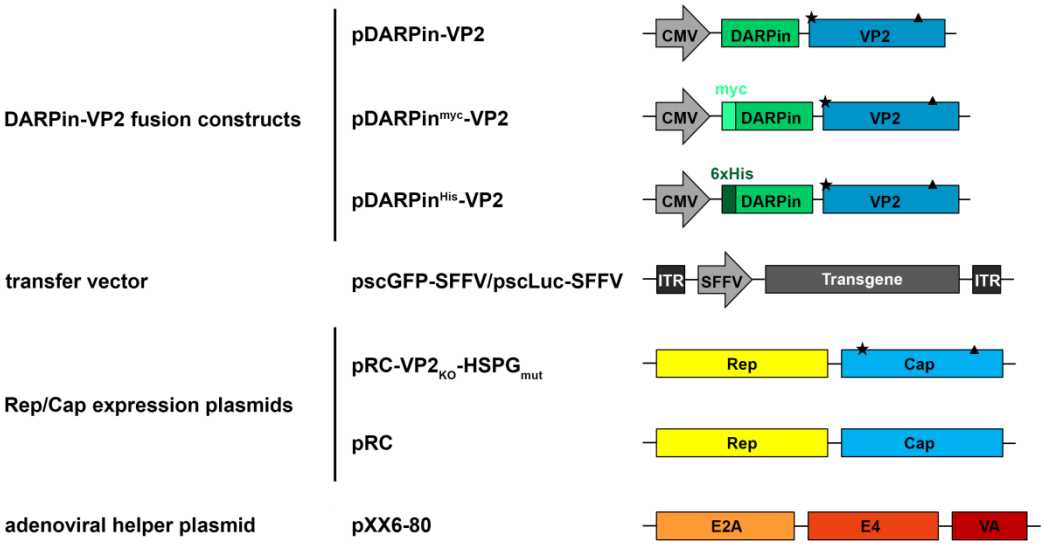

Figure 25: Schematic drawing of constructs used for AAV production. The transfer vector, the AAV2 plasmid pRC-VP2$_{KO}$-HSPG$_{mut}$, the adenoviral helper plasmid pXX6-80 and a pDARPin-VP2 construct shown here are required for production of targeted AAV vectors. Unmodified VP2 expression was prevented by mutating the VP2 start codons in pDARPin-VP2 and pRC-VP2$_{KO}$-HSPG$_{mut}$ (labeled by stars). For ablation of HSPG binding, two point mutations (R585A and R588A) were introduced (labeled by triangles). The unmodified pRC plasmid which is used for production of AAV2 encodes the AAV2 rep and cap proteins. Plasmid pXX6-80 provides the sequences for the essential adenoviral helper genes E2A, E4 and VA RNA necessary for AAV production. All transgenes were placed under control of the SSFV promoter and flanked by inverted terminal repeats (ITR). Immunological tags (myc and 6x His) of pDARPin^{myc}-VP2 or pDARPin^{His}-VP2 are indicated.

A minimal set of adenoviral helper genes are described to be sufficient for AAV production (Xiao et al, 1998). Transfection of HEK-293 or HEK-293T cells with pXX6-80 provides the required early adenoviral proteins E2A, E4 and VA RNA (Figure 25). As fourth plasmid, the transfer vector encoding the transgene under control of the SFFV promoter in self-complementary format (McCarty, 2008, Münch 2013) is needed. Upon co-transfection of these plasmids, AAV vector particles are produced and can be harvested and purified using iodixanol gradient purification.

3.2.1.1 EpCAM-specific DARPin can be incorporated into AAV particles

Besides particles presenting the EpCAM-specific DARPin Ec1 (EpCAM-AAV) (Stefan et al, 2011), Her2-AAV and AAV2 particles were generated as controls. In contrast to AAV2 particles, Her2-AAV is thought to present up to five DARPin molecules protruding from the five-fold symmetry axis. If Ec1 was successfully incorporated, resulting particles are assumed to look similar (Figure 26A).

One of the crucial prerequisites for gene transfer activity of receptor-targeted AAVs is the integrity of the virus capsid. Only if the fusion of DARPin-VP2 is not affecting virus assembly, infectious particles with high titers can be produced. Therefore, particles were

purified by iodixanol gradient centrifugation and then coated onto Nickel200 grids and stained with uranyl acetate to analyze virus morphology (Figure 26B). All three vector preparations revealed structurally intact particles in typical AAV shape. More importantly, not only empty vector particles which can be distinguished by the dark circle in their center but also genome-packaged (full) AAV particles were detected which indicates that infectious particles have been produced. In general, empty particles were overrepresented (data not shown) which is in accordance with data published for the Her2-AAV (Münch et al, 2013) as well as reports of a ten-fold excess of empty over genome-packaged AAV2 (Grimm et al, 1999; Drittanti et al, 2001; Sommer et al, 2003; Park et al, 2006).

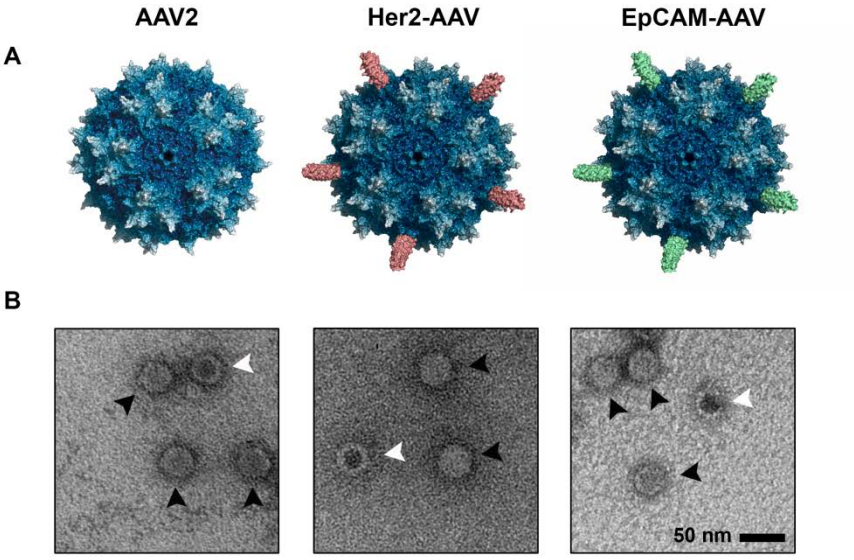

Figure 26: Incorporation of DARPins does not alter virus morphology. (A) Schematic illustration of AAV2, Her2-AAV and EpCAM-AAV particles. For surface exposure of the DARPin molecules (pink or green), the N-terminus of the VP2 protein has to be located at the pore complex. Illustrations were created using Pymol and PDB files 1LP3 (Xie et al, 2002) and 2XEE (Kramer et al, 2010) without exact modeling of the DARPin-AAV particle (Münch et al, 2013). (B) Electron micrographs of AAV particles. AAV2, Her2-AAV or EpCAM-AAV were coated on Ni200 grids and negative stained with uranyl acetate. Full and empty capsids are marked by black and white arrow heads, respectively. Micrographs were taken on a Zeiss EM109. Scale bar, 50 nm.

After having demonstrated that EpCAM-AAV exhibited AAV2-like morphology, vector particles were analyzed for their protein composition by western blot analysis. Capsid proteins of unmodified AAV2, Her2-AAV or EpCAM-AAV vector preparations were detected using the capsid-specific antibody B1. AAV2 structural proteins migrated according to their expected molecular weights of 90 kDa (VP1), 72 kDa (VP2) and 60 kDa (VP3) (Rose et al, 1971) (Figure 27A). Interestingly, vector particles harboring the two point mutations to abolish HSPG binding are described to migrate slower than the non-mutated proteins (Boucas et al, 2009; Münch et al, 2013) which was also true for Her2-AAV and EpCAM-AAV vector

preparations. The unmodified VP2 protein was absent in both targeting vector particles as a consequence of the mutated start codon. Instead, the DARPin-VP2 protein shifted to 89 kDa which overlaps with the VP1 protein. That the DARPin-VP2 band migrated at the same height as VP1 was demonstrated by western blot analysis of cell lysates from cells transfected with the plasmid encoding either VP1/Ec1-VP2/VP3 (Figure 27B, lane 1) or Ec1-VP2/VP3 (Figure 27B, lane 2).

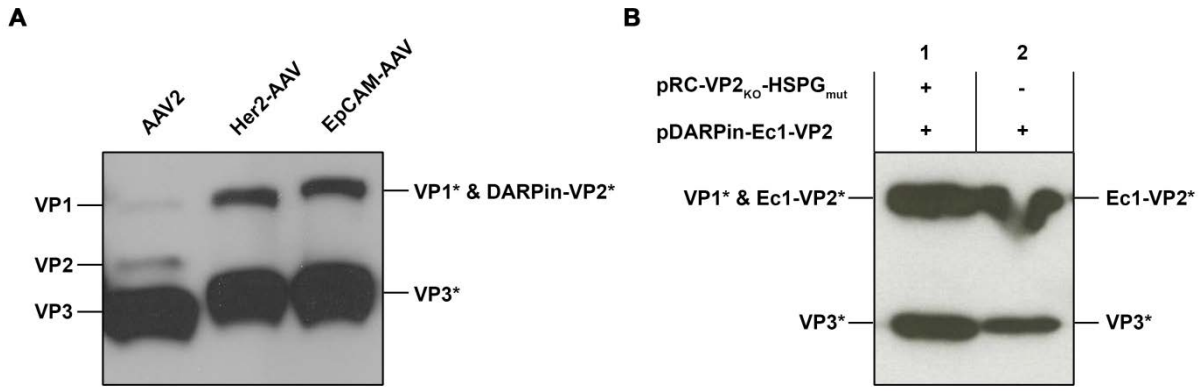

Figure 27: Western blot analysis of AAV vector particles and cell lysates. (A) Iodixanol gradient-purified vector particles were analyzed by western blot. Structural proteins of AAV2, Her2-AAV or EpCAM-AAV were detected using the capsid-specific antibody B1 recognizing a common epitope at the C-terminus of all three capsid proteins. (B) HEK-293T cells were transfected with pXX6-80, pscGFP-SFFV and the indicated plasmids. After 48 hours, cell lysates were prepared and analyzed by western blotting in co-operation with Prof. Dr. H. Büning (Köln). Structural proteins were detected using the capsid-specific antibody B1. VP variants with R585A and R588A mutations are marked by asterisks.

To show that EpCAM-VP2 was not only incorporated into vector particles but that the DARPin was also surface exposed, a myc-tag was fused to the N-terminal end of the Ec1 coding sequence using the primers Myc-for/DARPin$_{corr}$-rev. The amplified PCR product was inserted into the pDARPin-9.29-VP2 plasmid via *AgeI/BsrGI* replacing the Her2/neu-specific DARPin and resulting in the plasmid pDARPin-Ec1^{Myc}-VP2 (Figure 25). Subsequently, EpCAM^{Myc}-AAV particles were generated by replacing plasmid pDARPin-Ec1-VP2 with pDARPin-Ec1^{Myc}-VP2 for transfection.

EpCAM^{Myc}-AAV, Her2^{Myc}-AAV and AAV2 particles were incubated on ELISA plates pre-coated with anti-myc antibody and after several washing steps, bound particles were detected with the capsid specific antibody A20. Both, EpCAM^{Myc}-AAV and Her2^{Myc}-AAV, led to clear ELISA signals correlating with the number of applied vector particles (Figure 28). In contrast, no signals above background were detectable for the negative control AAV2. This assay proved that the myc-tag was accessible from outside the particle indicating that the DARPin was surface exposed as well.

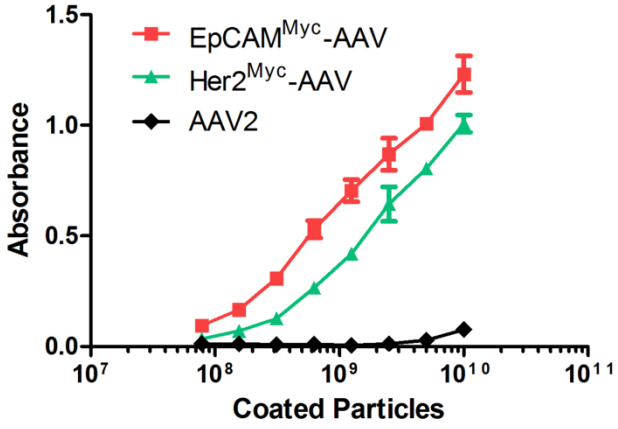

Figure 28: DARPin Ec1 displayed on the surface of AAV vector particles is accessible. Iodixanol gradient-purified AAV2, Her2^{Myc}-AAV or EpCAM^{Myc}-AAV vector preparations were bound to ELISA plates pre-coated with anti-myc antibody. After several washing steps, bound vector particles were detected using the capsid-specific antibody A20. AAV2 particles (not displaying a DARPin) served as negative control, Her2^{Myc}-AAV as positive control (n = 3; means ± SD are shown). (Münch et al, 2015)

After having demonstrated that AAVs presenting the EpCAM-specific DARPin were of AAV-like morphology and protein composition, one of the remaining concerns was the influence of the Ec1-VP2 fusion protein on the vector particle production. It was already shown in Figure 26 that genome-packaged AAVs were produced, but it was still unclear whether genomic titers were affected. Even small alterations in the AAV capsids are described to alter capsid to genome ratios und thus potentially impair packaging efficiency (Wu et al, 2000; Wu et al, 2006a).

For the analysis of EpCAM-AAV preparations, the number of genome packaged AAVs (genomic titer) was determined by qPCR as described previously (Theiss et al, 2003) using a primer pair specific for an *egfp* gene sequence (0.71 kbps) (Münch et al, 2013). As standard for quantification, defined copy numbers of the transfer vector pscGFP-SFFV were used. Genomic titers of EpCAM-AAV proved to be in the same range as that of unmodified AAV2 and were even slightly higher than that of Her2-AAV (Figure 29A).

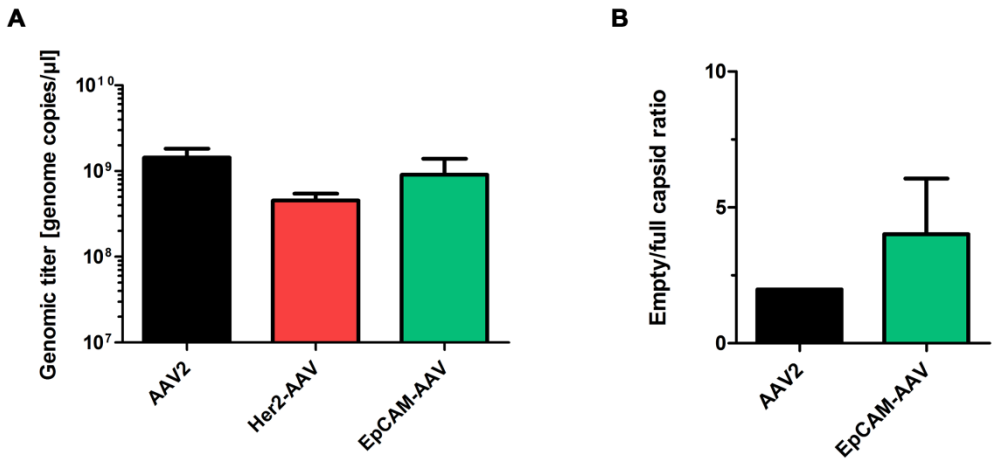

Figure 29: Ec1-VP2 fusion protein does not disturb particle production. (A) Genomic titers of AAV2, Her2-AAV and EpCAM-AAV were determined by qPCR detecting the *egfp* gene (n = 3; means ± SD are shown). (B) The number of vector particles was determined by capsid ELISA using the capsid-specific antibody A20 which recognizes a conformational epitope of assembled particles. The ratio between empty and genome-packaged (full) particles is shown (AAV2 n = 1; EpCAM-AAV n = 3; means ± SD are shown). (Münch et al, 2015)

To analyze the influence on the packaging efficiency, capsid titers were determined by sandwich ELISA (Grimm et al, 1999). Then, the ratio of total particles and genome-packaged particles reflecting the packaging efficiency can be determined. A ratio above 1 indicates an excess of empty over full particles, which is expected for recombinant AAV. The ratio for EpCAM-AAV was increased compared to AAV2 (Figure 29B). But it had been described previously that ratios below or equal to 50 are considered to be wild-type phenotype (Kern et al, 2003) suggesting that mutation of the HSPG-binding site as well as the Ec1-VP2 fusion protein had negligible effects on the capsid structure.

3.2.2 EpCAM-AAV is specific for human EpCAM

As demonstrated in the previous chapter, capsid integrity was not affected by the incorporation of the Ec1-VP2 fusion protein. Particles displayed the EpCAM-specific DARPin as described before for the Her2/neu DARPin.

AAV vector preparations were evaluated for their capacity to target receptor-positive cells. For this, the absence of off-targeting by ablation of the natural tropism as well as effective redirection and binding to the receptor of choice are essential.

3.2.2.1 Selective transduction of receptor-positive cells by EpCAM-AAV

To assess if the incorporation of the DARPin in combination with introduction of the two point mutations to ablate HSPG binding equipped the EpCAM-AAV with a restricted tropism for EpCAM$^+$ cells, transduction of receptor-positive and -negative cell lines was performed. As EpCAM-positive cells the breast cancer cell lines MDA-MB-453 and MCF-7 were used. The glioblastoma cell line LNT-229 served as negative control. The EpCAM expression pattern was confirmed by flow cytometry (Figure 30A).

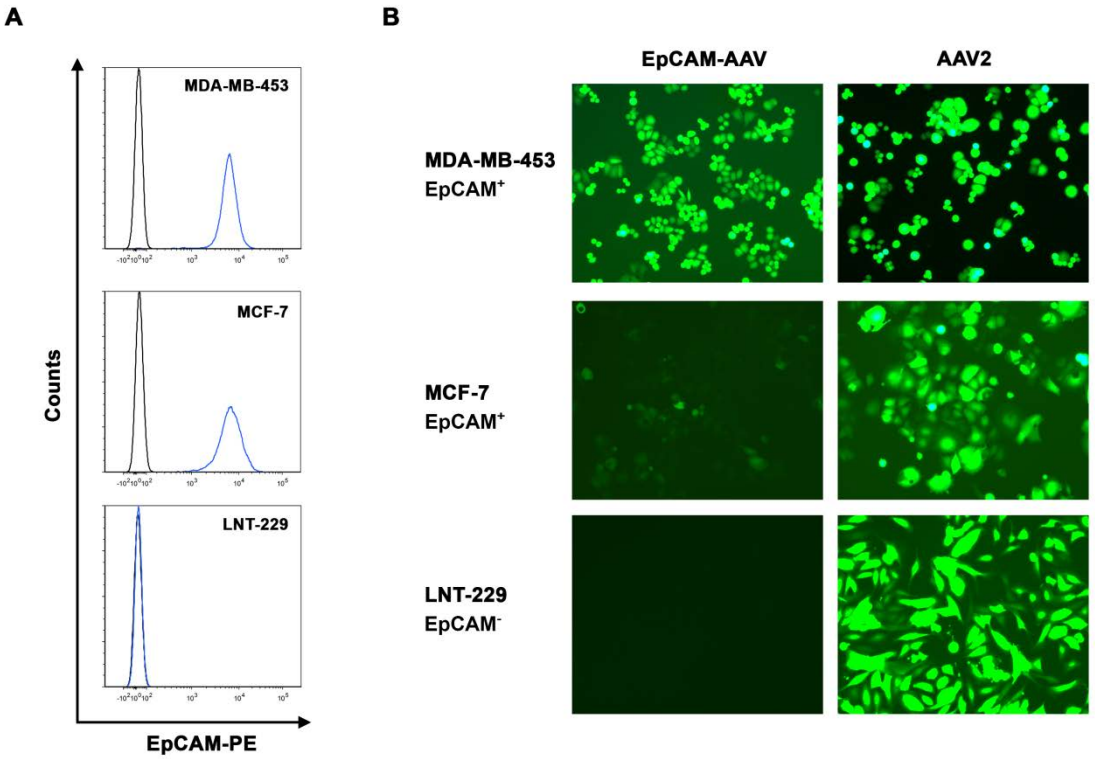

Figure 30: EpCAM-AAV specifically transduces EpCAM-positive cells. (A) EpCAM expression level of the indicated cell lines was determined by flow cytometry using the EpCAM-specific antibody anti-CD326-PE. (B) EpCAM-positive (MDA-MB-453 and MCF-7) and EpCAM-negative cells (LNT-229) were transduced with EpCAM-AAV or AAV-2 (GOI = 70,000). 48 h after transduction cells were analyzed by fluorescence microscopy. (Münch et al, 2015)

Two days after transduction of all three cell lines with either EpCAM-AAV or the unmodified AAV2 as control vector, GFP expression was assessed by fluorescence microscopy. EpCAM-AAV exclusively transduced MDA-MB-453 and MCF-7 cells but not the receptor-negative LNT-229 cells, whereas transduction with AAV2 resulted in GFP expression in all three cell lines (Figure 30B). In general, AAV2 transduced cells more efficiently than EpCAM-AAV when the same GOI was applied. This might be due to the fact, that not all genome-packaged EpCAM-AAVs necessarily incorporated the Ec1-VP2 fusion protein. It is described that only VP1 and VP3 capsid proteins can give rise to intact AAV particles. If this holds true for

EpCAM-AAV preparations, particles not able to bind to EpCAM or HSPG were present during transduction but do not contribute to gene transfer. These data confirm that EpCAM-AAV exhibits the desired receptor specificity.

3.2.2.2 EpCAM-AAV binds to human but not mouse EpCAM

In chapter 3.2.2.1 the specificity of EpCAM-AAV for receptor-positive human cells has been proven. But among different species, the amino acid sequence of EpCAM is highly conserved. Antibodies raised against the human EpCAM protein showed cross-reactivity against the homologous proteins in mice, rats and non-human primates (Zaloudik et al, 1997). The murine EpCAM shows 81% homology to its human counterpart as determined by alignment of protein sequences using Clustal Omega (Sievers et al, 2011; Goujon et al, 2010; McWilliam et al, 2013), which makes it a good candidate as DARPin Ec1 binding partner. To evaluate whether EpCAM-AAV was not only EpCAM-specific but also restricted to bind only the human protein, competition experiments were performed using the soluble form of the extracellular domains of human und murine EpCAM. AAV2 or EpCAM-AAV particles were incubated with increasing concentrations of recombinant protein and subsequently used to transduce MDA-MB-453. Transduction by EpCAM-AAV decreased only in presence of human but not mouse EpCAM, while no effect was observed for AAV2 particles pre-incubated with both forms of the soluble receptor (Figure 31). Competition with the extracellular domain was clearly dose-dependent

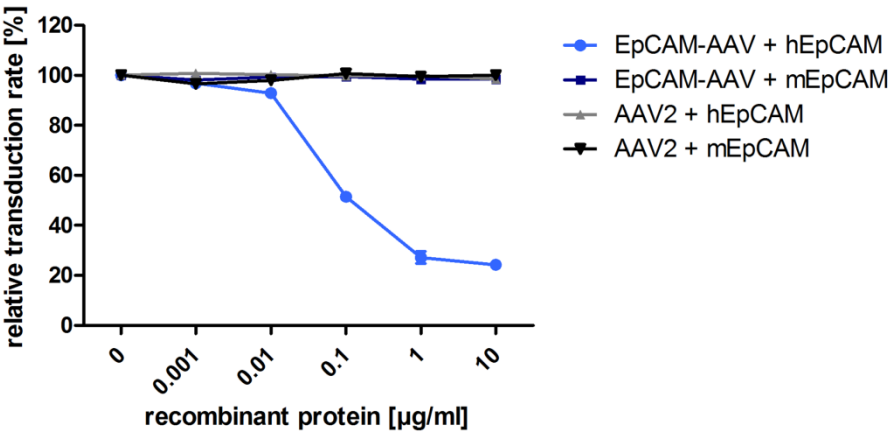

Figure 31: Transduction mediated by EpCAM-AAV is human EpCAM dependent. EpCAM-AAV (GOI=10,000) was incubated for 1 h at 4°C with increasing amounts of the entire extracellular domain of human (hEpCAM) or murine EpCAM (mEpCAM) as competitor. Following incubation, MDA-MB-453 cells were transduced and analyzed for GFP expression by flow cytometry 72 h post transduction. AAV-2 (not displaying a DARPin) (GOI 350) served as control. Data are normalized to the transduction efficiency measured without preincubation with recombinant protein (n = 3; means ± SD are shown). (Münch et al, 2015)

Accordingly, EpCAM-AAV was able to distinguish between the human and murine EpCAM protein. Its specificity for human EpCAM and the selective transduction was further confirmed by this competition experiment.

3.2.2.3 Transduction efficiency is receptor density-dependent

In the previous chapters, EpCAM-AAV has been proven to specifically transduce receptor-positive cells. But transduction of cells is not an experiment with a simple binary outcome. The efficiency may be dependent on vector properties such as titer or avidity for its receptor but it might also be influenced by cell characteristics as for example the receptor density. That efficient transduction mediated by receptor-targeted vectors depends on the target receptor density was not only shown for Her2/neu-targeted LVs (Münch et al, 2011) but also for Her2/neu-targeted AAVs (Münch et al, 2013), using a panel of CHO cells expressing the human Her2/neu protein with different densities.

Therefore, the cDNA sequence of human EpCAM (NCIB reference sequence NM_002354) was cloned into the pS-EGFP-I-puro-W transfer vector resulting in the bicistronic plasmid pS-hEpCAM-I-puro-W. In this construct both reading frames are linked by an internal ribosome entry site (IRES) which allows protein synthesis of the second gene product from a translation initiation site within the messenger RNA.

A VSVG-pseudotyped lentiviral vector packaging the hEpCAM-I-puro sequence was produced. After transduction of CHO-K1 cells, cells were put under selection pressure using puromycin for two weeks. The resulting CHO-EpCAM bulk cell population was stained for EpCAM expression and single cells were sorted. Screening of 30 single clones revealed cells expressing low, medium and high levels of EpCAM (Figure 32A).

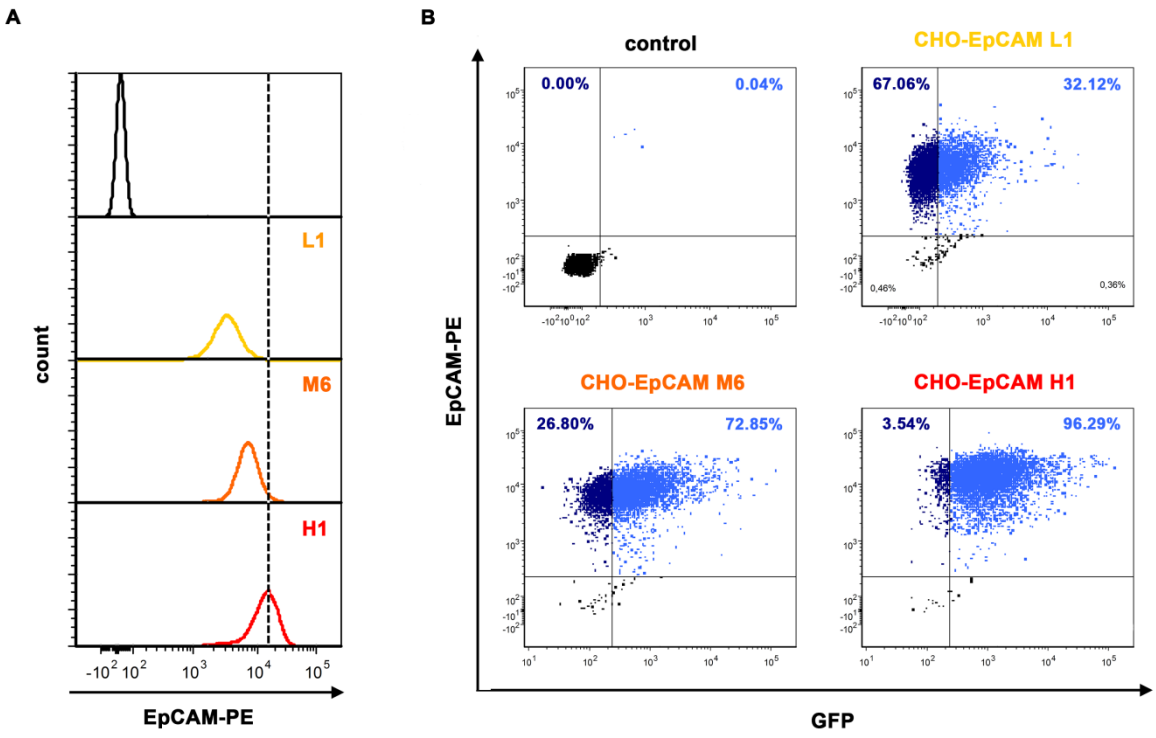

Figure 32: Receptor density influences transduction efficiency of EpCAM-AAV. (A) EpCAM expression of stably transduced CHO-EpCAM cell clones. CHO-K1 cells were transduced with a VSVG-pseudotyped lentiviral vector transferring the genes for human EpCAM and puromycin resistance. After selection of puromycin resistant cells, the bulk population was stained using an anti-EpCAM-PE antibody and single clones were obtained by fluorescence-activated cell sorting. After cultivation and fluorescence cytometry, a low (L1), medium (M6) and high (H1) EpCAM-expressing cell clone was chosen. Histograms are shown. Parental CHO-K1 cells (black) were used as negative control. (B) CHO-EpCAM clones L1, M6 and H1 were transduced with EpCAM AAV (GOI=80.000) and analyzed 72 h later for EGFP expression and EpCAM expression. Untransduced and unstained cells are shown as control.

The single cell clones CHO-EpCAM L1, M6 and H1 were transduced by EpCAM-AAV particles and analyzed for GFP and EpCAM expression three days later. Although all three clones were 100% EpCAM-positive and readily transduced, the strongest transduction efficiency was observed on CHO-EpCAM H1 cells, representing the highest target receptor expression of all three cell lines (Figure 32B). Here, almost all cells were GFP-positive whereas only 73% CHO-EpCAM M6 and 32% CHO-EpCAM L1 cells were transduced. These data prove that transduction mediated by EpCAM-AAV is clearly dependent on receptor density.

3.2.3 DARPin usage is flexible

In the previous chapters it was shown that the generation of EpCAM-targeted AAV vector particles was successful. Transduction of cell lines exclusively relied on the attachment of the EpCAM-specific DARPin Ec1 to its receptor. Ec1 evolved from the DARPin EPh1 which was selected by SRP phage display from a library using the biotinylated extracellular domain

of EpCAM as target (Stefan et al, 2011). Another available EpCAM-specific DARPin called Ac1 was selected by ribosome display and descended from DARPin C9 (Winkler et al, 2009) (Table 3). Both parental DARPins were subjected to directed evolution using error-prone PCR followed by new rounds of off-rate selection using ribosome display in solution to improve their affinities (Stefan et al, 2011). Additionally, a C-cap designed to be more stable (Interlandi et al, 2008) was introduced.

Table 3: Applied EpCAM-specific DARPins.

	Ec1[c]	**Ac1**[c]
K_D (nmol/l)[a]	0.068	0.12 & 75[d]
DARPin type[b]	N3C	N3C
Selection method	SRP phage display	Ribosome display

[a] Dissociation constant, [b] Number of ankyrin repeats; N represents the N-capping repeat, internal binding repeats are indicated by numbers, C represents the C-capping repeat, [c] (Stefan et al, 2011), [d] biphasic dissociation

The Ac1 coding sequence was amplified by PCR using the primer pair DARPin-for/DARPin$_{corr}$-rev and was subsequently inserted into the *AgeI/BsrGI* digested pDARPin-Ec1-VP2 plasmid, thereby replacing the Ec1 coding sequence. The resulting pDARPin-Ac1-VP2 and pDARPin-Ec1-VP2 were used to produce three independent Ac1-AAV and Ec1-AAV (elsewhere termed EpCAM-AAV) small scale vector preparations. Vector particles were not iodixanol gradient-purified and instead cleared lysates were used for analysis of genomic titers and transduction efficiency.

Genomic titers for both vector types were in the same range of about 10^8 genome copies/µl but titers of Ac1-AAV were slightly but significantly lower than Ec1-AAV titers (Figure 33A).

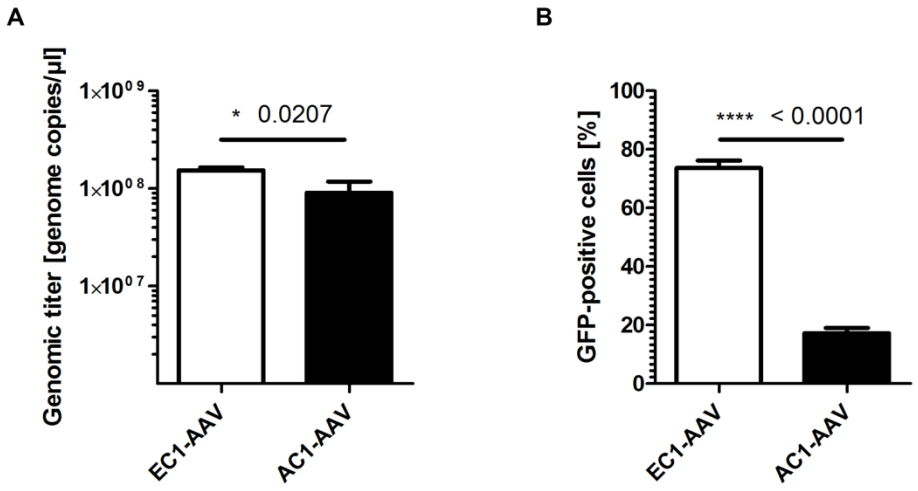

Figure 33: Ec1 is better suited as targeting ligand for AAVs than Ac1. (A) Genomic titers of AAVs displaying the EpCAM-specific DARPin Ec1 (Ec1-AAV) or Ac1 (Ac1-AAV) were determined by qPCR detecting the *egfp* gene (n = 3; means ± SD are shown). (B) CHO-EpCAM bulk cells were transduced with Ec1-AAV or Ac1-AAV (GOI = 62.5000) and percentage of GFP-positive cells was determined by flow cytometry 72 h later (n = 3; means ± SD are shown; *, $P < 0.05$; ****, $P < 0.0001$; by unpaired t test).

For the evaluation of the gene transfer efficiency, CHO-EpCAM cells were transduced with equal genomic copy numbers of Ec1-AAV or Ac1-AAV and analyzed three days later by flow cytometry. Remarkably, Ec1-AAV transduced up to 75% of all cells whereas Ac1-AAV was only able to mediate gene transfer into 20% CHO-EpCAM cells (Figure 33B). This result was highly significant and indicated that DARPin Ec1 was better suited for retargeting AAVs than DARPin Ac1.

Nevertheless, DARPin Ac1 can be used to retarget AAV vector particles although Ec1-AAV performed better. For this reason, Ec1-AAV was used in all further experiments.

3.2.4 Affinity purification of EpCAM-AAV

As a result of an expanded application and a growing selection of viral vectors in biomedical research and gene therapy, sophisticated purification methods need to be implemented to ensure quality, efficacy and safety of the product. Chromatography-based methods such as gel filtration, ion-exchange and affinity chromatography have become well-established in the field of AAV vector development. These techniques enable purification of large-scale productions but are also used to remove possible contaminants or byproducts.

In order to separate DARPin-displaying from -deficient AAV particles, the DARPin-VP2 has to have a His tag at the N-terminus of the DARPin to allow immobilized metal ion affinity chromatography (IMAC). The principle of this purification method is based on the formation of chelate complexes between the hexa-histidine tag of the vector particle and the nickel ions

of the stationary phase. This interaction results in retention of DARPin-displaying AAVs and flow through of DARPin-deficient particles. By competition of binding to the nickel ions using the aromatic heterocycle imidazole, the DARPin-displaying vector particles can then be eluted. The combination of iodixanol gradient purification to remove empty particles and subsequent IMAC to enrich DARPin-displaying AAVs (Figure 34) is the key to not only prevent off-targeting *in vivo* but also to enhance gene delivery efficiency (Münch, 2013).

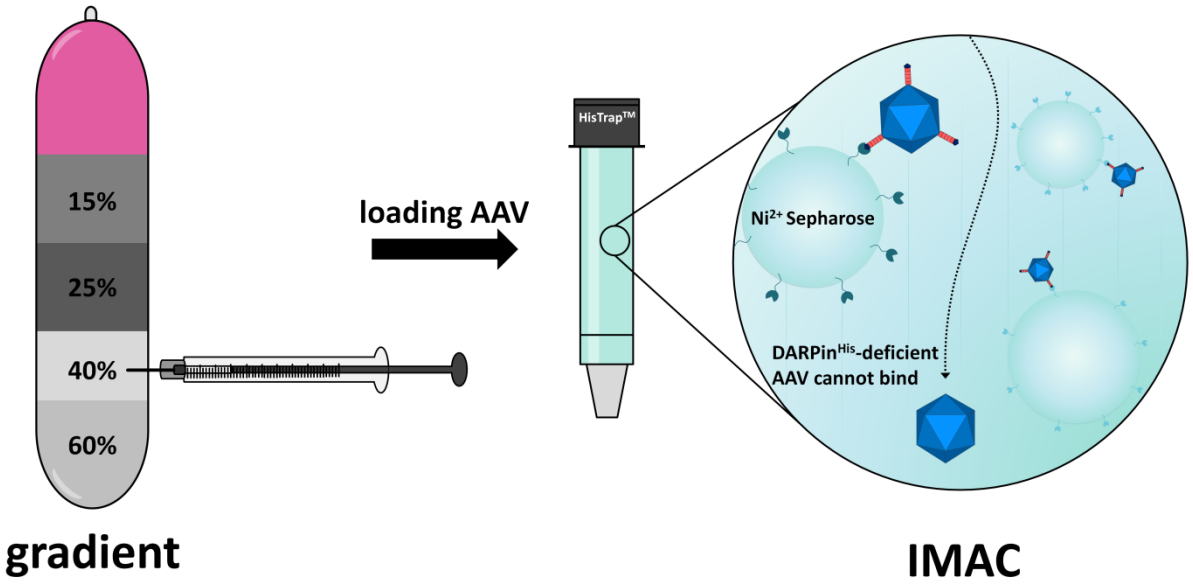

Figure 34: Separation of DARPin-displaying from DARPin-deficient vector particles. Schematic drawing of the two-step procedure including density gradient centrifugation followed by immobilized metal ion affinity chromatography (IMAC), which separates DARPin-displaying AAV particles carrying a hexa-histidine-tag at the N-terminus of the DARPin from DARPin-deficient particles. (Münch et al, 2015)

The same two-step purification procedure was applied to EpCAM-AAV and its transferability as well as potency of purified particles was evaluated.

3.2.4.1 Analysis of IMAC-purified EpCAM-AAV

In order to affinity purify EpCAM-AAV, the Ec1-VP2 fusion protein had to be equipped with a hexa-histidine tag. Therefore, the Ec1 coding sequence was amplified by PCR using the primers His-for and $DARPin_{corr}$-rev. The PCR product was inserted into the *AgeI/BsrGI* digested plasmid pDARPin-Ec1-VP2, resulting in the plasmid pDARPin-$Ec1^{His}$-VP2. This construct gives rise to the Ec1-VP2 fusion protein with the His tag fused to the N-terminal end of the DARPin molecule (Figure 25). The same position was used for the myc tag in

chapter 3.2.1.1 indicating that this was well tolerated for capsid assembly. For the production of EpCAM^{His}-AAV particles the already described production system (3.2.1) was used.

To set up the IMAC purification of EpCAM^{His}-AAV, several parameters had to be determined such as binding conditions, flow rate and retention time. The purification protocol for Her2^{His}-AAV particles was used as starting point (Münch, 2013). Iodixanol gradient-purified EpCAM^{His}-AAV particles were diluted in binding buffer containing 20 mM imidazole to prevent unspecific binding to the HisTrap column. Loading of vector particles to the equilibrated column was performed at 0.1 ml/min using a HPLC system to allow slow binding and complex formation. Monitoring of absorbance at 280 nm revealed a high peak upon vector particle loading and subsequent decline during washing phase (Figure 35A). The elution conditions of EpCAM^{His}-AAV were determined by performing a linear elution gradient from 20-500 mM imidazole. Analysis of collected fractions revealed that functional EpCAM^{His}-AAV vector particles started to elute at an imidazole concentration of 250 mM (data not shown). To stringently elute DARPin-displaying particles within only a few fractions, a step gradient was used. After loading of particles and subsequent washing with 20 mM imidazole, a single elution step with 300 mM imidazole for five column volumes followed by washing with 500 mM imidazole was performed (Figure 35B). Unfortunately, the imidazole used in these experiments was UV-active, resulting in strong absorbance upon increase of imidazole concentration to 300 or 500 mM. Eventually, signals arising from eluted vector particles could be superimposed by imidazole signals. Thus, further analysis of collected fractions for content of AAVs was obligatory.

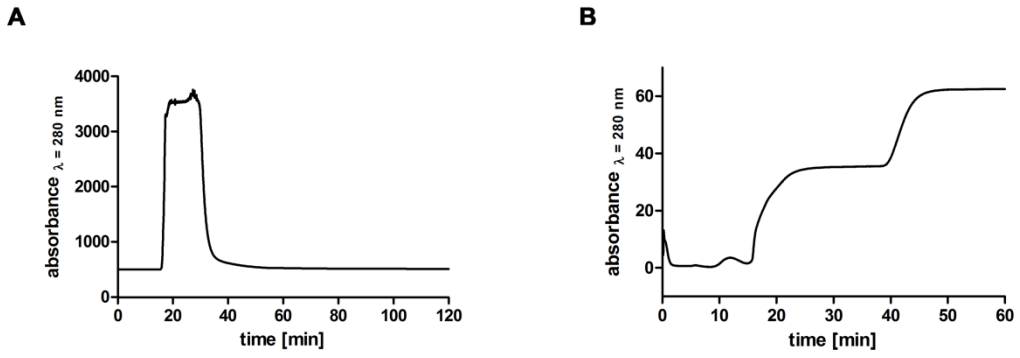

Figure 35: Step gradient affinity purification of EpCAM^{His}-AAV. (A) Vector particles were diluted in binding buffer containing 20 mM imidazole and loaded onto a HisTrap column (min 15-30) using a HPLC system. The column was washed with 15 column volumes binding buffer. (B) AAV vector particles were eluted from the column using buffer containing 300 mM imidazole (min 15-40) followed by final elution with buffer containing 500 mM imidazole (min 40-60). Representative absorbance profiles of vector particle loading (A) and elution (B) are shown.

Collected fractions were analyzed by dot blot using the capsid-specific antibody B1. Strong signals were detected for the loading fractions which was well in accordance with the loading profile. The most prominent signal intensities were observed for fractions 7-10 (Figure 36A). In contrast, no capsid signals were detected in the washing fractions and only 3 dots (51-53) appeared in the elution fractions. Although these signals were comparably weak and faint, it seemed that eluted particles were at least concentrated in only a few fractions (Figure 36A) and correlated with the corresponding elution profile.

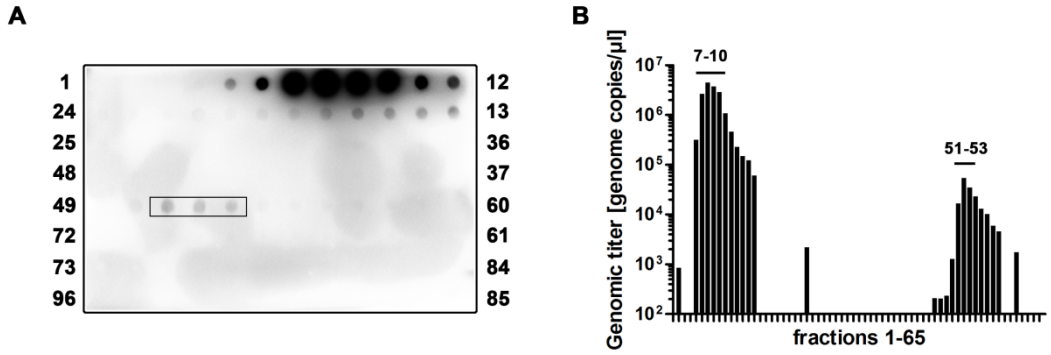

Figure 36: IMAC purification of EpCAM^{His}-AAV. (A) 80 fractions collected during column loading (1-10), washing (11-49) and elution (50-80) were analyzed by dot blot using the capsid protein specific antibody B1. Fractions were loaded in alternating order from top-left to bottom-left. Elution fractions (51-53) with the strongest signals are indicated. (B) Genomic titers of corresponding fractions were determined by qPCR detecting the *egfp* gene. Loading (7-10) and elution (51-53) fractions with the strongest signals are indicated.

Based on the dot blot results, a few fractions were selected and genomic titers were determined by qPCR using *egfp*-specific primers. Pre-loading fraction 3 was used to determine the background of the experiment which was around 10^3 genome copies/µl. Only slightly higher values resulted from washing fractions indicating that they did not contain a relevant number of AAV particles. Loading fractions 7-10 revealed to have the highest titers whereas elution fractions 51-53 had at least 10-fold lower genomic titers (Figure 36B). This discrepancy was expected since dot blotting already revealed a vast excess of capsids in the loading fractions.

Due to very high imidazole concentrations in higher number fractions and the fact that this was not very well tolerated by cells (data not shown), only fractions 1-65 were used to transduce CHO-EpCAM cells. Flow cytometry analysis revealed, that similar if not higher transduction was achieved when the same volume of elution fractions 51-53 was used to transduce cells than with loading fractions 7-10 (Figure 37A). Combined with data obtained from qPCR, this clearly showed that eluted particles were more infectious although they had significantly lower titers. In accordance with previous AAV IMAC experiments, it is safe to

assume that particles in fractions 51-53 were displaying the Ec1 DARPin and therefore bound to the HisTrap column and were able to specifically transduce EpCAM-positive cells. A considerable amount of AAVs in loading fractions 7-10 contained a genome but were most likely DARPin-deficient and could not transduce CHO-EpCAM cells.

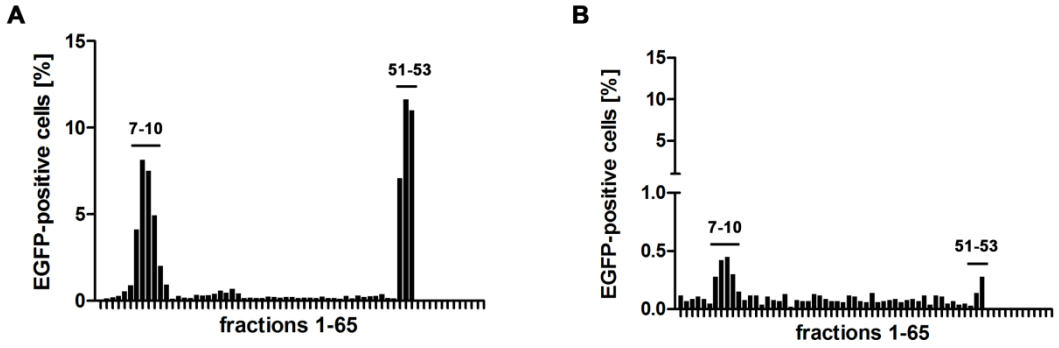

Figure 37: IMAC-purified EpCAM^{His}-AAV transduces receptor-positive cells. 20 µl of the collected fractions of EpCAM-AAV IMAC purification were used to transduce (A) CHO-EpCAM or (B) CHO-K1 cells. Cells were analyzed 72h later for EGFP expression. Only the first 65 fractions were included to avoid to high imidazole concentrations killing the cells. Eventually, only in fractions 1-53 were enough cells alive to analyze EGFP expression. Loading fractions 7-10 and elution fractions 51-53 are indicated.

Nevertheless, the transduction that was observed for loading fractions 7-10 was either based on unspecific transduction of VP1/VP3-only particles or these fractions still contained EpCAM^{His}-AAV, implying that not all vector particles were able to bind to the HisTrap column. For clarification, receptor-negative CHO-K1 cells were transduced with 20 µl of the same fractions as before. In case transduction was due to unspecific VP1/VP3-only particle cell entry, the same transduction efficiency as on CHO-EpCAM cells would be observed on CHO-K1 cells. But EGFP expression 72 hours after transduction was negligible for all fractions. If at all, slightly higher transduction efficiency in the range of 0.5% was observed for loading fractions 7-10 (Figure 37B). Thus, transduction of CHO-EpCAM cells with loading fractions must have been caused by DARPin-displaying EpCAM^{His}-AAV particles that were not able to bind to the column. This indicates that although it was possible to purify EpCAM^{His}-AAV using IMAC, the procedure was still not as efficient as described for Her2^{His}-AAV (Münch, 2013). One possible explanation might be, that the His tag interacts with the modified C-cap or the ankyrin repeats of the Ec1 DARPin preventing efficient binding to the HisTrap column. To further improve the purification, column binding conditions could be modified to be less stringent and to allow more AAV particles to bind.

3.2.4.2 Enhanced transduction of purified EpCAM^{His}-AAV

Analysis of IMAC-purified EpCAM^{His}-AAVs had demonstrated that particles were able to bind the column material and were still infectious and specifically transduced EpCAM-positive cells. Although AAV vector particles are inherently more stable and less affected by storage conditions such as pH, salt concentrations and temperature compared to the enveloped lentiviral vectors, downstream processes of AAV IMAC purification must ensure their integrity. In addition, buffer conditions were already shown to be critical for transduced cells which might be especially pronounced for primary material and *in vivo* applications. Therefore, respective elution fractions were pooled and dialyzed against PBS to get rid of high salt and imidazole concentrations. In parallel, the same procedure was performed for EpCAM^{His}-AAV that was only iodixanol-gradient but not IMAC purified.

Resulting vector particle suspensions were analyzed by qPCR and an equal number of genome copies were used to transduce MDA-MB-453 or CHO-EpCAM cells. In general, transduction efficiency on MDA-MB-453 cells was higher than on CHO-EpCAM cells (Figure 38).

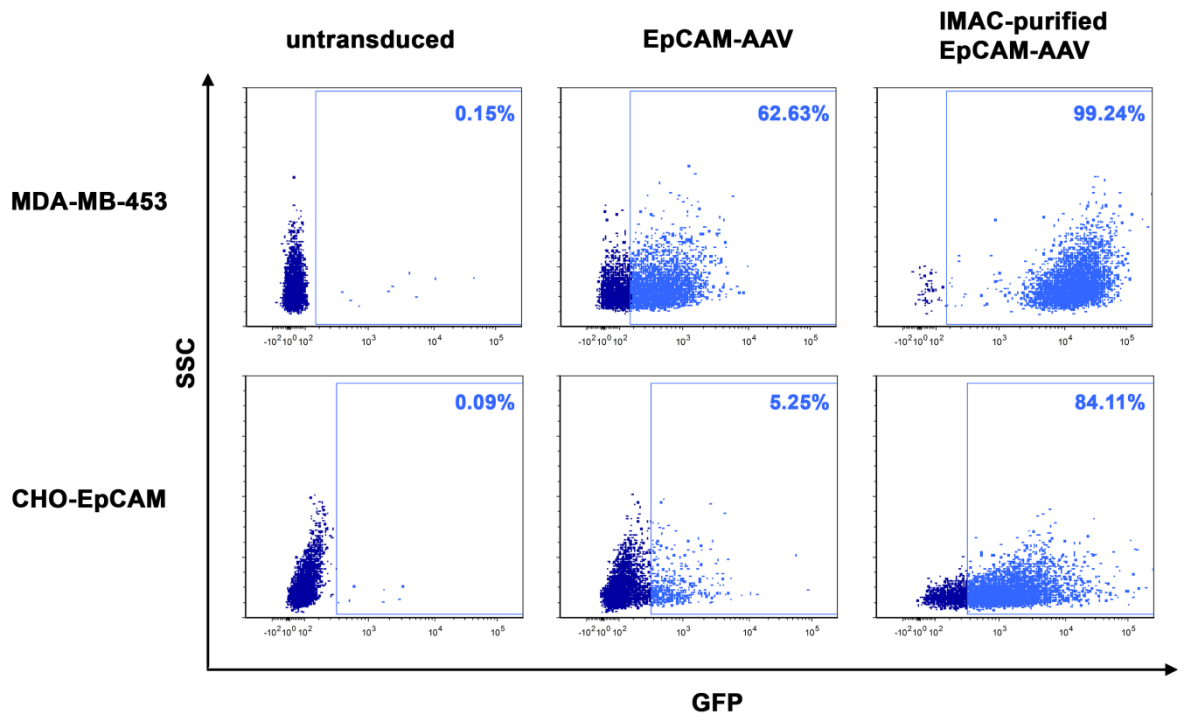

Figure 38: IMAC purification enhances EpCAM-AAV-mediated transduction. (A) MDA-MB-453 or (B) CHO-EpCAM cells were transduced with conventionally purified EpCAM^{His}-AAV or IMAC-purified EpCAM-AAV (GOI 60,000, each) or were left untransduced. Transgene expression was analyzed by flow cytometry 72 h post transduction as a measure of transduction. (Münch et al, 2015)

Remarkably, transduction was strongly enhanced with IMAC-purified EpCAM^{His}-AAV. Percentage of GFP-expressing cells increased from 63% to 99% and the same tendency was true for the mean fluorescent intensity of MDA-MB-453 cells. Transduction with conventionally purified EpCAM^{His}-AAV resulted in only 5% of GFP-positive CHO-EpCAM cells but increased more than 10-fold with IMAC-purified EpCAM^{His}-AAV (Figure 38). These data clearly show that IMAC-purified AAV vector particles are superior in transduction of receptor-positive cells due to the depletion of genome-packaged but DARPin-deficient vector particles.

3.2.5 Non-malignant epithelial cells are less susceptible for EpCAM-AAV than tumor cells

The results described in the previous chapters prove that AAV vectors can be designed to specifically and efficiently target EpCAM-positive tumor cells. But EpCAM is not only abundantly expressed on primary tumors and metastases of most epithelial malignancies, it is also expressed in normal epithelial tissues (Simon et al, 2013).

Therefore, non-malignant epithelial cells could potentially be a target for EpCAM-AAV. Depending on the application of the vector this might be critical. In a therapeutical setting with the aim of targeting and killing tumor cells *in vivo* it may cause severe side effects if healthy cells were affected as well. To verify the susceptibility of non-malignant EpCAM-positive cells to EpCAM-AAV, primary epithelial cells were transduced. Additionally, gene transfer into mice transgenic for human EpCAM was monitored.

3.2.5.1 Transduction of primary human mammary epithelial cells

To determine whether EpCAM-AAV would be able to transduce normal epithelial cells, primary cells were obtained and cultivated. Since breast cancer derived tumor cell lines MDA-MB-453 and MCF-7 were shown to be susceptible for EpCAM-AAV (3.2.2.1 and 3.2.2.2), human mammary epithelial cells (HMECs) isolated from adult female breast tissue were chosen for this experiment.

Expression of EpCAM as well as Her2/neu was confirmed by staining against both antigens and subsequent flow cytometry analysis. The whole cell population was positive for both cell surface marker, although Her2/neu expression seemed to be a bit more homogenous (Figure 39A). In general, expression was moderate compared to expression levels observed on tumor cell lines.

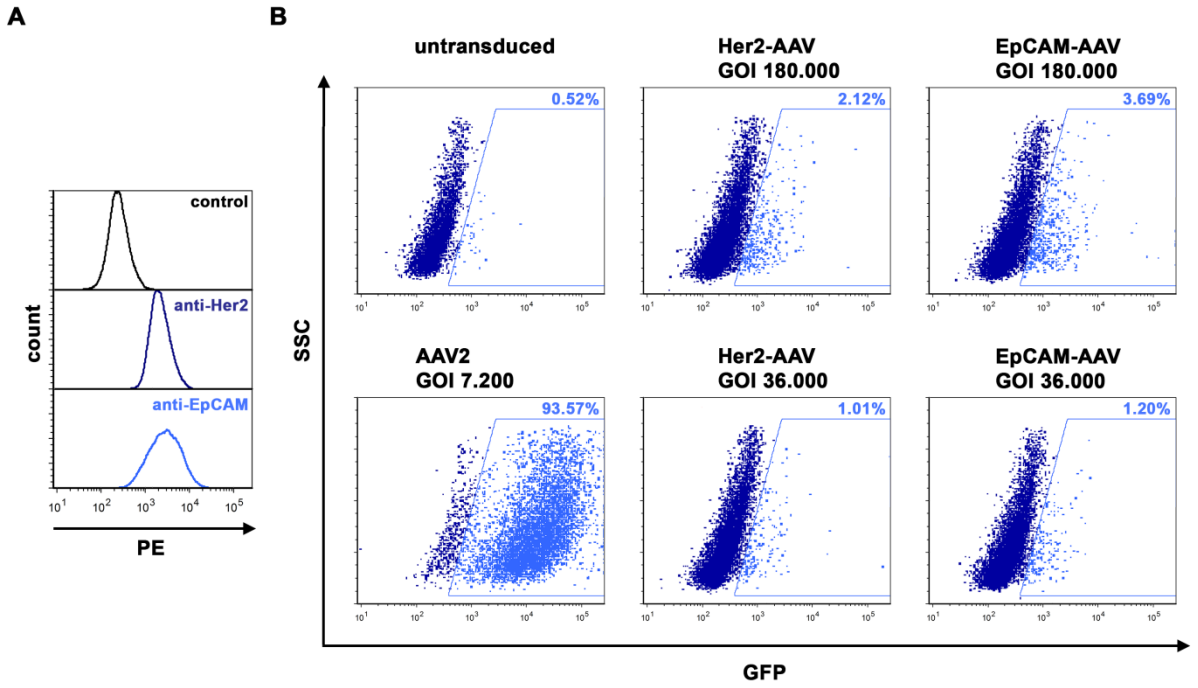

Figure 39: Transduction of human mammary epithelial cells (HMECs) using AAV vectors. (A) Primary HMECs isolated from adult female breast tissue were obtained from LONZA and cultivated as recommended. After passaging twice, cells were stained with anti-Her2-PE or anti-EpCAM-PE antibody and analyzed for respective surface expression. (B) HMECS were either transduced with AAV2 (GOI 7.200) or with one of the targeted vectors Her2-AAV or EpCAM-AAV with high (upper panel) or low (lower panel) GOI. After three days, cells were analyzed for GFP expression by flow cytometry.

Primary HMECs were then transduced with AAV2, Her2-AAV or EpCAM-AAV. Analysis of GFP expression 72 h later revealed a strong transduction of cells that were incubated with AAV2. In contrast, transduction with either Her2-AAV or EpCAM-AAV at a GOI of 36.000 resulted in only a few GFP-positive cells. Even when a 25-fold higher GOI than with AAV2 was used to transduce HMECs, only 2-4% of cells were GFP-positive. These data demonstrate that while HMECs are generally susceptible for AAV transduction, they were only poorly transduced by EpCAM-AAV.

3.2.5.2 Administration of EpCAM-AAV into mice transgenic for hEpCAM

One of the challenges of developing medical products targeting human proteins is the lack of relevant *in vivo* models to study biodistribution, efficacy and side effects. A way to avoid these problems is the use of transgenic animals. McLaughlin et al. generated a mouse model expressing the human EpCAM epithelial-specifically in a pattern very similar to that observed in humans (McLaughlin et al, 2001). These mice were bred and analyzed for transgene expression and then used to evaluate gene transfer by EpCAM-AAV into normal epithelial

tissue *in vivo*. For this purpose, EpCAM-AAV was equipped with the luciferase transgene to allow non-invasive monitoring of gene transfer.

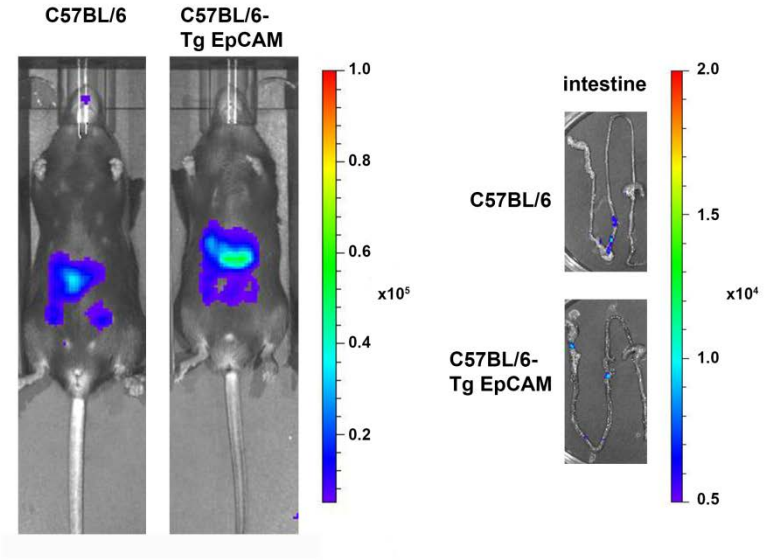

Figure 40: *In vivo* administration of EpCAM-AAV. EpCAM-AAV transferring the *luciferase* gene (2×10^{10} vector genomes) was i.p. injected into C57BL/6 or C57BL/6-Tg EpCAM mice. Three days after vector administration luciferase signals were analyzed by *in vivo* imaging. Luciferase signal intensity is expressed as photons/second/square centimeter/steradian.

Three days after i.p. vector administration into C57BL/6 wildtype and C57BL/6 Tg EpCAM transgenic mice, weak luciferase signals were detected in the abdomen of both mice (Figure 40). Further analysis revealed that the signals originated from the intestines but that they did not significantly differ in intensity from another. This indicates that normal epithelial tissue expressing human EpCAM may not be susceptible for EpCAM-AAV *in vivo* but that the observed signals were rather due to minimal unspecific uptake of the vector particles in wildtype and transgenic animals.

3.2.6 Detection and modification of tumor cells using EpCAM-AAV

EpCAM is a surface marker of human epithelial tissue and derived cancer cells but intriguingly it is also described to be expressed on cancer stem cells (CSCs) and circulating tumor cells (CTC) of various histotypes (Visvader & Lindeman, 2008; Gires et al, 2009; Pantel et al, 2008). CTCs are tumor cells that have disseminated from the primary tumor and circulate in the peripheral blood. To fathom whether EpCAM-AAV could be useful in CTC research and diagnosis, its capacity to find its target cells even when they are strongly underrepresented was evaluated.

3.2.6.1 EpCAM-AAV specifically detects strongly underrepresented tumor cells

One of the prerequisites for this approach was that even a few tumor cells could be detected when they were strongly underrepresented in a cell mixture. To verify whether EpCAM-AAV could be used to detect and modify tumor cells in patient samples, a number of preliminary experiments were performed.

Therefore, healthy human donor blood was used to purify PBMCs by density gradient centrifugation. PBMCs were then mixed in different ratios with MDA-MB-453 cells following transduction with EpCAM-AAV. Expression of GFP as well as the tumor surface marker EpCAM was analyzed two days later by flow cytometry (Figure 41A).

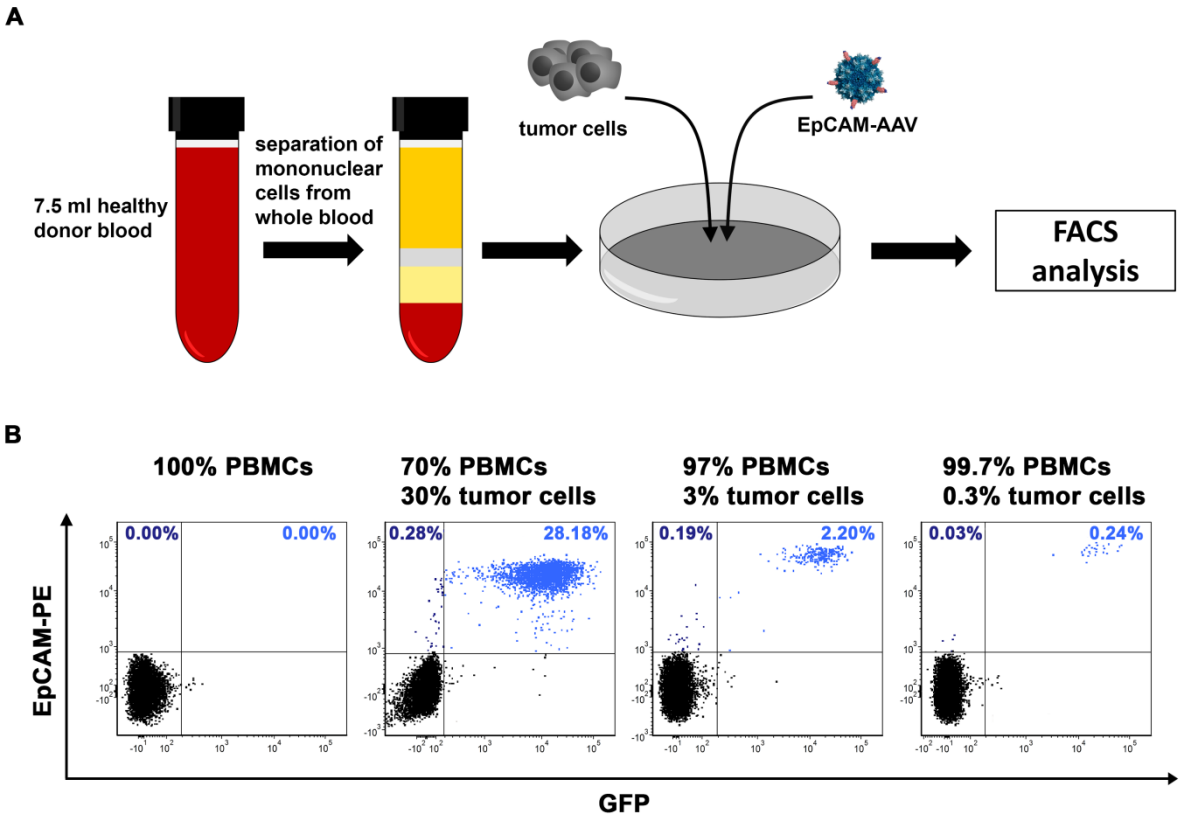

Figure 41: EpCAM-AAV specifically detects strongly underrepresented tumor cells mixed with human PBMC. (A) Schematic drawing of the experimental outline. Human PBMCs were purified by density gradient centrifugation (30 min, 1800 rpm) using Histopaque. Remaining erythrocytes were subsequently lysed (20 min, 37°C, 0.86% ammonium chloride) and cells were washed with PBS. PBMCs alone or mixed in the indicated ratios with MDA-MB-453 cells were transduced with EpCAM-AAV (GOI=1,500). After 48 h cells were analyzed by flow cytometry for EpCAM and GFP expression (as a measure of transduction). (B) Samples were analyzed for EpCAM using an anti-EpCAM-PE antibody and GFP expression. Representative flow cytometry data are shown. (Münch et al, 2015)

A sample exclusively containing PBMCs was transduced with EpCAM-AAV as control. And as expected, neither EpCAM nor GFP expression could be detected demonstrating that no unspecific antibody staining or transduction of PBMCs occurred. In PBMC/MDA-MB-453

mixtures, EpCAM-AAV basically tracked all of the tumor cells, even when these made up only 0.3% of all cells. The fluorescence intensity of these cells was at least 100-fold above that of EpCAM-negative cells (Figure 41B). Thus, EpCAM-AAV was able to specifically detect strongly underrepresented tumor cells with remarkable efficiency.

3.2.6.2 EpCAM-AAV detects low numbers of tumor cells in human blood

As shown in the previous chapter, EpCAM-AAV was able to discriminate between EpCAM-positive and -negative cells within a cell mixture. But in this experiment, mononuclear cells were already purified and separated from whole blood before they were mixed with tumor cells. Eventually, blood samples of cancer patients with circulating tumor cells are a greater challenge. Not only are tumor cells usually very rare, but the whole sample is more complex. Therefore, this situation was mimicked by mixing MDA-MB-453 tumor cells into whole human blood of healthy donors (Figure 42A). Density gradient centrifugation was performed as described above before addition of EpCAM-AAV and 48 h cultivation. Subsequently, samples were stained with anti-EpCAM-PE and anti-CD45-APC antibody, fixed and analyzed by flow cytometry. Debris, doublets and high $CD45^+$ cells (marker for hematopoietic cells) were excluded. Whereas no transduction by EpCAM-AAV was observed when no tumor cells were present, the vector detected more than 90% of tumor cells (constituting between several thousand down to a few hundred cells) present in several million blood cells (Figure 42B).

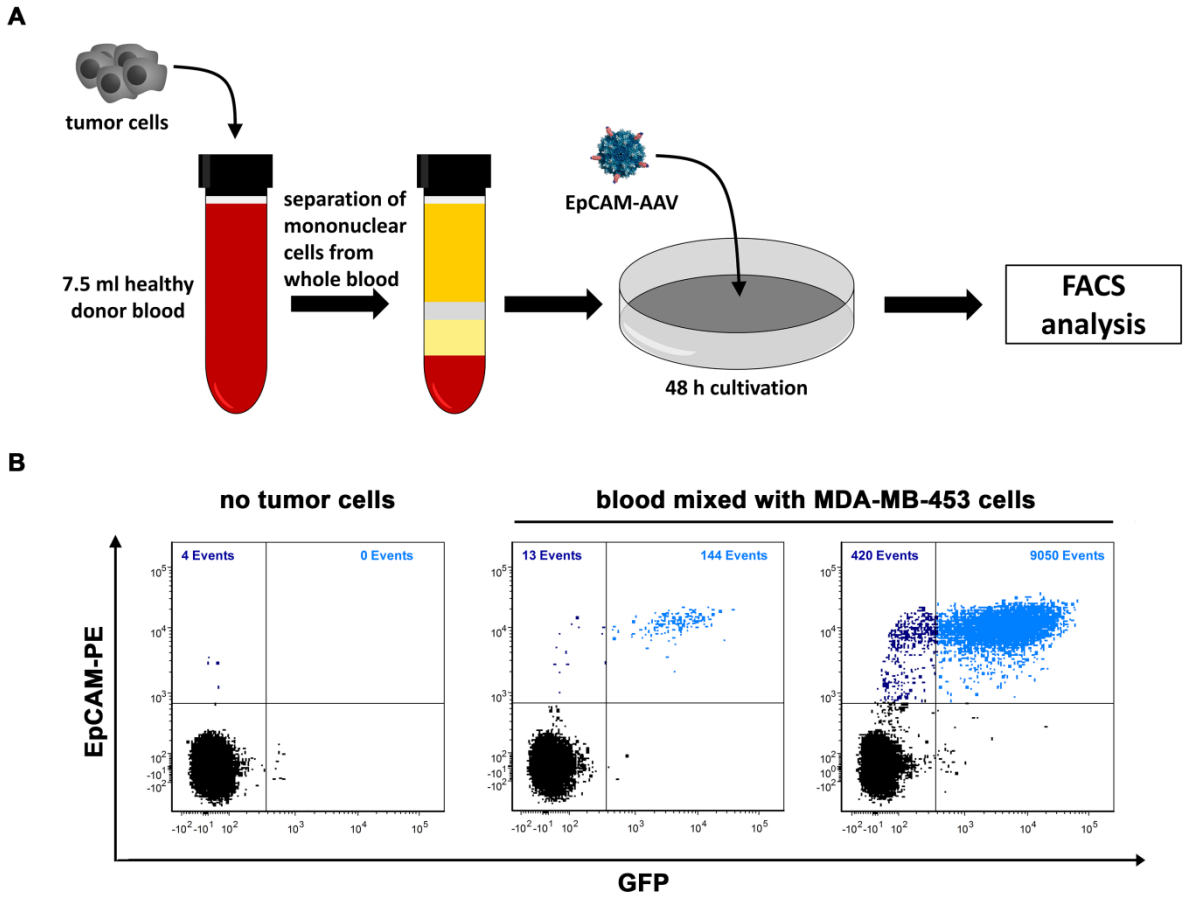

Figure 42: EpCAM-AAV detects low numbers of tumor cells in human blood. (A) Workflow of the experimental procedure. Varying numbers of MDA-MB-453 tumor cells were mixed with 7.5 ml whole human donor blood and mononuclear cells were separated via density gradient centrifugation. The cell mixture was then transduced with EpCAM-AAV, cultivated for 48 h and analyzed by flow cytometry for EpCAM and GFP expression. (B) FACS data of a sample containing whole blood without addition of MDA-MB-453 cells (left) or sample 3 (middle) and 4 (right) also shown in Table 4. Representative dot plots are shown. The number of events in each of the two gates containing EpCAM-positive cells is indicated. (Münch et al, 2015)

Remarkably, even when less than 100 tumor cells were present, most of these were tracked by EpCAM-AAV (Table 4). Interestingly, in control samples without tumor cells a few EpCAM-positive cells were detected by the anti-EpCAM antibody but none of these events were GFP-positive, suggesting that this approach may be less prone to false-positive signals than available detection systems that rely on antibodies.

Table 4: Data overview of seven samples and controls.

	total cells	$EpCAM^+$ cells	$EpCAM^+GFP^+$ cells	$EpCAM^-$ GFP^+ cells	transduced $EpCAM^+$ cells [%]
sample 1	5,689,640	44,078	41,777	250	94.78
sample 2	5,974,121	11,577	11,042	12	95.38
sample 3	6,252,561	9,470	9,050	24	95.56
sample 4	5,818,601	157	144	3	91.72
sample 5	4,001,921	92	79	1	85.87
sample 6	6,611,121	17	12	10	70.59
sample 7	3,603,443	7	6	17	85.71
control 1	5,690,000	4	0	8	0
control 2	4,004,080	17	0	5	0
control 3	6,318,040	2	0	18	0

Samples 1-7 contained decreasing numbers of MDA-MB-453 tumor cells. Control 1 and 2 contained no tumor cells but were incubated with EpCAM-AAV, while control 3 contained neither tumor cells nor vector. (Münch et al, 2015)

These data clearly indicate, that EpCAM-AAV is able to detect and modify a few tumor cells present in a complex blood sample. Although many parameters have yet to be optimized, the newly generated and characterized EpCAM-AAV could be a useful tool in CTC research.

4 Discussion

Viral vectors have evolved to powerful tools in research and development and have proven to be indispensable in gene therapy. Nowadays, increasing efforts are being made to design and engineer these vectors to meet the requirements of researchers, clinicians and patients. Guaranteeing safe and efficacious gene transfer remains one of the main challenges in vectorology, driving the development of selective receptor-targeted viral vectors. The general concept of redirecting viruses to a receptor of choice is based on two simple principles: i) ablation of natural receptor recognition and ii) introduction of a targeting ligand to alter the viral tropism. Using this strategy, lentiviral and AAV vectors targeting cell surface receptors of choice were developed in this thesis. Lentiviral vectors pseudotyped with the MV glycoproteins and a third receptor attachment protein were generated as tool to challenge the MV membrane fusion model for a better understanding of the MV biology and as potential gene therapy vectors. The novel EpCAM-targeted AAV was generated for the detection and modification of rare cell populations.

4.1 Implications for the mechanism of measles virus-triggered membrane fusion

Attachment to cellular receptors and entry into the host cell are the first steps in viral infection. Cell entry by enveloped viruses depends on fusion of the viral envelope with the host cell membrane either directly at the cell surface or following virus internalization. This critical event is mediated by viral glycoproteins which are highly regulated to ensure proper timing and localization of the fusion. Membrane fusion involving two different viral glycoproteins is especially complex and less well understood than that of viruses having receptor attachment and membrane fusion combined in a single protein. As representatives of the first group, MV H and F are known to act concertedly to mediate cell entry. It is assumed that fusion is triggered upon binding of H to one of the three MV receptors, leading to conformational changes in H that are passed on to F (fusion-helper function of H). This thesis describes the generation of lentiviral vectors pseudotyped with engineered MV envelope protein complexes in which receptor attachment and fusion-helper function of H have been separated onto two transmembrane proteins to study the MV fusion mechanism.

4.1.1 Lentiviral particles as core for the MV glycoproteins

For engineering the MV glycoprotein complex and eventually separating the receptor attachment function from H, the MV-pseudotyped LV targeting system established by Funke et al. (Funke et al, 2008) was modified. HIV-1-derived lentiviral vectors were pseudotyped with cytoplasmic tail-truncated variants of F and H. The latter harbored the four point mutations Y481A, R533A, S548L and F549S to ablate natural receptor recognition (Vongpunsawad et al, 2004) and thereby remove receptor attachment function from H. Instead of presenting a targeting ligand fused to H, the system was complemented by an artificial third transmembrane protein binding to Her2/neu. Vectors pseudotyped with this envelope triad conferring receptor attachment, fusion-helper and fusion function transduced Her2/neu-positive cells efficiently and even revealed higher or equal infectivity compared to the convential targeting vector or unmodified MV-LV. This is the first demonstration that in such a setting a paramyxovirus protein complex mediates cell entry equally well as in the two-transmembrane-protein-based setting. Transfer of receptor attachment to a third transmembrane protein has been described for a totally different enveloped virus, i.e. the alphavirus Sindbis virus. Also in this case, lentiviral vectors were pseudotyped. Though receptor attachment was mediated by membrane-bound CD20-specific antibody (Yang et al, 2006), vector particle cell entry relied on endocytic uptake and, more importantly, was triggered by low pH and not receptor contact. Moreover, substantial background transduction was observed even in the absence of the target receptor due to a residual receptor recognition of the Sindbis E2 protein (Zhang et al, 2010) clearly revealing the differences between both systems.

The decision to use MV-pseudotyped lentiviral vectors instead of the virus itself was based on rational considerations: i) LVs can be more easily engineered and generated from plasmid DNA and ii) the modified MV glycoproteins used for pseudotyping exhibit a receptor usage identical to that of unmodified MV glycoproteins (Funke et al, 2008; Frecha et al, 2008). Because of alterations required for incorporation of H and F into the lentiviral envelope, one could argue that these proteins behave differently in the LV setting. But cytoplasmic tail-truncated variants FΔ30 and HΔ18 have been successfully used for the retargeting of lentiviral vectors (Funke et al, 2008; Anliker et al, 2010). Previous studies demonstrated that the cytoplasmic tail of F is not required for cell surface expression and membrane fusion (Moll et al, 2002). Likewise, H can be truncated by 20 amino acids without losing its fusion-helper function (Moll et al, 2002). A recombinant MV with FΔ30 and HΔ20 was fully infectious and replication-competent, although glycoprotein incorporation rates were reduced upon

cytoplasmic tail truncation (Moll et al, 2002; Cathomen et al, 1998b). Interestingly, it has also been suggested that these truncations enhance the fusogenicity of F and H (Cathomen et al, 1998b) implying that the MV glycoprotein complex in $D^{9.29}$-LV particles may be in a preactivated state. It is, however, evident from data in this thesis that the fusion-helper function of H is required for $D^{9.29}$-LV cell entry and that close contact of cells and vector particles is not sufficient for fusion initiation. Identical to MV characteristics, $D^{9.29}$-LV cell entry was pH-independent and sensitive towards the F protein-specific fusion inhibitory peptide (FIP) as well as neutralizing antibodies. In addition, the H/F fusion machinery of $D^{9.29}$-LV was active only in presence of the target receptor Her2/neu.

4.1.2 Do further receptors for MV exist?

Generally, these data could also be explained by the existence of a so far unidentified MV coreceptor. Since $D^{9.29}$-LV transduced both human and hamster Her2/neu-positive cells, such a coreceptor must be expressed in both species. All data available cannot explicitly exclude this possibility but data supporting the idea of a MV coreceptor have not been published except for a report in 2007 in which neurokinin-1 was proposed as potential coreceptor for F on neurons (Makhortova et al, 2007). In 2010, Watanabe et al. reported that cyclophilin B, among others serving as CD147 ligand, was incorporated into the membranes of MV virions (Watanabe et al, 2010). They demonstrated that the binding partner CD147 is involved in MV infection of HEK-293 cells, since CD147-specific antibodies significantly reduced MV infectivity. Furthermore, MV infectivity was slightly increased on CHO cells stably expressing CD147 in comparison to parental CHO cells. Initially, they suggested that CD147 could be the up to that time unidentified MV receptor on epithelial cells. Although this was later contradicted by the identification of nectin-4 (Mühlebach et al, 2011; Noyce et al, 2011), the cyclophilin B/CD147 interaction can possibly be seen as a natural counterpart of the $D^{9.29}$/Her2/neu interaction. One of the main differences in both settings are the protein-protein interaction affinities, which are high for $D^{9.29}$ and Her2/neu (Zahnd et al, 2007; Steiner et al, 2008) and presumably orders of magnitudes lower for cyclophilin B and CD147 (Pakula et al, 2007). Consequently, $D^{9.29}$-LV particles were substantially more active in entering cells in the absence of natural receptor attachment. In concordance with a putative F coreceptor as well as data presented by Watanabe et al. and in this thesis, one can conclude that attachment of particles to cells is sufficient to trigger MV fusion without a need for H itself binding to a receptor.

4.1.3 The H/F interaction

In recent years, many groups worked on understanding the structural and molecular interplay of H and F as well as H and its receptors. Structural analysis of H head domains bound to SLAM revealed new insights into the mechanism of fusion triggering. Two discrete forms of the H/SLAM tetrameric assembly were identified and were suggested to represent a prefusion form of H immediately after receptor binding and a postfusion receptor-bound form (Hashiguchi et al, 2011b). The reorganization that takes place from form I to form II is interpreted as shift of the noncovalent H dimer-dimer interface while the dimer structure itself remains intact (Hashiguchi et al, 2011b; Plemper et al, 2011). Still, it is widely assumed that the H heads are not responsible for the direct interplay between H and F but rather a H-stalk/F interaction (Ader et al, 2012; Apte-Sengupta et al, 2013; Navaratnarajah et al, 2012; Paal et al, 2009). Biochemical and mutational analyses mapped the so-called central fusion activation segment to stalk residues 84-117 (Navaratnarajah et al, 2012; Navaratnarajah et al, 2014). Data of this thesis show that conformational and/or structural changes can be triggered even if receptor binding is carried out not by H but by an additional protein. The fact that $D^{9.29}$-LV was not able to enter cells in the absence of H or when the H/F complex formation was impaired ($H^{*}_{mut}\Delta 18$) indicates a need for H to interact with F in order to achieve membrane fusion.

This was corroborated by neutralization experiments shown in Figure 21. $D^{9.29}$-LV cell entry was blocked by three out of four MV H-specific monoclonal antibodies. Putative epitopes of all four antibodies can be mapped on the globular head domain of H. According to this model, K71 and K29 bind in close proximity to the natural receptor binding sites and correspondingly to the introduced mutations in H_{mut}, whereas Nc32 and L77 epitopes are located more distantly (Figure 43). Furthermore, the MAbs L77 and K71 have recently been shown to neutralize MV-LV vectors (Kneissl et al, 2012). Steric hindrance effects and thus prevention of Her2/neu binding by the antibodies were excluded. Interestingly, Tahara et al. identified the so-called antigenic site *vi*, which is located at the bottom, membrane-proximal site of the H blade and acts as effective neutralization epitope (Figure 43). In contrast to many neutralizing antibodies inhibiting the receptor binding, antibodies binding to the *vi* site seem to interfere with H/F interaction (Tahara et al, 2013). The epitope of L77, which was most efficient in neutralizing $D^{9.29}$-LV, is in spatial proximity to the *vi* site. This indicates and supports the idea that H plays an active and indispensable role in the membrane fusion process of $D^{9.29}$-LV.

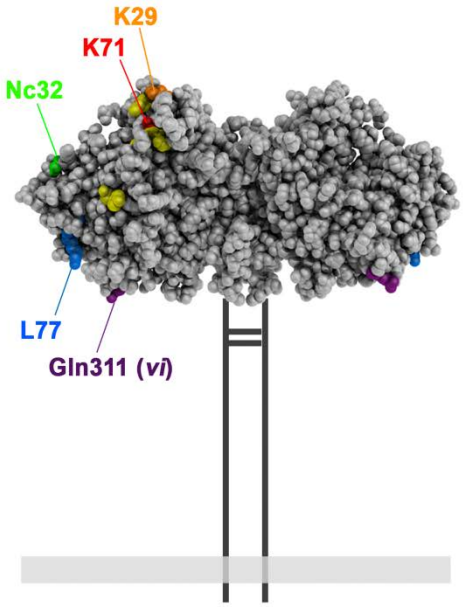

Figure 43: Putative antibody epitopes on the H globular head domains. (A) Sphere representation of the H dimer crystal structure (Hashiguchi et al, 2007). The stalk, transmembrane, and cytoplasmic regions are depicted as vertical lines, with two horizontal lines indicating disulfide bonds. Putative antibody binding sites are indicated in orange, red, green, and blue. Residues mutated in $H_{mut}\Delta18$ to ablate natural receptor tropism are shown in yellow. Antigenic site *vi* is shown in purple (Tahara et al, 2013). The virus membrane is illustrated as a light gray box. Protein Data Bank [PDB] ID 2ZB5; modified with PyMOL.

4.1.4 Conformational changes to activate membrane fusion

Currently, two alternative conformations for the H head domains shape new MV fusion mechanism concepts. The so-called “heads-up” conformation with heads located above the stalks is derived from soluble H heads cocrystallized with their receptor (Hashiguchi et al, 2011b). The relatively new idea of a “heads-down” conformation relies on structures obtained from entire hemagglutinin-neuraminidase (HN) ectodomains of the cognate Newcastle disease virus (NDV) and the parainfluenza virus 5 (PIV5) (Yuan et al, 2011; Welch et al, 2013). In this conformation, the heads of both or only one HN dimer, respectively, are tilted and form interactions with the sides of the stalks. According to the stalk exposure model described for other paramyxoviruses (Yuan et al, 2011; Bose et al, 2014), the heads-down conformation blocks HN-stalk/F interactions. Upon receptor binding, the heads move up and uncover residues in the HN stalks that can interact with and ultimately activate F. But it has been noted, that unlike other paramyxoviruses, MV glycoproteins already form a complex within the cell which would require at least a one head-up/one head-down configuration to allow the association of H and F (Navaratnarajah et al, 2014; Mateo et al, 2014). Thus, further rearrangements would be necessary for MV fusion triggering. Similarly, the so-called three-step safety-catch model describes the pre-fusion complex in a heads-down conformation

(Brindley et al, 2014). The crucial difference to the first model is that despite the heads-down conformation, the F interaction site in the H stalk is accessible. After assembly of H/F_0 complexes in the endoplasmic reticulum, the F protein is proteolytically matured which in turn reduces the strength of the H/F interaction. This is assumed to prepare the complex for physical separation upon fusion triggering. The H heads act as safety catch to suppress spontaneous reorganization of the central stalk region. Only after receptor binding and transition into the heads-up conformation the central stalks are unwinded triggering refolding of F (Brindley et al, 2014).

The absolute necessity of H binding to one of its receptors for fusion triggering is challenged by data described in this thesis but also by a report of a recombinant MV incorporating a headless H (Brindley et al, 2013). It was shown that the stabilized H-stem was sufficient for triggering membrane fusion although the virus was severely growth impaired. Here, spontaneous rearrangements of the central stalk region seemed to serve as molecular trigger. Altogether, it is not direct binding of an MV receptor to H that induces fusion and, possibly, also heads-down to heads-up transition, but rather short-range changes in the microenvironment of H and F (Plemper et al, 2011), such as the close proximity of the target cell membrane mediated by binding of $D^{9.29}$ to Her2/neu (Figure 44). These then drive irreversible changes and ultimately membrane fusion.

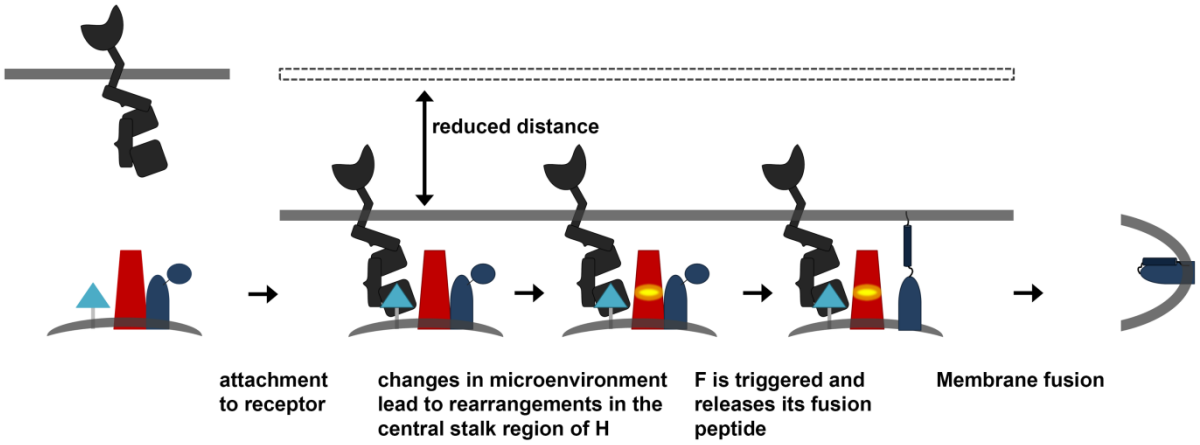

Figure 44: MV fusion mechanism model with separated receptor attachment and fusion-helper function. H (red), F (dark blue) and $D^{9.29}$ (light blue and gray) reside in close proximity in the viral membrane. Upon attachment of $D^{9.29}$ to its receptor (dark grey), viral and cellular membranes are in close contact and the microenvironment of the MV glycoprotein complex changes. This leads to rearrangements in the central stalk region of H (depicted in yellow) which ultimately triggers F, release of the fusion peptide and membrane fusion.

Taking the colocalization of $D^{9.29}$ with the MV glycoproteins into account, $D^{9.29}$ possibly replaces one of the H dimers physically and functionally or closely associates with the MV

complex, thereby transcomplementing the receptor binding-deficient $H_{mut}\Delta 18$. This is reminiscent of work by Brindley et al. demonstrating transcomplementation of the MV fusion complex by combining an H dimer deficient for F triggering but able to bind to MV receptors with an H dimer competent for F triggering but lacking receptor binding function (Brindley et al, 2012).

4.2 Targeting AAVs by protein display

Even before AAV crystal structures had become available, several groups aimed at modifying the viral capsid to alter its tropism or equip it with desirable features such as enhanced transduction or evasion of neutralizing antibodies. Already in 1999, Girod et al. demonstrated that insertional mutagenesis at position 587 can lead to transduction of cells that are normally resistant to AAV2 (Girod et al, 1999). Insertion of the 14-amino-acid peptide L14 containing an RGD motif resulted in vector particles binding to cellular integrin receptors. Although many other positions have been experimentally tested, peptide ligands inserted at position 587/588 dominated due to their location at the apex of the second highest peak of the AAV capsid (Xie et al, 2002). Only position 453, which is even more exposed on the viral capsid, proved to be equivalent or superior when an RGD-containing peptide was inserted (Boucas et al, 2009). Peptide ligands of up to 34 amino acids incorporated into the capsid have been shown to be tolerated and to enhance transduction levels in endothelial cells, tumor cell lines, cardiomyoblasts and several other cell types (Schaffer et al, 2008). However, the limitation of peptide length as well as the absence of secondary and tertiary structures often resulted in only low affinity peptides and thus a weak receptor-ligand interaction.

Consequently, the display of whole proteins may open up new possibilities leading to more versatile AAV retargeting systems. First reports of a scFv directed against CD34 fused to the N-terminus of VP2 (Yang et al, 1998) proved that this position can be used to incorporate large proteins. However, intact viral particles were only produced in the presence of unmodified VP1, VP2 and VP3 in addition to scFv-VP2, titers were severely compromised compared to wildtype AAV2 and natural receptor binding sites were still present (Yang et al, 1998). Similarly, others were not able to efficiently re-direct AAV with scFv-VP2 fusion proteins. AAV2 incorporating anti-GluRD, anti-CD30, anti-CA19 or anti-CEA scFv-VP2 were not able to specifically transduce targets cells (Boucas, Jorge Miguel Martins, 2008; Reul, 2013). One possible explanation could be that scFv fused to VP2 cannot properly fold due to the fact that AAV capsid assembly takes place in the nucleus which does not allow the

formation of disulfide bonds usually required for scFv folding (Reul, 2013).

Extending this approach, Lux et al. fused GFP to the VP2 N-terminus in order to enable visualization of AAV trafficking through the cell (Lux et al, 2005). Contrary to what had been published before (Yang et al, 1998; Warrington et al, 2004), they were able to show that particles incorporating GFP-VP2 did not require unmodified VP2 complementation and that GFP-tagged virions were fully infectious. Since all of these studies reported that large proteins can be incorporated into the AAV capsid using the VP2 N-terminus, if only physically and not functionally as seen for scFvs, Münch et al. chose this position for the fusion with a Her2/neu-specific DARPin in combination with capsid mutations to ablate HSPG-binding (Münch et al, 2013). DARPins are ideal alternative binding proteins in the context of AAV retargeting because they are of small size, highly stable, lack disulfide bonds and can be selected using high-throughput library screens to become a high affinity binder to a given antigen (Stumpp & Amstutz, 2007). The resulting Her2-AAV was the first fully retargeted AAV with high affinity and selectivity for Her2/neu-positive tumor cells *in vitro* and *in vivo*.

In this thesis, the same retargeting strategy was employed to develop AAV vectors that specifically transduce EpCAM-positive cells. For this purpose, two different DARPins, namely Ec1 and Ac1, which were previously selected to bind to EpCAM, were used. They were selected by two different methods and were also shown to differ in affinities. While Ec1 binds to EpCAM with picomolar affinity, association and dissociation of Ac1 is rather biphasic and lies in the nanomolar range (Table 3). It was speculated that Ac1 recognizes an epitope on EpCAM which is present in two different conformations and is bound with two different affinities (Stefan et al, 2011). In contrast, only Ec1 competed for binding with the anti-EpCAM antibody MOC31 proving that epitopes of these two DARPins were not overlapping. Thus, it was expected that they behaved differently as targeting ligands for AAV vectors. And indeed, Ec1-AAV produced slightly higher titers and, more importantly, transduced EpCAM-positive cells more efficiently. Possible explanations for these differences include, but are not limited to, the higher affinity of Ec1 to EpCAM or its binding epitope. It might be that efficient uptake of the AAV only occurs when binding to EpCAM is extremely stable. Alternatively, the Ac1 epitope could be less accessible for a whole virus particle. Since EpCAM is a highly glycosylated protein, binding of Ac1-AAV could be sterically deterred. Of course the superiority of Ec1-AAV could also rely on effects inherent to AAV vector particle production. It was shown in chapter 3.2.1.1 that Ec1-VP2 did not affect packaging efficiency in general. But what remains unknown is the percentage of genome packaged

versus empty DARPin-presenting particles. Eventually, it could be that incorporation of Ac1-VP2 is more prone to result in empty particles than incorporation of Ec1-VP2. In this case, less functional EpCAM-targeted particles would be present in Ac1-AAV preparations leading to lower transduction efficiencies. Interestingly, when used as targeting ligand in the lentiviral vector context, DARPin Ac1 results in higher titer vectors than Ec1 (Bender and Buchholz, unpublished). This clearly demonstrates, that characteristics of targeting ligands in soluble form or even in combination with another viral vector may not reflect its potential in the AAV retargeting system.

An alternative approach to retarget AAVs relies on indirect coupling of the targeting ligand (Figure 45). In contrast to strategies described above, the targeting ligand itself is not genetically fused to the AAV capsid but interacts and associates with the viral vector and the cell surface receptor.

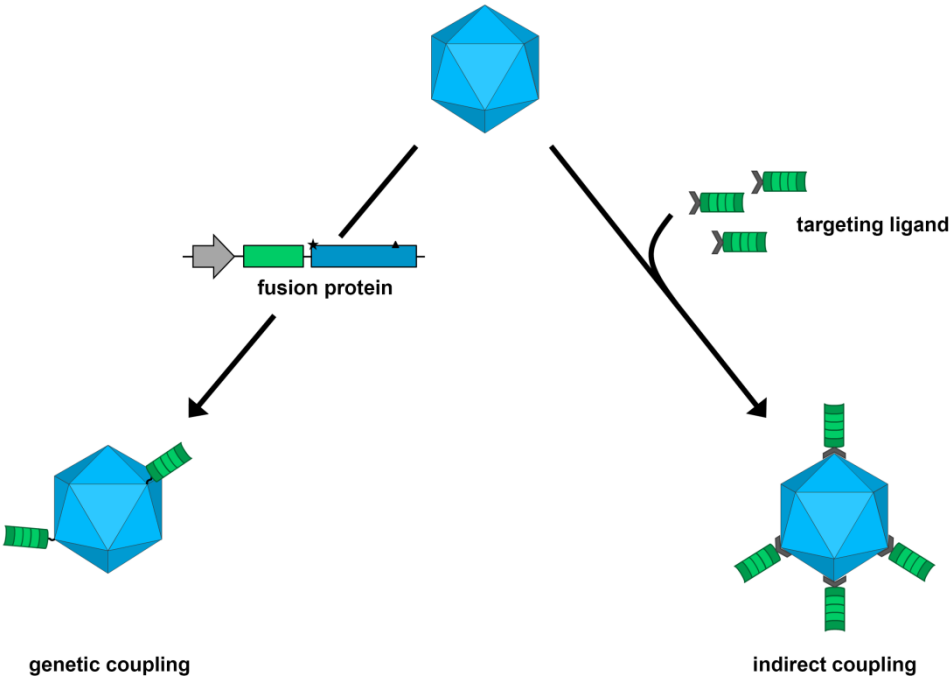

Figure 45: AAV protein display retargeting strategies. Retargeting of AAV vectors can be achieved by either genetic (left) or indirect (right) coupling of the targeting ligand with the capsid.

Bartlett et al. demonstrated that a bispecific F(ab'γ)$_2$ antibody directed against the $\alpha_{IIb}\beta_3$ integrin and the AAV capsid mediated attachment to and transduction of megakaryocytes (Bartlett et al, 1999). Additionally, two groups reported that the high affinity avidin-biotin interaction can be used as molecular bridge between the AAV capsid and the targeting ligand (Ponnazhagan et al, 2002; Arnold et al, 2006). The main advantages of the indirect coupling

are that (i) there is no need for a detailed structural understanding of the AAV or the AAV fusion proteins, (ii) that the maximal number of targeting ligands is not limited by the number of VP2 proteins and (iii) that one AAV vector batch can easily be combined with several different targeting ligands. However, this retargeting approach relies on a reversible and maybe even transient interaction of capsid and targeting ligand which may be a limiting factor for vector uptake and *in vivo* administration (Büning et al, 2003; Kwon & Schaffer, 2008).
Possibly, the future of AAV retargeting will benefit from combining the best features of different strategies. Post-translational but covalent coupling of a targeting ligand to the AAV capsid could be achieved by so-called copper-free click chemistry. This strain-promoted azido-alkyne cycloaddition has recently been used to couple fluorescent dyes to the plant virus cowpea chlorotic mottle virus (Hommersom et al, 2014) and to functionalize DARPin molecules (Simon et al, 2012). Therefore, this method may be suitable to team up AAV and DARPin in an even more flexible way.

4.3 Applications of receptor-targeted viral vectors

In this thesis, receptor targeting of lentiviral and AAV vectors for different applications has been demonstrated, proving the versatility of this approach. While both vector types are promising tools, possible limitations, drawbacks and comparisons to other systems will be discussed.

4.3.1 $D^{9.29}$-LV and derivatives as gene therapy vector

$D^{9.29}$-LV has proven to be a valuable tool to investigate the MV fusion mechanism, but vectors pseudotyped with such an envelope triad may also represent a novel targeting concept for lentiviral vectors. $D^{9.29}$-LV mediated stable gene transfer and exhibited a 26-fold better infectivity-to-particle ratio than the conventional 9.29-LV, where the targeting ligand is fused directly to H. Explanations for this enhanced gene transfer activity include, but are not limited to, an increased stability of the MV glycoprotein complex, improved conformation and/or presentation of the targeting ligand, or establishment of a more suitable distance between LV and target cell membrane (Buchholz et al, 1996). It is known that the biophysical properties of the targeting ligand can influence and decrease transport of the H-targeting ligand fusion protein to the plasma membrane (Friedel et al). Likewise, the H protein type-II transmembrane protein topology could disturb the binding capability of some targeting ligands. Circumventing the need for a direct modification of H may therefore be beneficial.

As proof of concept for the applicability of $D^{9.29}$-LV for *in vivo* gene transfer, the vector transferring the luciferase gene was systemically injected into mice xenografted with a subcutaneously growing SK-OV-3 tumor. Bioluminescence signals were exclusively detected in the tumor tissue, proving its targeting potential. While replication-competent vectors and oncolytic viruses are the weapons of choice in tumor therapy, $D^{9.29}$-LV may prove useful for functional genomics studies in tumor biology.

One drawback of this targeting system is that targeting ligands don't seem to be universally exchangeable. Transduction of cells expressing CD4, CD20, CD30 or CD8 using the respective vector particles was not successful. In some cases, titers improved upon insertion of a linker between transmembrane domain and targeting ligand. This helix-forming peptide linker designed to compensate the distance of the 9.29 to G3 Her2/neu binding sites consists of $A(EAAAK)_nA$ repeats and was already described to effectively separate bifunctional fusion proteins (Arai et al, 2001). Assuming that the length of helix per residue corresponds to 1.5 Å (Brändén & Tooze, 1991) and that one helical turn consists of 3.6 residues (Berg et al, 2007), a helical linker with seven repeats results in round about 10 turns and has a length of 55 Å. At that time, it was only known that DARPin 9.29 was directed against domain I, II or III (Steiner et al, 2008) but not yet the exact binding site. If binding occurred somewhere along domain III or II, the distance to the G3 binding domain IV would be in the range of 50-60 Å (using Pymol and PDB file 1N8Z, (Cho et al, 2003)). Consequently, the DARPin G3 was one of the targeting ligands benefitting the most, proving that vectors based on this targeting concept can be optimized by altering the length of the linker between PDGFR transmembrane domain and the targeting ligand.

4.3.2 EpCAM-AAV in CTC research

EpCAM is a surface marker of human epithelial tissue and derived cancer cells but intriguingly it is also described to be expressed on cancer stem cells (CSCs) and circulating tumor cells (CTC) of various histotypes (Visvader & Lindeman, 2008; Gires et al, 2009; Pantel et al, 2008). CTCs are tumor cells that have disseminated from the primary tumor and circulate in the peripheral blood. Equipped with the capacity to initiate new tumors and strong invading potential, a subpopulation of CTCs is responsible for the formation of metastases and their presence is believed to be an indicator of poor prognosis (Baccelli et al, 2013; Pantel et al, 2008). Understandably, the detection and characterization of these cells has gained considerable attention in recent years. One of the problems in this field is that CTCs are

usually present only in low numbers in the blood of many cancer patients and that extremely sensitive and reliable techniques are required. The most commonly used methods rely on antibody-mediated detection of EpCAM-positive CTCs. One of the systems, an automated immunomagnetic enrichment and staining system called CellSearch, was already approved by the US Food and Drug Administration for monitoring treatment effectiveness of patients with metastatic breast, colon and prostate cancer (Hayes et al, 2006; Cohen et al, 2008; de Bono, Johann S et al, 2008). However, these techniques only allow staining of CTCs via binding of fluorophore-coupled antibodies to the cell surface. As a viral vector, EpCAM-AAV provides antibody-like specificity combined with the possibility to modify these cells either to express a fluorescence protein of choice or any other desired transgene that can be packaged. Proof of principle experiments demonstrated that EpCAM-AAV specifically and efficiently detected tumor cells strongly underrepresented in human blood at a high signal-to-noise ratio. However, this has to be confirmed with patient material in direct comparison to state of the art methods to make a realistic assessment of the vector. If necessary, several parameters can still be further optimized. These include use of single-stranded AAV vectors which may offer a second layer of specificity. The second strand synthesis prior to transgene expression is hampered in cells of the hematopoietic system, but proceeds efficiently in tumor cells (Hacker et al, 2005; Schuhmann et al, 2010). Additionally, further optimizing the affinity purification for EpCAM-AAV and thereby increasing the yield of DARPin-displaying particles will be beneficial.

One source for false-positive signals in CTC detection may arise from transduction of non-malignant epithelial cells present in the blood sample. With the exception of epidermal keratinocytes, gastric parietal cells, hepatocytes, thymic cortical epithelial and myoepithelial cells, epithelial cells throughout the body are EpCAM-positive and can be stained using an anti-EpCAM antibody in immunohistochemical studies (Momburg et al, 1987; Schmelzer & Reid, 2008). Nevertheless, the expression profile of EpCAM in non-malignant and malignant tissues is different. Variable levels are found in normal epithelial cells, whereas EpCAM is usually highly overexpressed in tumor cells (Spizzo et al, 2011). Moreover, the distribution of EpCAM molecules at the surface of tumor cells seems to be homogenous, while it is only found at the basolateral membrane in normal tissues (Balzar et al, 1999; McLaughlin et al, 2001). The resulting limited *in vivo* accessibility of non-malignant tissues was confirmed by i.v. administration of the EpCAM-specific monoclonal antibody MOC31 into tumor bearing mice (McLaughlin et al, 2001). Similar observations were made with the EpCAM-AAV presenting the DARPin Ec1 which is directed against the same epitope as MOC31. The fact

that transduction mediated by EpCAM-AAV was clearly receptor density-dependent and that primary human mammary epithelial cells as well as mice transgenic for human EpCAM were less susceptible for EpCAM-AAV argues that a strong preference for tumor cells is inherent to the vector particles.

It has been suggested that in some cases characterization of CTCs by EpCAM is not sufficient to detect the real metastases initiating cells (Baccelli et al, 2013). In part, this could be accounted for by a possible epithelial-to-mesenchymal transition (EMT) of carcinoma cells which can result in at least a partial downregulation of EpCAM (Kalluri & Weinberg, 2009; Yu et al, 2013). This further highlights the potential of EpCAM-AAV in CTC research because permanent labelling of EpCAM-positive CTCs without the need for fixation, as required for other methods such as the CellSearch system, could be useful in functional EMT studies as well.

5 References

Abel T (2013) *Targeted gene delivery to hematopoietic progenitor & specialized endothelial cells.* Dissertation, Frankfurt

Abel T, El Filali E, Waern J, Schneider IC, Yuan Q, Münch RC, Hick M, Warnecke G, Madrahimov N, Kontermann RE, Schüttrumpf J, Müller UC, Seppen J, Ott M & Buchholz CJ (2013) Specific gene delivery to liver sinusoidal and artery endothelial cells. *Blood* **122:** 2030–2038

Ader N, Brindley MA, Avila M, Origgi FC, Langedijk, Johannes P M, Örvell C, Vandevelde M, Zurbriggen A, Plemper RK & Plattet P (2012) Structural rearrangements of the central region of the morbillivirus attachment protein stalk domain trigger F protein refolding for membrane fusion. *J. Biol. Chem.* **287:** 16324–16334

Ageichik A, Buchholz CJ & Collins MK (2011) Lentiviral vectors targeted to MHC II are effective in immunization. *Hum. Gene Ther.* **22:** 1249–1254

Aiuti A, Biasco L, Scaramuzza S, Ferrua F, Cicalese MP, Baricordi C, Dionisio F, Calabria A, Giannelli S, Castiello MC, Bosticardo M, Evangelio C, Assanelli A, Casiraghi M, Di Nunzio S, Callegaro L, Benati C, Rizzardi P, Pellin D & Di Serio C et al (2013) Lentiviral hematopoietic stem cell gene therapy in patients with Wiskott-Aldrich syndrome. *Science* **341:** 1233151

Akache B, Grimm D, Pandey K, Yant SR, Xu H & Kay MA (2006) The 37/67-kilodalton laminin receptor is a receptor for adeno-associated virus serotypes 8, 2, 3, and 9. *J. Virol.* **80:** 9831–9836

Akkina RK, Walton RM, Chen ML, Li QX, Planelles V & Chen IS (1996) High-efficiency gene transfer into CD34+ cells with a human immunodeficiency virus type 1-based retroviral vector pseudotyped with vesicular stomatitis virus envelope glycoprotein G. *J. Virol* **70:** 2581–2585

Anderson BD, Nakamura T, Russell SJ & Peng K (2004) High CD46 receptor density determines preferential killing of tumor cells by oncolytic measles virus. *Cancer Res.* **64:** 4919–4926

Anliker B, Abel T, Kneissl S, Hlavaty J, Caputi A, Brynza J, Schneider IC, Münch RC, Petznek H, Kontermann RE, Koehl U, Johnston ICD, Keinänen K, Müller UC, Hohenadl C,

Monyer H, Cichutek K & Buchholz CJ (2010) Specific gene transfer to neurons, endothelial cells and hematopoietic progenitors with lentiviral vectors. *Nat. Methods* **7:** 929–935

Apte-Sengupta S, Navaratnarajah CK & Cattaneo R (2013) Hydrophobic and charged residues in the central segment of the measles virus hemagglutinin stalk mediate transmission of the fusion-triggering signal. *J. Virol.* **87:** 10401–10404

Apte-Sengupta S, Negi S, Leonard, Vincent H J, Oezguen N, Navaratnarajah CK, Braun W & Cattaneo R (2012) Base of the measles virus fusion trimer head receives the signal that triggers membrane fusion. *J. Biol. Chem.* **287:** 33026–33035

Arai R, Ueda H, Kitayama A, Kamiya N & Nagamune T (2001) Design of the linkers which effectively separate domains of a bifunctional fusion protein. *Protein Eng.* **14:** 529–532

Arnold GS, Sasser AK, Stachler MD & Bartlett JS (2006) Metabolic biotinylation provides a unique platform for the purification and targeting of multiple AAV vector serotypes. *Molecular therapy : the journal of the American Society of Gene Therapy* **14:** 97–106

Asokan A, Hamra JB, Govindasamy L, Agbandje-McKenna M & Samulski RJ (2006) Adeno-associated virus type 2 contains an integrin alpha5beta1 binding domain essential for viral cell entry. *J. Virol.* **80:** 8961–8969

Asokan A, Schaffer DV & Samulski RJ (2012) The AAV vector toolkit: poised at the clinical crossroads. *Mol. Ther.* **20:** 699–708

Avota E, Müller N, Klett M & Schneider-Schaulies S (2004) Measles virus interacts with and alters signal transduction in T-cell lipid rafts. *J. Virol.* **78:** 9552–9559

Baccelli I, Schneeweiss A, Riethdorf S, Stenzinger A, Schillert A, Vogel V, Klein C, Saini M, Bäuerle T, Wallwiener M, Holland-Letz T, Höfner T, Sprick M, Scharpff M, Marmé F, Sinn HP, Pantel K, Weichert W & Trumpp A (2013) Identification of a population of blood circulating tumor cells from breast cancer patients that initiates metastasis in a xenograft assay. *Nat. Biotechnol.* **31:** 539–544

Balzar M, Winter MJ, Boer CJ de & Litvinov SV (1999) The biology of the 17-1A antigen (Ep-CAM). *J. Mol. Med.* **77:** 699–712

Bartlett JS, Kleinschmidt J, Boucher RC & Samulski RJ (1999) Targeted adeno-associated virus vector transduction of nonpermissive cells mediated by a bispecific F(ab'gamma)2 antibody. *Nat. Biotechnol.* **17:** 181–186

Bell JC (2014) Taming measles virus to create an effective cancer therapeutic. *Mayo Clin. Proc.* **89:** 863–865

Berg JM, Tymoczko JL & Stryer L (2007) *Biochemistry: Jeremy M. Berg, John L. Tymoczko, Lubert Stryer.* W.H.Freeman & Co Ltd, New York

Berns KI (1974) Molecular biology of the adeno-associated viruses. *Curr. Top. Microbiol. Immunol.* **65:** 1–20

Biffi A, Montini E, Lorioli L, Cesani M, Fumagalli F, Plati T, Baldoli C, Martino S, Calabria A, Canale S, Benedicenti F, Vallanti G, Biasco L, Leo S, Kabbara N, Zanetti G, Rizzo WB, Mehta, Nalini A L, Cicalese MP & Casiraghi M et al (2013) Lentiviral hematopoietic stem cell gene therapy benefits metachromatic leukodystrophy. *Science* **341:** 1233158

Bleker S, Pawlita M & Kleinschmidt JA (2006) Impact of capsid conformation and Rep-capsid interactions on adeno-associated virus type 2 genome packaging. *J. Virol.* **80:** 810–820

Bleker S, Sonntag F & Kleinschmidt JA (2005) Mutational analysis of narrow pores at the fivefold symmetry axes of adeno-associated virus type 2 capsids reveals a dual role in genome packaging and activation of phospholipase A2 activity. *J. Virol.* **79:** 2528–2540

Bluming AZ & Ziegler JL (1971) Regression of Burkitt's lymphoma in association with measles infection. *Lancet* **2:** 105–106

Bose S, Song AS, Jardetzky TS & Lamb RA (2014) Fusion activation through attachment protein stalk domains indicates a conserved core mechanism of paramyxovirus entry into cells. *Journal of Virology* **88:** 3925–3941

Boucas J, Lux K, Huber A, Schievenbusch S, von Freyend, Miriam John, Perabo L, Quadt-Humme S, Odenthal M, Hallek M & Büning H (2009) Engineering adeno-associated virus serotype 2-based targeting vectors using a new insertion site-position 453-and single point mutations. *J Gene Med* **11:** 1103–1113

Boucas, Jorge Miguel Martins (2008) *Engineering AAV-2 Targeting Vectors: A New Insertion Site and scFv Driven Vectors.* Dissertation, Köln

Brändén C & Tooze J (1991) *Introduction to protein structure.* Garland Pub., New York

Brindley MA, Chaudhury S & Plemper RK (2014) Measles Virus Glycoprotein Complexes Preassemble Intracellularly and Relax During Transport to the Cell Surface in Preparation for Fusion. *Journal of Virology*

Brindley MA, Suter R, Schestak I, Kiss G, Wright ER & Plemper RK (2013) A Stabilized Headless Measles Virus Attachment Protein Stalk Efficiently Triggers Membrane Fusion. *Journal of Virology*

Brindley MA, Takeda M, Plattet P & Plemper RK (2012) Triggering the measles virus membrane fusion machinery. *Proc. Natl. Acad. Sci. U.S.A.* **109:** E3018-27

Buchholz CJ, Mühlebach MD & Cichutek K (2009) Lentiviral vectors with measles virus glycoproteins - dream team for gene transfer? *Trends Biotechnol.* **27:** 259–265

Buchholz CJ, Schneider U, Devaux P, Gerlier D & Cattaneo R (1996) Cell entry by measles virus: long hybrid receptors uncouple binding from membrane fusion. *J. Virol.* **70:** 3716–3723

Büning H, Perabo L, Coutelle O, Quadt-Humme S & Hallek M (2008) Recent developments in adeno-associated virus vector technology. *J Gene Med* **10:** 717–733

Büning H, Ried MU, Perabo L, Gerner FM, Huttner NA, Enssle J & Hallek M (2003) Receptor targeting of adeno-associated virus vectors. *Gene therapy* **10:** 1142–1151

Burova E & Ioffe E (2005) Chromatographic purification of recombinant adenoviral and adeno-associated viral vectors: methods and implications. *Gene Ther.* **12 Suppl 1:** S5-17

Cao L, During M & Xiao W (2002) Replication competent helper functions for recombinant AAV vector generation. *Gene Ther.* **9:** 1199–1206

Cathomen T, Mrkic B, Spehner D, Drillien R, Naef R, Pavlovic J, Aguzzi A, Billeter MA & Cattaneo R (1998a) A matrix-less measles virus is infectious and elicits extensive cell fusion: consequences for propagation in the brain. *EMBO J.* **17:** 3899–3908

Cathomen T, Naim HY & Cattaneo R (1998b) Measles viruses with altered envelope protein cytoplasmic tails gain cell fusion competence. *J. Virol.* **72:** 1224–1234

Cattaneo R, Rebmann G, Schmid A, Baczko K, ter Meulen V & Billeter MA (1987) Altered transcription of a defective measles virus genome derived from a diseased human brain. *EMBO J.* **6:** 681–688

Cho H, Mason K, Ramyar KX, Stanley AM, Gabelli SB, Denney DW & Leahy DJ (2003) Structure of the extracellular region of HER2 alone and in complex with the Herceptin Fab. *Nature* **421:** 756–760

Choi VW, McCarty DM & Samulski RJ (2005) AAV hybrid serotypes: improved vectors for gene delivery. *Curr Gene Ther* **5:** 299–310

Clark KR, Sferra TJ & Johnson PR (1997) Recombinant adeno-associated viral vectors mediate long-term transgene expression in muscle. *Hum. Gene Ther.* **8:** 659–669

Cohen SJ, Punt, Cornelis J A, Iannotti N, Saidman BH, Sabbath KD, Gabrail NY, Picus J, Morse M, Mitchell E, Miller MC, Doyle GV, Tissing H, Terstappen, Leon W M M & Meropol NJ (2008) Relationship of circulating tumor cells to tumor response, progression-free survival, and overall survival in patients with metastatic colorectal cancer. *J. Clin. Oncol.* **26:** 3213–3221

Cronin J, Zhang X & Reiser J (2005) Altering the tropism of lentiviral vectors through pseudotyping. *Curr Gene Ther* **5:** 387–398

Dalerba P, Cho RW & Clarke MF (2007) Cancer stem cells: models and concepts. *Annu. Rev. Med.* **58:** 267–284

Daya S & Berns KI (2008) Gene therapy using adeno-associated virus vectors. *Clin. Microbiol. Rev.* **21:** 583–593

de Bono, Johann S, Scher HI, Montgomery RB, Parker C, Miller MC, Tissing H, Doyle GV, Terstappen, Leon W W M, Pienta KJ & Raghavan D (2008) Circulating tumor cells predict survival benefit from treatment in metastatic castration-resistant prostate cancer. *Clin. Cancer Res.* **14:** 6302–6309

Demaison C, Parsley K, Brouns G, Scherr M, Battmer K, Kinnon C, Grez M & Thrasher AJ (2002) High-level transduction and gene expression in hematopoietic repopulating cells using a human immunodeficiency [correction of imunodeficiency] virus type 1-based lentiviral vector containing an internal spleen focus forming virus promoter. *Hum. Gene Ther.* **13:** 803–813

Dörig RE, Marcil A, Chopra A & Richardson CD (1993) The human CD46 molecule is a receptor for measles virus (Edmonston strain). *Cell* **75:** 295–305

Drittanti L, Jenny C, Poulard K, Samba A, Manceau P, Soria N, Vincent N, Danos O & Vega M (2001) Optimised helper virus-free production of high-quality adeno-associated virus vectors. *J Gene Med* **3:** 59–71

Drouin LM & Agbandje-McKenna M (2013) Adeno-associated virus structural biology as a tool in vector development. *Future Virol* **8:** 1183–1199

Erlenhoefer C, Wurzer WJ, Löffler S, Schneider-Schaulies S, ter Meulen V & Schneider-Schaulies J (2001) CD150 (SLAM) is a receptor for measles virus but is not involved in viral contact-mediated proliferation inhibition. *J. Virol.* **75:** 4499–4505

Ferrari FK, Samulski T, Shenk T & Samulski RJ (1996) Second-strand synthesis is a rate-limiting step for efficient transduction by recombinant adeno-associated virus vectors. *J. Virol.* **70:** 3227–3234

Finkelshtein D, Werman A, Novick D, Barak S & Rubinstein M (2013) LDL receptor and its family members serve as the cellular receptors for vesicular stomatitis virus. *Proceedings of the National Academy of Sciences* **110:** 7306–7311

Fisher KJ, Gao GP, Weitzman MD, DeMatteo R, Burda JF & Wilson JM (1996) Transduction with recombinant adeno-associated virus for gene therapy is limited by leading-strand synthesis. *J. Virol.* **70:** 520–532

Flemming A (2012) Regulatory watch: pioneering gene therapy on brink of approval. *Nat Rev Drug Discov* **11:** 664

Frecha C, Costa C, Negre D, Gauthier E, Russell SJ, Cosset F & Verhoeyen E (2008) Stable transduction of quiescent T cells without induction of cycle progression by a novel lentiviral vector pseudotyped with measles virus glycoproteins. *Blood* **112:** 4843–4852

Friedel T, Hanisch LJ, Muth A, Honegger A, Abken H, Plückthun A, Buchholz CJ & Schneider IC *Receptor-targeted lentiviral vectors are exceptionally sensitive towards the biophysical properties of the displayed single-chain Fv.* Manuscript under consideration.

Friedmann T & Roblin R (1972) Gene therapy for human genetic disease? *Science* **175:** 949–955

Funke S, Maisner A, Mühlebach MD, Koehl U, Grez M, Cattaneo R, Cichutek K & Buchholz CJ (2008) Targeted cell entry of lentiviral vectors. *Mol. Ther.* **16:** 1427–1436

Galanis E, Hartmann LC, Cliby WA, Long HJ, Peethambaram PP, Barrette BA, Kaur JS, Haluska PJ, Aderca I, Zollman PJ, Sloan JA, Keeney G, Atherton PJ, Podratz KC, Dowdy SC, Stanhope CR, Wilson TO, Federspiel MJ, Peng K & Russell SJ (2010) Phase I trial of intraperitoneal administration of an oncolytic measles virus strain engineered to express carcinoembryonic antigen for recurrent ovarian cancer. *Cancer Res.* **70:** 875–882

Gires O, Klein CA & Baeuerle PA (2009) On the abundance of EpCAM on cancer stem cells. *Nat. Rev. Cancer* **9:** 143; author reply 143

Girod A, Ried M, Wobus C, Lahm H, Leike K, Kleinschmidt J, Deléage G & Hallek M (1999) Genetic capsid modifications allow efficient re-targeting of adeno-associated virus type 2. *Nature medicine* **5:** 1052–1056

Girod A, Wobus CE, Zádori Z, Ried M, Leike K, Tijssen P, Kleinschmidt JA & Hallek M (2002) The VP1 capsid protein of adeno-associated virus type 2 is carrying a phospholipase A2 domain required for virus infectivity. *J. Gen. Virol.* **83:** 973–978

Goujon M, McWilliam H, Li W, Valentin F, Squizzato S, Paern J & Lopez R (2010) A new bioinformatics analysis tools framework at EMBL-EBI. *Nucleic Acids Res.* **38:** W695-9

Govindasamy L, DiMattia MA, Gurda BL, Halder S, McKenna R, Chiorini JA, Muzyczka N, Zolotukhin S, Agbandje-McKenna M, Govindasamy L, DiMattia MA, Gurda BL, Halder S, McKenna R, Chiorini JA, Muzyczka N & Zolotukhin S (2013) Structural Insights into Adeno-Associated Virus Serotype 5. *Journal of Virology* **87:** 11187–11199

Govindasamy L, Padron E, McKenna R, Muzyczka N, Kaludov N, Chiorini JA & Agbandje-McKenna M (2006) Structurally mapping the diverse phenotype of adeno-associated virus serotype 4. *J. Virol.* **80:** 11556–11570

Grieger JC, Snowdy S & Samulski RJ (2006) Separate basic region motifs within the adeno-associated virus capsid proteins are essential for infectivity and assembly. *J. Virol.* **80:** 5199–5210

Grimm D, Kern A, Pawlita M, Ferrari F, Samulski R & Kleinschmidt J (1999) Titration of AAV-2 particles via a novel capsid ELISA: packaging of genomes can limit production of recombinant AAV-2. *Gene Ther.* **6:** 1322–1330

Gross S (1971) Measles and leukaemia. *Lancet* **1:** 397–398

Gurda BL, DiMattia MA, Miller EB, Bennett A, McKenna R, Weichert WS, Nelson CD, Chen W, Muzyczka N, Olson NH, Sinkovits RS, Chiorini JA, Zolotutkhin S, Kozyreva OG, Samulski RJ, Baker TS, Parrish CR & Agbandje-McKenna M (2013) Capsid antibodies to different adeno-associated virus serotypes bind common regions. *J. Virol.* **87:** 9111–9124

Hacker UT, Wingenfeld L, Kofler DM, Schuhmann NK, Lutz S, Herold T, King, Susan B S, Gerner FM, Perabo L, Rabinowitz J, McCarty DM, Samulski RJ, Hallek M & Büning H (2005) Adeno-associated virus serotypes 1 to 5 mediated tumor cell directed gene transfer and improvement of transduction efficiency. *The journal of gene medicine* **7:** 1429–1438

Hashiguchi T, Kajikawa M, Maita N, Takeda M, Kuroki K, Sasaki K, Kohda D, Yanagi Y & Maenaka K (2007) Crystal structure of measles virus hemagglutinin provides insight into effective vaccines. *Proc. Natl. Acad. Sci. U.S.A* **104:** 19535–19540

Hashiguchi T, Maenaka K & Yanagi Y (2011a) Measles Virus Hemagglutinin: Structural Insights into Cell Entry and Measles Vaccine. *Front. Microbio.* **2**

Hashiguchi T, Ose T, Kubota M, Maita N, Kamishikiryo J, Maenaka K & Yanagi Y (2011b) Structure of the measles virus hemagglutinin bound to its cellular receptor SLAM. *Nat Struct Mol Biol* **18:** 135–141

Hayes DF, Cristofanilli M, Budd GT, Ellis MJ, Stopeck A, Miller MC, Matera J, Allard WJ, Doyle GV & Terstappen, Leon W W M (2006) Circulating tumor cells at each follow-up time point during therapy of metastatic breast cancer patients predict progression-free and overall survival. *Clin. Cancer Res.* **12:** 4218–4224

Hernandez LD, Hoffman LR, Wolfsberg TG & White JM (1996) Virus-cell and cell-cell fusion. *Annu. Rev. Cell Dev. Biol.* **12:** 627–661

Hirano A, Ayata M, Wang AH & Wong TC (1993) Functional analysis of matrix proteins expressed from cloned genes of measles virus variants that cause subacute sclerosing panencephalitis reveals a common defect in nucleocapsid binding. *J. Virol.* **67:** 1848–1853

Hirano A, Wang AH, Gombart AF & Wong TC (1992) The matrix proteins of neurovirulent subacute sclerosing panencephalitis virus and its acute measles virus progenitor are functionally different. *Proc. Natl. Acad. Sci. U.S.A.* **89:** 8745–8749

Hogue IB, Grover JR, Soheilian F, Nagashima K & Ono A (2011) Gag induces the coalescence of clustered lipid rafts and tetraspanin-enriched microdomains at HIV-1 assembly sites on the plasma membrane. *J. Virol.* **85:** 9749–9766

Hommersom CA, Matt B, van der Ham, A, Cornelissen, J J L M & Katsonis N (2014) Versatile post-functionalization of the external shell of cowpea chlorotic mottle virus by using click chemistry. *Organic & biomolecular chemistry* **12:** 4065–4069

Hsu EC, Iorio C, Sarangi F, Khine AA & Richardson CD (2001) CDw150(SLAM) is a receptor for a lymphotropic strain of measles virus and may account for the immunosuppressive properties of this virus. *Virology* **279:** 9–21

http://www.nobelprize.org *All Nobel Prizes in Physiology or Medicine.* http://www.nobelprize.org/nobel_prizes/medicine/laureates/. 01 October 2014

http://www.wiley.co.uk/genmed/clinical *Gene Therapy Clinical Trials Worldwide.* http://www.wiley.com/legacy/wileychi/genmed/clinical/. 10 October 2014

Interlandi G, Wetzel SK, Settanni G, Plückthun A & Caflisch A (2008) Characterization and further stabilization of designed ankyrin repeat proteins by combining molecular dynamics simulations and experiments. *J. Mol. Biol.* **375:** 837–854

Iorio RM, Melanson VR & Mahon PJ (2009) Glycoprotein interactions in paramyxovirus fusion. *Future Virology* **4:** 335–351

Ito M, Iwasaki M, Takeda M, Nakamura T, Yanagi Y & Ohno S (2013) Measles virus nonstructural C protein modulates viral RNA polymerase activity by interacting with host protein SHCBP1. *J. Virol.* **87:** 9633–9642

Iwasaki M, Takeda M, Shirogane Y, Nakatsu Y, Nakamura T & Yanagi Y (2009) The matrix protein of measles virus regulates viral RNA synthesis and assembly by interacting with the nucleocapsid protein. *J. Virol.* **83:** 10374–10383

Jost C, Schilling J, Tamaskovic R, Schwill M, Honegger A & Plückthun A (2013) Structural basis for eliciting a cytotoxic effect in HER2-overexpressing cancer cells via binding to the extracellular domain of HER2. *Structure* **21:** 1979–1991

Kalluri R & Weinberg RA (2009) The basics of epithelial-mesenchymal transition. *J. Clin. Invest.* **119:** 1420–1428

Kashiwakura Y, Tamayose K, Iwabuchi K, Hirai Y, Shimada T, Matsumoto K, Nakamura T, Watanabe M, Oshimi K & Daida H (2005) Hepatocyte growth factor receptor is a coreceptor for adeno-associated virus type 2 infection. *J. Virol.* **79:** 609–614

Kay MA (2011) State-of-the-art gene-based therapies: the road ahead. *Nat Rev Genet* **12:** 316–328

Kern A, Schmidt K, Leder C, Müller OJ, Wobus CE, Bettinger K, Von der Lieth, C W, King JA & Kleinschmidt JA (2003) Identification of a heparin-binding motif on adeno-associated virus type 2 capsids. *J. Virol.* **77:** 11072–11081

King JA, Dubielzig R, Grimm D & Kleinschmidt JA (2001) DNA helicase-mediated packaging of adeno-associated virus type 2 genomes into preformed capsids. *EMBO J.* **20:** 3282–3291

Kneissl S, Abel T, Rasbach A, Brynza J, Schneider-Schaulies J & Buchholz CJ (2012) Measles virus glycoprotein-based lentiviral targeting vectors that avoid neutralizing antibodies. *PLoS ONE* **7:** e46667

Knipe DM & Fields BN (2007) *Fields' virology.* Lippincott Williams & Wilkins, Philadelphia

Koch-Nolte F, Reyelt J, Schössow B, Schwarz N, Scheuplein F, Rothenburg S, Haag F, Alzogaray V, Cauerhff A & Goldbaum FA (2007) Single domain antibodies from llama effectively and specifically block T cell ecto-ADP-ribosyltransferase ART2.2 in vivo. *FASEB J.* **21:** 3490–3498

Kotin RM, Siniscalco M, Samulski RJ, Zhu XD, Hunter L, Laughlin CA, McLaughlin S, Muzyczka N, Rocchi M & Berns KI (1990) Site-specific integration by adeno-associated virus. *Proc. Natl. Acad. Sci. U.S.A.* **87:** 2211–2215

Kotterman MA & Schaffer DV (2014) Engineering adeno-associated viruses for clinical gene therapy. *Nat. Rev. Genet.* **15:** 445–451

Kramer MA, Wetzel SK, Plückthun A, Mittl PRE & Grütter MG (2010) Structural determinants for improved stability of designed ankyrin repeat proteins with a redesigned C-capping module. *J. Mol. Biol.* **404:** 381–391

Kronenberg S, Böttcher B, von der Lieth, Claus W, Bleker S & Kleinschmidt JA (2005) A conformational change in the adeno-associated virus type 2 capsid leads to the exposure of hidden VP1 N termini. *J. Virol.* **79:** 5296–5303

Kronenberg S, Kleinschmidt JA & Böttcher B (2001) Electron cryo-microscopy and image reconstruction of adeno-associated virus type 2 empty capsids. *EMBO reports* **2:** 997–1002

Kwon I & Schaffer DV (2008) Designer gene delivery vectors: molecular engineering and evolution of adeno-associated viral vectors for enhanced gene transfer. *Pharm. Res.* **25:** 489–499

Langhorst MF, Reuter A & Stuermer, C A O (2005) Scaffolding microdomains and beyond: the function of reggie/flotillin proteins. *Cell. Mol. Life Sci.* **62:** 2228–2240

Lerch TF, Xie Q & Chapman MS (2010) The structure of adeno-associated virus serotype 3B (AAV-3B): insights into receptor binding and immune evasion. *Virology* **403:** 26–36

Liebert UG, Flanagan SG, Loffler S, Baczko K, ter Meulen V & Rima BK (1994) Antigenic determinants of measles virus hemagglutinin associated with neurovirulence. *J Virol* **68:** 1486–1493

Liljeroos L, Huiskonen JT, Ora A, Susi P & Butcher SJ (2011) Electron cryotomography of measles virus reveals how matrix protein coats the ribonucleocapsid within intact virions. *Proceedings of the National Academy of Sciences* **108:** 18085–18090

Litvinov SV, Velders MP, Bakker HA, Fleuren GJ & Warnaar SO (1994) Ep-CAM: a human epithelial antigen is a homophilic cell-cell adhesion molecule. *J. Cell Biol.* **125:** 437–446

Liu ML, Winther BL & Kay MA (1996) Pseudotransduction of hepatocytes by using concentrated pseudotyped vesicular stomatitis virus G glycoprotein (VSV-G)-Moloney murine leukemia virus-derived retrovirus vectors: comparison of VSV-G and amphotropic vectors for hepatic gene transfer. *J. Virol.* **70:** 2497–2502

Lux K, Goerlitz N, Schlemminger S, Perabo L, Goldnau D, Endell J, Leike K, Kofler DM, Finke S, Hallek M & Büning H (2005) Green fluorescent protein-tagged adeno-associated virus particles allow the study of cytosolic and nuclear trafficking. *J. Virol.* **79:** 11776–11787

Maetzel D, Denzel S, Mack B, Canis M, Went P, Benk M, Kieu C, Papior P, Baeuerle PA, Munz M & Gires O (2009) Nuclear signalling by tumour-associated antigen EpCAM. *Nat. Cell Biol.* **11:** 162–171

Makhortova NR, Askovich P, Patterson CE, Gechman LA, Gerard NP & Rall GF (2007) Neurokinin-1 enables measles virus trans-synaptic spread in neurons. *Virology* **362:** 235–244

Malim MH & Emerman M (2008) HIV-1 accessory proteins--ensuring viral survival in a hostile environment. *Cell Host Microbe* **3:** 388–398

Mateo M, Navaratnarajah CK & Cattaneo R (2014) Structural basis of efficient contagion: measles variations on a theme by parainfluenza viruses. *Curr Opin Virol* **5:** 16–23

McCarty DM (2008) Self-complementary AAV vectors; advances and applications. *Mol. Ther.* **16:** 1648–1656

McCarty DM, Fu H, Monahan PE, Toulson CE, Naik P & Samulski RJ (2003) Adeno-associated virus terminal repeat (TR) mutant generates self-complementary vectors to overcome the rate-limiting step to transduction in vivo. *Gene Ther.* **10:** 2112–2118

McCarty DM, Monahan PE & Samulski RJ (2001) Self-complementary recombinant adeno-associated virus (scAAV) vectors promote efficient transduction independently of DNA synthesis. *Gene Ther.* **8:** 1248–1254

McLaughlin PM, Harmsen MC, Dokter WH, Kroesen BJ, van der Molen, H, Brinker MG, Hollema H, Ruiters MH, Buys CH & de Leij, L F (2001) The epithelial glycoprotein 2 (EGP-

2) promoter-driven epithelial-specific expression of EGP-2 in transgenic mice: a new model to study carcinoma-directed immunotherapy. *Cancer Res.* **61:** 4105–4111

McWilliam H, Li W, Uludag M, Squizzato S, Park YM, Buso N, Cowley AP & Lopez R (2013) Analysis Tool Web Services from the EMBL-EBI. *Nucleic Acids Res.* **41:** W597-600

Miest TS & Cattaneo R (2014) New viruses for cancer therapy: meeting clinical needs. *Nat. Rev. Microbiol.* **12:** 23–34

Mingozzi F & High KA (2007) Immune responses to AAV in clinical trials. *Curr Gene Ther* **7:** 316–324

Mingozzi F, High KA, Mingozzi F & High KA (2013) Immune responses to AAV vectors: overcoming barriers to successful gene therapy. *Blood* **122:** 23–36

Moeller K, Duffy I, Duprex P, Rima B, Beschorner R, Fauser S, Meyermann R, Niewiesk S, ter Meulen V & Schneider-Schaulies J (2001) Recombinant measles viruses expressing altered hemagglutinin (H) genes: functional separation of mutations determining H antibody escape from neurovirulence. *J. Virol.* **75:** 7612–7620

Moll M, Klenk H & Maisner A (2002) Importance of the cytoplasmic tails of the measles virus glycoproteins for fusogenic activity and the generation of recombinant measles viruses. *Journal of Virology* **76:** 7174–7186

Momburg F, Moldenhauer G, Hämmerling GJ & Möller P (1987) Immunohistochemical study of the expression of a Mr 34,000 human epithelium-specific surface glycoprotein in normal and malignant tissues. *Cancer Res.* **47:** 2883–2891

Moss WJ & Griffin DE (2006) Global measles elimination. *Nat Rev Micro* **4:** 900–908

Msaouel P, Iankov ID, Allen C, Russell SJ & Galanis E (2012) Oncolytic measles virus retargeting by ligand display. *Methods Mol. Biol.* **797:** 141–162

Mühlebach MD, Mateo M, Sinn PL, Prüfer S, Uhlig KM, Leonard, Vincent H J, Navaratnarajah CK, Frenzke M, Wong XX, Sawatsky B, Ramachandran S, McCray PB, Cichutek K, Messling V von, Lopez M & Cattaneo R (2011) Adherens junction protein nectin-4 is the epithelial receptor for measles virus. *Nature* **480:** 530–533

Münch RC (2013) *A rational approach for targeted cell entry of adeno-associated viral vectors.* Dissertation, Heidelberg

Münch RC, Janicki H, Völker I, Rasbach A, Hallek M, Büning H & Buchholz CJ (2013) Displaying high-affinity ligands on adeno-associated viral vectors enables tumor cell-specific and safe gene transfer. *Mol. Ther.* **21:** 109–118

Münch RC, Muth A, Muik A, Friedel T, Schmatz J, Dreier B, Trkola A, Plückthun A, Büning H & Buchholz CJ (2015) Off-target-free gene delivery by affinity-purified receptor-targeted viral vectors. *Nature communications* **6:** 6246

Münch RC, Mühlebach MD, Schaser T, Kneissl S, Jost C, Plückthun A, Cichutek K & Buchholz CJ (2011) DARPins: an efficient targeting domain for lentiviral vectors. *Mol. Ther.* **19:** 686–693

Münz M, Kieu C, Mack B, Schmitt B, Zeidler R & Gires O (2004) The carcinoma-associated antigen EpCAM upregulates c-myc and induces cell proliferation. *Oncogene* **23:** 5748–5758

Nakamura T, Peng K, Harvey M, Greiner S, Lorimer, Ian A J, James CD & Russell SJ (2005) Rescue and propagation of fully retargeted oncolytic measles viruses. *Nat. Biotechnol.* **23:** 209–214

Naldini L, Blömer U, Gallay P, Ory D, Mulligan R, Gage FH, Verma IM & Trono D (1996) In vivo gene delivery and stable transduction of nondividing cells by a lentiviral vector. *Science* **272:** 263–267

Nam H, Lane MD, Padron E, Gurda B, McKenna R, Kohlbrenner E, Aslanidi G, Byrne B, Muzyczka N, Zolotukhin S & Agbandje-McKenna M (2007) Structure of adeno-associated virus serotype 8, a gene therapy vector. *J. Virol.* **81:** 12260–12271

Naniche D, Varior-Krishnan G, Cervoni F, Wild TF, Rossi B, Rabourdin-Combe C & Gerlier D (1993) Human membrane cofactor protein (CD46) acts as a cellular receptor for measles virus. *J. Virol* **67:** 6025–6032

Navaratnarajah CK, Kumar S, Generous A, Apte-Sengupta S, Mateo M & Cattaneo R (2014) The measles virus hemagglutinin stalk: structures and functions of the central fusion activation and membrane-proximal segments. *J. Virol.* **88:** 6158–6167

Navaratnarajah CK, Leonard, V H J & Cattaneo R (2009) Measles virus glycoprotein complex assembly, receptor attachment, and cell entry. *Curr. Top. Microbiol. Immunol.* **329:** 59–76

Navaratnarajah CK, Negi S, Braun W, Cattaneo R, Navaratnarajah CK, Negi S, Braun W & Cattaneo R (2012) Membrane fusion triggering: three modules with different structure and

function in the upper half of the measles virus attachment protein stalk. *Journal of Biological Chemistry* **287:** 38543–38551

Ng R, Govindasamy L, Gurda BL, McKenna R, Kozyreva OG, Samulski RJ, Parent KN, Baker TS & Agbandje-McKenna M (2010) Structural characterization of the dual glycan binding adeno-associated virus serotype 6. *J. Virol.* **84:** 12945–12957

Norrby E (1971) The effect of a carbobenzoxy tripeptide on the biological activities of measles virus. *Virology* **44:** 599–608

Noyce RS, Bondre DG, Ha MN, Lin L, Sisson G, Tsao M, Richardson CD & Rall GF (2011) Tumor Cell Marker PVRL4 (Nectin 4) Is an Epithelial Cell Receptor for Measles Virus. *PLoS Pathog* **7:** e1002240

Opie SR, Warrington KH, Agbandje-McKenna M, Zolotukhin S & Muzyczka N (2003) Identification of amino acid residues in the capsid proteins of adeno-associated virus type 2 that contribute to heparan sulfate proteoglycan binding. *J. Virol.* **77:** 6995–7006

Paal T, Brindley MA, St. Clair C, Prussia A, Gaus D, Krumm SA, Snyder JP, Plemper RK, Paal T, Brindley MA, St Clair C, Prussia A, Gaus D, Krumm SA, Snyder JP & Plemper RK (2009) Probing the Spatial Organization of Measles Virus Fusion Complexes // Probing the spatial organization of measles virus fusion complexes. *Journal of Virology* **83:** 10480–10493

Pakula R, Melchior A, Denys A, Vanpouille C, Mazurier J & Allain F (2007) Syndecan-1/CD147 association is essential for cyclophilin B-induced activation of p44/42 mitogen-activated protein kinases and promotion of cell adhesion and chemotaxis. *Glycobiology* **17:** 492–503

Pantel K, Brakenhoff RH & Brandt B (2008) Detection, clinical relevance and specific biological properties of disseminating tumour cells. *Nat. Rev. Cancer* **8:** 329–340

Park JY, Lim B, Lee K, Kim Y & Jo E (2006) Scalable production of adeno-associated virus type 2 vectors via suspension transfection. *Biotechnol. Bioeng.* **94:** 416–430

Pereira DJ, McCarty DM & Muzyczka N (1997) The adeno-associated virus (AAV) Rep protein acts as both a repressor and an activator to regulate AAV transcription during a productive infection. *J. Virol.* **71:** 1079–1088

Philpott NJ, Gomos J, Berns KI & Falck-Pedersen E (2002) A p5 integration efficiency element mediates Rep-dependent integration into AAVS1 at chromosome 19. *Proc. Natl. Acad. Sci. U.S.A.* **99:** 12381–12385

Plemper RK, Brindley MA, Iorio RM & Manchester M (2011) Structural and Mechanistic Studies of Measles Virus Illuminate Paramyxovirus Entry. *PLoS Pathog* **7:** e1002058

Plemper RK, Hammond AL & Cattaneo R (2001) Measles virus envelope glycoproteins hetero-oligomerize in the endoplasmic reticulum. *J. Biol. Chem.* **276:** 44239–44246

Ponnazhagan S, Mahendra G, Kumar S, Thompson JA & Castillas M (2002) Conjugate-based targeting of recombinant adeno-associated virus type 2 vectors by using avidin-linked ligands. *J. Virol.* **76:** 12900–12907

Popa-Wagner R, Porwal M, Kann M, Reuss M, Weimer M, Florin L & Kleinschmidt JA (2012) Impact of VP1-specific protein sequence motifs on adeno-associated virus type 2 intracellular trafficking and nuclear entry. *J. Virol.* **86:** 9163–9174

Qing K, Mah C, Hansen J, Zhou S, Dwarki V & Srivastava A (1999) Human fibroblast growth factor receptor 1 is a co-receptor for infection by adeno-associated virus 2. *Nat. Med.* **5:** 71–77

Rasbach A (2010) *Receptor attachment is not required for the measles virus hemagglutinin membrane fusion-helper function.* Diplomarbeit, Frankfurt am Main

Rasbach A, Abel T, Münch RC, Boller K, Schneider-Schaulies J & Buchholz CJ (2013) The receptor attachment function of measles virus hemagglutinin can be replaced with an autonomous protein that binds Her2/neu while maintaining its fusion-helper function. *J. Virol.* **87:** 6246–6256

Reiser J, Harmison G, Kluepfel-Stahl S, Brady RO, Karlsson S & Schubert M (1996) Transduction of nondividing cells using pseudotyped defective high-titer HIV type 1 particles. *Proc. Natl. Acad. Sci. U.S.A.* **93:** 15266–15271

Reul J (2013) *Oberflächen-Engineering von AAV-Vektorpartikeln zur Präsentation von Antikörperfragmenten.* Diplomarbeit, Frankfurt am Main

Richardson CD & Choppin PW (1983) Oligopeptides that specifically inhibit membrane fusion by paramyxoviruses: studies on the site of action. *Virology* **131:** 518–532

Richardson JH, Child LA & Lever AM (1993) Packaging of human immunodeficiency virus type 1 RNA requires cis-acting sequences outside the 5' leader region. *J. Virol.* **67:** 3997–4005

Riedl P, Moll M, Klenk H & Maisner A (2002) Measles virus matrix protein is not cotransported with the viral glycoproteins but requires virus infection for efficient surface targeting. *Virus Res.* **83:** 1–12

Riley-Vargas RC, Gill DB, Kemper C, Liszewski MK & Atkinson JP (2004) CD46: expanding beyond complement regulation. *Trends Immunol.* **25:** 496–503

Rose JA, Maizel JV, Inman JK & Shatkin AJ (1971) Structural proteins of adenovirus-associated viruses. *J. Virol.* **8:** 766–770

Runkler N, Pohl C, Schneider-Schaulies S, Klenk H & Maisner A (2007) Measles virus nucleocapsid transport to the plasma membrane requires stable expression and surface accumulation of the viral matrix protein. *Cell. Microbiol.* **9:** 1203–1214

Russell SJ, Federspiel MJ, Peng K, Tong C, Dingli D, Morice WG, Lowe V, O'Connor MK, Kyle RA, Leung N, Buadi FK, Rajkumar SV, Gertz MA, Lacy MQ & Dispenzieri A (2014) Remission of disseminated cancer after systemic oncolytic virotherapy. *Mayo Clin. Proc.* **89:** 926–933

Russell SJ & Peng KW (2009) Measles virus for cancer therapy. *Curr. Top. Microbiol. Immunol.* **330:** 213–241

Sakuma T, Barry MA & Ikeda Y (2012) Lentiviral vectors: basic to translational. *Biochem. J.* **443:** 603–618

Samulski RJ, Zhu X, Xiao X, Brook JD, Housman DE, Epstein N & Hunter LA (1991) Targeted integration of adeno-associated virus (AAV) into human chromosome 19. *EMBO J.* **10:** 3941–3950

Sato H, Yoneda M, Honda T & Kai C (2012) Morbillivirus receptors and tropism: multiple pathways for infection. *Front Microbiol* **3:** 75

Schaffer DV, Koerber JT & Lim K (2008) Molecular engineering of viral gene delivery vehicles. *Annual review of biomedical engineering* **10:** 169–194

Schambach A, Zychlinski D, Ehrnstroem B & Baum C (2013) Biosafety features of lentiviral vectors. *Hum. Gene Ther.* **24:** 132–142

Schmelzer E & Reid LM (2008) EpCAM expression in normal, non-pathological tissues. *Front. Biosci.* **13:** 3096–3100

Schuhmann NK, Pozzoli O, Sallach J, Huber A, Avitabile D, Perabo L, Rappl G, Capogrossi MC, Hallek M, Pesce M & Büning H (2010) Gene transfer into human cord blood-derived CD34(+) cells by adeno-associated viral vectors. *Experimental Hematology* **38:** 707–717

Schweizer A, Rusert P, Berlinger L, Ruprecht CR, Mann A, Corthésy S, Turville SG, Aravantinou M, Fischer M, Robbiani M, Amstutz P & Trkola A (2008) CD4-specific designed ankyrin repeat proteins are novel potent HIV entry inhibitors with unique characteristics. *PLoS Pathog.* **4:** e1000109

Sievers F, Wilm A, Dineen D, Gibson TJ, Karplus K, Li W, Lopez R, McWilliam H, Remmert M, Söding J, Thompson JD & Higgins DG (2011) Fast, scalable generation of high-quality protein multiple sequence alignments using Clustal Omega. *Mol. Syst. Biol.* **7:** 539

Simon M, Stefan N, Plückthun A & Zangemeister-Wittke U (2013) Epithelial cell adhesion molecule-targeted drug delivery for cancer therapy. *Expert Opin Drug Deliv* **10:** 451–468

Simon M, Zangemeister-Wittke U & Plückthun A (2012) Facile double-functionalization of designed ankyrin repeat proteins using click and thiol chemistries. *Bioconjug. Chem.* **23:** 279–286

Sommer JM, Smith PH, Parthasarathy S, Isaacs J, Vijay S, Kieran J, Powell SK, McClelland A & Wright JF (2003) Quantification of adeno-associated virus particles and empty capsids by optical density measurement. *Mol. Ther.* **7:** 122–128

Sompayrac L (2002) *How pathogenic viruses work.* Jones and Bartlett Publishers, Boston

Sonntag F, Schmidt K & Kleinschmidt JA (2010) A viral assembly factor promotes AAV2 capsid formation in the nucleolus. *Proc. Natl. Acad. Sci. U.S.A.* **107:** 10220–10225

Spizzo G, Fong D, Wurm M, Ensinger C, Obrist P, Hofer C, Mazzoleni G, Gastl G & Went P (2011) EpCAM expression in primary tumour tissues and metastases: an immunohistochemical analysis. *J. Clin. Pathol.* **64:** 415–420

Stefan N, Martin-Killias P, Wyss-Stoeckle S, Honegger A, Zangemeister-Wittke U & Plückthun A (2011) DARPins recognizing the tumor-associated antigen EpCAM selected by phage and ribosome display and engineered for multivalency. *J. Mol. Biol.* **413:** 826–843

Steiner D, Forrer P & Plückthun A (2008) Efficient selection of DARPins with sub-nanomolar affinities using SRP phage display. *J. Mol. Biol.* **382:** 1211–1227

Steiner D, Forrer P, Stumpp MT & Pluckthun A (2006) Signal sequences directing cotranslational translocation expand the range of proteins amenable to phage display. *Nat Biotechnol* **24:** 823–831

Stumpp MT & Amstutz P (2007) DARPins: a true alternative to antibodies. *Curr Opin Drug Discov Devel* **10:** 153–159

Summerford C, Bartlett JS & Samulski RJ (1999) AlphaVbeta5 integrin: a co-receptor for adeno-associated virus type 2 infection. *Nat. Med.* **5:** 78–82

Summerford C & Samulski RJ (1998) Membrane-associated heparan sulfate proteoglycan is a receptor for adeno-associated virus type 2 virions. *J. Virol.* **72:** 1438–1445

Suryanarayana K, Baczko K, ter Meulen V & Wagner RR (1994) Transcription inhibition and other properties of matrix proteins expressed by M genes cloned from measles viruses and diseased human brain tissue. *J. Virol.* **68:** 1532–1543

Tahara M, Ito Y, Brindley MA, Ma X, He J, Xu S, Fukuhara H, Sakai K, Komase K, Rota PA, Plemper RK, Maenaka K & Takeda M (2013) Functional and structural characterization of neutralizing epitopes of measles virus hemagglutinin protein. *J. Virol.* **87:** 666–675

Tahara M, Takeda M & Yanagi Y (2007) Altered interaction of the matrix protein with the cytoplasmic tail of hemagglutinin modulates measles virus growth by affecting virus assembly and cell-cell fusion. *J. Virol.* **81:** 6827–6836

Tatsuo H, Ono N, Tanaka K & Yanagi Y (2000) SLAM (CDw150) is a cellular receptor for measles virus. *Nature* **406:** 893–897

Theiss HD, Kofler DM, Büning H, Aldenhoff A, Kaess B, Decker T, Baumert J, Hallek M & Wendtner C (2003) Enhancement of gene transfer with recombinant adeno-associated virus (rAAV) vectors into primary B-cell chronic lymphocytic leukemia cells by CpG-oligodeoxynucleotides. *Exp. Hematol.* **31:** 1223–1229

Tseng Y & Agbandje-McKenna M (2014) Mapping the AAV Capsid Host Antibody Response toward the Development of Second Generation Gene Delivery Vectors. *Front Immunol* **5:** 9

Vasileva A & Jessberger R (2005) Precise hit: adeno-associated virus in gene targeting. *Nat. Rev. Microbiol.* **3:** 837–847

Vincent S, Gerlier D & Manié SN (2000) Measles virus assembly within membrane rafts. *J. Virol.* **74:** 9911–9915

Visvader JE & Lindeman GJ (2008) Cancer stem cells in solid tumours: accumulating evidence and unresolved questions. *Nat Rev Cancer* **8:** 755–768

Völkel T, Müller R & Kontermann RE (2004) Isolation of endothelial cell-specific human antibodies from a novel fully synthetic scFv library. *Biochem. Biophys. Res. Commun.* **317:** 515–521

Vongpunsawad S, Oezgun N, Braun W & Cattaneo R (2004) Selectively receptor-blind measles viruses: Identification of residues necessary for SLAM- or CD46-induced fusion and their localization on a new hemagglutinin structural model. *J. Virol* **78:** 302–313

Walters RW, Agbandje-McKenna M, Bowman VD, Moninger TO, Olson NH, Seiler M, Chiorini JA, Baker TS & Zabner J (2004) Structure of adeno-associated virus serotype 5. *J. Virol.* **78:** 3361–3371

Wang Z, Ma H, Li J, Sun L, Zhang J & Xiao X (2003) Rapid and highly efficient transduction by double-stranded adeno-associated virus vectors in vitro and in vivo. *Gene Ther.* **10:** 2105–2111

Warrington KH, Gorbatyuk OS, Harrison JK, Opie SR, Zolotukhin S & Muzyczka N (2004) Adeno-associated virus type 2 VP2 capsid protein is nonessential and can tolerate large peptide insertions at its N terminus. *J. Virol.* **78:** 6595–6609

Watanabe A, Yoneda M, Ikeda F, Terao-Muto Y, Sato H & Kai C (2010) CD147/EMMPRIN acts as a functional entry receptor for measles virus on epithelial cells. *J. Virol.* **84:** 4183–4193

Welch BD, Yuan P, Bose S, Kors CA, Lamb RA & Jardetzky TS (2013) Structure of the parainfluenza virus 5 (PIV5) hemagglutinin-neuraminidase (HN) ectodomain. *PLoS Pathogens* **9:** e1003534

Winkler J, Martin-Killias P, Plückthun A & Zangemeister-Wittke U (2009) EpCAM-targeted delivery of nanocomplexed siRNA to tumor cells with designed ankyrin repeat proteins. *Mol. Cancer Ther.* **8:** 2674–2683

Wu J, Zhao W, Zhong L, Han Z, Li B, Ma W, Weigel-Kelley KA, Warrington KH & Srivastava A (2007) Self-complementary recombinant adeno-associated viral vectors: packaging capacity and the role of rep proteins in vector purity. *Hum. Gene Ther.* **18:** 171–182

Wu P, Xiao W, Conlon T, Hughes J, Agbandje-McKenna M, Ferkol T, Flotte T & Muzyczka N (2000) Mutational analysis of the adeno-associated virus type 2 (AAV2) capsid gene and construction of AAV2 vectors with altered tropism. *J. Virol.* **74:** 8635–8647

Wu Z, Asokan A, Grieger JC, Govindasamy L, Agbandje-McKenna M & Samulski RJ (2006a) Single amino acid changes can influence titer, heparin binding, and tissue tropism in different adeno-associated virus serotypes. *J. Virol.* **80:** 11393–11397

Wu Z, Asokan A & Samulski RJ (2006b) Adeno-associated virus serotypes: vector toolkit for human gene therapy. *Mol. Ther.* **14:** 316–327

Xiao X, Li J & Samulski RJ (1998) Production of high-titer recombinant adeno-associated virus vectors in the absence of helper adenovirus. *J. Virol.* **72:** 2224–2232

Xie Q, Bu W, Bhatia S, Hare J, Somasundaram T, Azzi A & Chapman MS (2002) The atomic structure of adeno-associated virus (AAV-2), a vector for human gene therapy. *Proc. Natl. Acad. Sci. U.S.A.* **99:** 10405–10410

Yamashita T, Budhu A, Forgues M & Wang XW (2007) Activation of hepatic stem cell marker EpCAM by Wnt-beta-catenin signaling in hepatocellular carcinoma. *Cancer Res.* **67:** 10831–10839

Yang L, Bailey L, Baltimore D & Wang P (2006) Targeting lentiviral vectors to specific cell types in vivo. *Proc. Natl. Acad. Sci. U.S.A.* **103:** 11479–11484

Yang Q, Mamounas M, Yu G, Kennedy S, Leaker B, Merson J, Wong-Staal F, Yu M & Barber JR (1998) Development of novel cell surface CD34-targeted recombinant adenoassociated virus vectors for gene therapy. *Hum. Gene Ther.* **9:** 1929–1937

Yin H, Wen X, Paterson RG, Lamb RA & Jardetzky TS (2006) Structure of the parainfluenza virus 5 F protein in its metastable, prefusion conformation. *Nature* **439:** 38–44

Ylä-Herttuala S (2012) Endgame: glybera finally recommended for approval as the first gene therapy drug in the European union. *Mol. Ther.* **20:** 1831–1832

Young SM, McCarty DM, Degtyareva N & Samulski RJ (2000) Roles of adeno-associated virus Rep protein and human chromosome 19 in site-specific recombination. *J. Virol.* **74:** 3953–3966

Yu M, Bardia A, Wittner BS, Stott SL, Smas ME, Ting DT, Isakoff SJ, Ciciliano JC, Wells MN, Shah AM, Concannon KF, Donaldson MC, Sequist LV, Brachtel E, Sgroi D, Baselga J, Ramaswamy S, Toner M, Haber DA & Maheswaran S (2013) Circulating Breast Tumor Cells

Exhibit Dynamic Changes in Epithelial and Mesenchymal Composition. *Science* **339:** 580–584

Yuan P, Swanson KA, Leser GP, Paterson RG, Lamb RA & Jardetzky TS (2011) Structure of the Newcastle disease virus hemagglutinin-neuraminidase (HN) ectodomain reveals a four-helix bundle stalk. *Proceedings of the National Academy of Sciences of the United States of America* **108:** 14920–14925

Zahnd C, Pecorari F, Straumann N, Wyler E & Pluckthun A (2006) Selection and characterization of Her2 binding-designed ankyrin repeat proteins. *J Biol Chem* **281:** 35167–35175

Zahnd C, Wyler E, Schwenk JM, Steiner D, Lawrence MC, McKern NM, Pecorari F, Ward CW, Joos TO & Plückthun A (2007) A designed ankyrin repeat protein evolved to picomolar affinity to Her2. *J. Mol. Biol.* **369:** 1015–1028

Zaloudik J, Basak S, Nesbit M, Speicher DW, Wunner WH, Miller E, Ernst-Grotkowski C, Kennedy R, Bergsagel LP, Koido T & Herlyn D (1997) Expression of an antigen homologous to the human CO17-1A/GA733 colon cancer antigen in animal tissues. *Br. J. Cancer* **76:** 909–916

Zhang X, Kutner RH, Bialkowska A, Marino MP, Klimstra WB & Reiser J (2010) Cell-specific targeting of lentiviral vectors mediated by fusion proteins derived from Sindbis virus, vesicular stomatitis virus, or avian sarcoma/leukosis virus. *Retrovirology* **7:** 3

Zhou Q, Schneider IC, Edes I, Honegger A, Bach P, Schönfeld K, Schambach A, Wels WS, Kneissl S, Uckert W & Buchholz CJ (2012) T-cell receptor gene transfer exclusively to human CD8(+) cells enhances tumor cell killing. *Blood* **120:** 4334–4342

Zufferey R, Dull T, Mandel RJ, Bukovsky A, Quiroz D, Naldini L & Trono D (1998) Self-inactivating lentivirus vector for safe and efficient in vivo gene delivery. *J. Virol.* **72:** 9873–9880

Zufferey R, Nagy D, Mandel RJ, Naldini L & Trono D (1997) Multiply attenuated lentiviral vector achieves efficient gene delivery in vivo. *Nat Biotechnol* **15:** 871–875

Zygiert Z (1971) Hodgkin's disease: remissions after measles. *Lancet* **1:** 593

6 Abbreviations

α	anti
AAV	adeno-associated virus
APS	ammonium persulfate
ATCC	American Type Culture Collection
bp	base pair
BSA	bovine serum albumin
°C	degree Celsius
cap	capsid protein
CHO	Chinese hamster ovary
CMV	cytomegalovirus
Δ	delta
DARPin	designed ankyrin repeat protein
DMEM	Dulbecco's modified Eagle medium
DMSO	dimethyl sulfoxide
DNA	deoxyribonucleic acid
E. coli	Escherichia coli
EDTA	ethylenediaminetetraacetic acid
EGFP	enhanced green fluorescent protein
ELISA	enzyme-linked immunosorbent assay
EM	electron microscopy
Env	envelope protein
EpCAM	epithelial cell adhesion molecule
et al.	and others
F	fusion protein
FACS	fluorescence-activated cell sorting
FCS	fetal calf serum
FIP	fusion inhibitory peptide
for	forward
g	gram
GFP	green fluorescent protein
GOI	genomes per cell
H	hemagglutinin

HCl	hydrochloride
HEK	human embryonic kidney
Her2/neu	human epidermal growth factor receptor 2
his	hexa-histidine motif
HIV	human immunodeficiency virus
HMEC	human mammary epithelial cell
HN	hemagglutinin-neuraminidase
HPLC	high-performance liquid chromatography
HRP	horseradish peroxidase
HSPG	heparan sulfate proteoglycan
ITR	inverted terminal repeat
K	potassium
kDa	kilo Dalton
kg	kilogram
l	liter
LB	Luria-Bertani
luc	luciferase
LTR	long terminal repeat
LV	lentiviral vector
µ	micro
MAb	monoclonal antibody
Mg	Magnesium
MOI	multiplicity of infection
mRNA	messenger RNA
MV	measles virus
nb	nanobody
n.s.	not significant
NDV	Newcastle disease virus
ORF	open reading frame
PBMC	peripheral blood mononuclear cells
PBS	phosphate buffered saline
PBS M/K	PBS supplemented with Mg/K
PCR	polymerase chain reaction
PIV5	parainfluenza virus 5

rep	viral regulatory proteins
rev	reverse
RNA	ribonucleic acid
rpm	rounds per minute
scAAV	AAV vector with self-complementary genome
scFv	single chain Fragment variable
SDS	sodium dodecyl sulfate
SDS-PAGE	SDS polyacrylamide gel electrophoresis
SFFV	spleen focus forming virus
SLAM	signaling lymphocyte activation molecule
TEMED	tetramethylethylenediamine
Tris	tris(hydroxymethyl)aminomethane
t.u.	transducing unit
U	unit
V	volt
VP	viral protein
VSV	vesicular stomatitis virus
VSVG	envelope glycoprotein of VSV
wt	wildtype

7 Curriculum Vitae

Persönliche Informationen

Name	Anke Muth, geb. Rasbach
Geburtsdatum	27.07.1985
Geburtsort	Friedberg (Hessen)

Ausbildung & Berufserfahrung

Dezember 2014	Abgabe der Doktorarbeit am Fachbereich Biologie, TU Darmstadt Titel: Receptor-targeted viral vectors for basic and medical research
Juli 2011 – Dezember 2014	Stipendiatin am Paul-Ehrlich-Institut in Langen, Arbeitsgruppe von Prof. Dr. Christian Buchholz „Molekulare Biotechnologie und Gentherapie“
Oktober 2011 – Dezember 2011	Gastwissenschaftlerin an der Purdue University (Indiana, USA) in der Arbeitsgruppe von Prof. Dr. Michael G. Rossmann
November 2010 – Juni 2011	Wissenschaftliche Mitarbeiterin am Paul-Ehrlich-Institut in Langen in der Abteilung „Medizinische Biotechnologie“
Oktober 2005 – Oktober 2010	Studium der Biochemie an der Goethe Universität Frankfurt Studienabschluss: Diplom-Biochemikerin (Note: 1,0)
Juni 2005	Allgemeine Hochschulreife an der St. Lioba-Schule Bad Nauheim (Note: 1,7)

Stipendien & Auszeichnungen

Juli 2014 – Dezember 2014	Promotionsstipendium des Zell- und Gentherapie Zentrums der Landesoffensive zur Entwicklung Wissenschaftlich-Ökonomischer Exzellenz (LOEWE)
2014	„Travel Grant Award“ zum Meeting der American Society of Gene & Cell Therapy, Washington DC 2014
2014	„Best Presentation Award“ des PEI Retreats, Heidelberg 2014
2012	„Best Poster Award“ des Meetings der Deutschen Gesellschaft für Gentherapie, Frankfurt 2012
2012	“Travel Grant Award” zum Meeting der Deutschen Gesellschaft für Gentherapie, Frankfurt 2012
Juli 2011 – Juni 2014	Promotionsstipendium des Graduiertenkollegs 1172 „Biologicals“ der Deutschen Forschungsgemeinschaft

8 Danksagung

Ich möchte mich herzlich bei Prof. Dr. Christian Buchholz bedanken, der mir die Möglichkeit gegeben hat, meine Doktorarbeit in seiner Arbeitsgruppe am Paul-Ehrlich-Institut anzufertigen. Meine Projekte wären ohne seine hervorragende Betreuung, die stete Diskussionsbereitschaft und Förderung nicht möglich gewesen.

Prof. Dr. Beatrix Süß danke ich für die unkomplizierte und nette Betreuung am Fachbereich Biologie der TU Darmstadt, sowie für die Unterstützung im Rahmen des Graduiertenkollegs „Biologicals“.

Ein weiterer Dank geht an Prof. Dr. Harald Kolmar für die Bereitschaft, die Aufgabe des Zweitgutachters an der TU Darmstadt zu übernehmen.

Natürlich möchte ich mich auch bei allen Kooperationspartnern bedanken, mit denen ich im Laufe der Zeit zusammenarbeiten durfte. Auch wenn die Liste der Personen zu lang wäre, um sie hier aufzuführen, möchte ich hervorheben, dass diese Zusammenarbeiten ein wertvoller Bestandteil der letzten Jahre war.

Ganz besonders möchte ich mich bei „meinem Postdoc“ Robert sowie bei Sarah, Ruben, Johanna, Thorsten, Alex, Qi, Jessi, Irene, Tobi, Gundi, Ruth, Manu, Patricia, Anett und Dina bedanken. Ihr habt mit eurer unermüdlichen Hilfsbereitschaft, den unzähligen Diskussionen und der fantastischen Arbeitsatmosphäre maßgeblich zum Gelingen dieser Arbeit beigetragen. Ohne euch und ohne die Freundschaften, die in den letzten Jahren auch außerhalb des Labors entstanden sind, wäre die Zeit nicht annähernd so schön gewesen.

Danken möchte ich auch meiner Familie – allen voran meinen Eltern, meinen Geschwistern Heike und Frank und meinen Schwiegereltern Barbara und Volker – sowie meinen Freunden, die immer für mich da sind.

Ein riesiges Dankeschön geht auch an meinen Mann Sebastian, der mich in allen Lebenslagen unterstützt, auch in den unmöglichsten Situationen verständnisvoll und geduldig bleibt und mich zum Lachen bringt. Danke, dass du immer für mich da bist!

9 Ehrenwörtliche Erklärung

Ich erkläre hiermit ehrenwörtlich, dass ich die vorliegende Arbeit entsprechend den Regeln guter wissenschaftlicher Praxis selbstständig und ohne unzulässige Hilfe Dritter angefertigt habe.

Sämtliche aus fremden Quellen direkt oder indirekt übernommenen Gedanken sowie sämtliche von Anderen direkt oder indirekt übernommenen Daten, Techniken und Materialien sind als solche kenntlich gemacht. Die Arbeit wurde bisher bei keiner anderen Hochschule zu Prüfungszwecken eingereicht.

Darmstadt, den 18.12.2014

_____

(Anke Muth)